Revised Manuscript (with changes marked)

Current version (egusphere-2025-3248)

Probabilistic and Deterministic Seismic Hazard Assessments of the area comprised between west Gulf of Cádiz and east Alboran Sea

Adrián José Rosario Beltré[1,2], Carlos Paredes Bartolomé[1], Miguel Llorente Isidro[3]

[1] Department of Geological and Mining Engineering, Higher Technical School of Mines and Energy, Universidad Politécnica de Madrid (UPM), Ríos Rosas 21, 28003 Madrid, Spain
[2] Department of Geological Resources for the Ecological Transition, Geological Survey of Spain (IGME), Spanish National Research Council (CSIC), La Calera 1, 28760 Tres Cantos (Madrid), Spain
[3] Department of Geological Risk and Climatic Change, Geological Survey of Spain (IGME), Spanish National Research Council (CSIC), Rios Rosas 23, 28003 Madrid, Spain

Correspondence to: Adrián José Rosario Beltré (aj.rosario@igme.es); Carlos Paredes Bartolomé (carlos.paredes@upm.es); Miguel Llorente Isidro (m.llorente@igme.es)

Abstract.

The increased deployment of subsea infrastructures and the exploration of marine resources have heightened the need to assess seismic hazard on the seabed, especially in tectonically active offshore regions. The area between the Gulf of Cádiz and the Alboran Sea, which is rich in coastal and submarine assets, is located within the Ibero-Maghrebian Region (IMR) a seismically active region. While previous research has addressed seismic hazard in adjacent inland areas using deterministic and probabilistic approaches, few studies have focused on offshore zones. Moreover, existing models often overlook the amplification effects introduced by bathymetry and seafloor conditions, and they rely on ground motion prediction equations (GMPEs) derived from inland data. Consequently, seismic hazard in marine environments remains poorly constrained. This study aims to evaluate the feasibility and applicability of both probabilistic (PSHA) and deterministic (DSHA) seismic hazard assessments for submarine areas, using updated seismogenic zonation, a high-resolution bathymetric model, and GMPEs suitable for soft marine soils. The objective is to produce reliable peak ground acceleration (PGA) estimates at the seabed ~~and to examine the convergence of deterministic and probabilistic approaches~~ in a complex tectonic context. The analysis was conducted using the OpenQuake (OQ) engine for PSHA and a custom MATLAB© script for DSHA. The seismogenic sources and parameters were taken from the European Seismic Hazard Model (ESHM20), and four GMPEs ~~: IDR91, HZ23, NT24, and DKK24~~ were selected for their relevance to offshore or soft soil conditions. These GMPEs were benchmarked ~~validated~~ against six regional offshore earthquakes recorded in the IMR as a plausibility check. Hazard estimates were computed over a EMODnet bathymetric refined grid and expressed as PGA maps for various return periods (100, 475, 2475, and 5000 years). The results show that significant PGA values occur over key submarine fault systems such as the Gorringe Ridge, Horseshoe Plain, and Arzew Fault. ~~Offshore PGA estimates for return periods of 2475 years using NT24 and DKK24 are close to those derived from DSHA, settling convergence between methodologies.~~ A PSHA reference results for onshore site conditions and

clipped to the IMR was used as a methodological contrast to provide a reference for how the hazard results obtained amplify PGAs. The use of seabed-adapted GMPEs resulted in higher and more realistic PGA values compared to inland models. This study demonstrates the applicability of seismic hazard assessment methods to offshore environments and highlights the importance of incorporating seafloor conditions into hazard modelling. The findings offer a methodological basis for improving the seismic design of subsea infrastructure in tectonically complex marine regions such as the IMR.

1. Introduction

The majority of ocean infrastructures are anchored or seated on the seabed in some way (e.g., Guo et al., 2021; Rui et al., 2024). The stability of these assets may be compromised by the mechanical properties of the seafloor (e.g., Liu et al., 2021; Randolph and Gourvenec, 2017; Veiskarami et al., 2017). Earthquakes and the processes they trigger, such as tsunamis and landslides, affect the dynamic behaviour of the ground, with the potential to cause significant damage to infrastructures and facilities (Román-de la Sancha et al., 2022; Shan et al., 2022). Consequently, attention should be given to investigate local effects on offshore structures (e.g., Kee et al., 2023; Li et al., 2023) along with undersea seismic hazard and the influence of surrounding seismogenic sources (Ercilla et al., 2021; Karthigeyan, 2022). Coastal and offshore facilities should be designed to withstand earthquakes and their coseismic effects. In offshore settings, the water column, seabed morphology and compliant soft sediments rheology modify source-to-site path and site terms. The water layer alters impedance contrasts and incidence/refraction of P and /SV waves at the seafloor, shifts spectral content, and can lengthen significant duration at the seabed relative to adjacent onshore sites (Nakamura et al., 2015; Zhang et al. 2020; Dhakal and Kunugi, 2023; W. Chen et al., 2024b). These effects, together with basin geometry and bathymetric geography, motivate use of seabed-adapted GMPEs and 3-D distance metrics that include depth (e.g., R_{RUP}) when estimating seabed PGA (e.g., Chen et al., 2024a; Hu et al., 2020; Dhakal et al., 2021; Lan et al., 2021)Research show that the seawater layer and seafloor cohesion mainly influence how seismic energy is transmitted in marine environments (Chen et al., 2015, 2024; Lan et al., 2021). However, the strategies to evaluate undersea seismic hazard may not be entirely valid considering they rely on seismic response of emerged terrain.

The area encompassing the Strait of Gibraltar, between the Alboran Sea in the Mediterranean Sea and the Gulf of Cádiz in the Atlantic Ocean, is also known as the Ibero-Maghrebian Region (IMR) (Buforn et al., 1995). A substantial number of communication and energy cables (Submarine Cable Map, 2025) are present in the IMR. Major infrastructures are also located here, including oil and gas pipelines connecting Algeria and Morocco with Spain (Medgaz; https://www.medgaz.com/, last accessed 08/07/2025) and several offshore wind farms. Moreover, the European-African tunnel is planned to be developed in the IMR (SECEGSA; https://www.secegsa.gob.es/proyecto-del-enlace-fijo, last accessed 08/07/2025). These assets, among other issues, underscore the area's substantial geostrategic importance (Báez et al., 2021). The IMR is at the boundary between the Eurasian and Nubian tectonic plates (Buforn et al., 2016). It comprises the southern Iberian Peninsula and the Maghreb (Buforn et al., 1995), and it is considered to have a medium to moderate tectonic activity, with frequent seismicity due to the convergence of the tectonic plates. Significant and devastating earthquakes have been documented within the region (Buforn et al., 2015), some of which have triggered tsunamis and submarine landslides (Table 1). Consequently, a comprehensive Seismic Hazard Assessment (SHA) is of utmost relevance within the IMR.

Nowadays, there are two broad standard approaches to SHA (Hamidatou et al., 2024; Kumar et al., 2024): Deterministic Seismic Hazard Analysis (DSHA) and Probabilistic Seismic Hazard Analysis (PSHA; Reiter, 1990). These methods have also been criticised (Kossobokov and Panza, 2022). Currently, PSHA has been broadly adopted by the scientific community and for mitigation plans, whilst DSHA is still considered useful in worst-case scenario modelling situations (Grasso and Maugeri, 2012; Mostafa et al., 2019), commonly used by civil protection agencies. DSHA was the first methodology proposed in the late 1960s for the design of nuclear power plants and was later applied to other large industrial infrastructures (AEIS-IGN, 1979; NRC, 1973). DSHA and PSHA can complement each other, providing further information about the existing seismic hazard (Wang et al., 2012).

Table 1: Location, date and moment magnitude (M_w) of notable~~some large~~ earthquakes with causalities in the IMR.

Region	Location	Date	M_w	Casualties	Reference
Southern Iberian Peninsula	Malaga, Spain	10.09.1680	6.8	70	Goded et al. (2008)
	Lisbon, Portugal	11.01.1755	7.7 - 8.5	100,000	Chester (2001), Fonseca (2020), Mendes-Victor et al. (2009)
	Torrevieja, Alicante	03.21.1829	6.8 - 6.9	389	Silva et al. (2019)
	Andalusian, Spain	12.25.1884	6.5 - 6.7	839	Udias and Muñoz (1979)
	Adra, Almeria	06.16.1910	6.1	0	Stich et al. (2003)
	Cape St. Vincent, Portugal	02.28.1969	7.8	19	López Arroyo and Udías (1972)
North Africa	Oran, Algeria	09.10.1790	6.0 - 6.5	2,000	Ayadi and Bezzeghoud (2014)
	El-Asnam, Algeria	10.10.1980	7.3	2,633	Ayadi and Bezzeghoud (2014)
	Boumerdès, Algeria	05.21.2003	6.8	2,278	Ayadi and Bezzeghoud (2014)
	Al-Hoceima, Morocco	02.24.2004	6.3	629	Kariche et al. (2018)

Despite the significant record of earthquakes, submarine landslides and tsunamis in the IMR (Rodriguez et al., 2017; Vázquez et al., 2022), the area has not been updated in full SHA. The first attempt of SHA in IMR was made by Molina Palacios (1998). This work evaluates the seismic hazard in terms of intensities and PGAs of the Iberia-Africa contact zone by a probabilistic approach. This involved a seismic zonation using areal sources, applying available estimation tools to flat terrain, using ground motion prediction equations (GMPEs) from rocky inland areas, and relying on seismotectonic knowledge from the 1990s. Conversely, the emerged land around the IMR has exhaustive seismic hazard studies, using both deterministic and probabilistic approaches. For example, the PHSA method has been the most widely implemented (e.g., Crespo et al., 2014; Danciu et al., 2024; IGN-UPM, 2017; Salgado Gálvez et al., 2015). Neo-deterministic Seismic Hazard Assessment (NDSHA) has been applied for the Iberian Peninsula (García-Fernández et al., 2022) and DSHA for Sevilla city (Sá et al., 2021). In the North African part, Poggi et al. (2020) performed a PSHA, and Mourabit et al. (2014) also conducted an NDSHA approach in this region. At the European continental scale, the most recent work covers the Euro-Mediterranean region, where the IMR is located. A fully probabilistic framework was adopted in the implementation of the hazard model, using harmonised input datasets across national boundaries. The seismogenic zone mosaic uses the 2020 European Seismic Hazards Model (ESHM20) (Danciu et al., 2024) for PSHA hazard assessment. The ESHM20 model uses the same principles as the 2013 Seismic Hazard Harmonisation in Europe (SHARE) project model (ESHM13) (Wössner et al., 2015), with state-of-the-art procedures applied homogeneously to the pan-European region. However, the SHA gap in the marine environment persists, hence further assessment of large-scale seismic hazard under seabed conditions within the marine IMR is needed, taking into consideration earthquake characteristics and spatial distribution based on comprehensive undersea data. In order fill this gap, this study has used seismic zoning and parameters from the ESHM20 (Danciu et al., 2021a, 2024). The novelty of this work also involves the use of attenuation functions derived from analogous marine regions regarding their seismotectonic context, considering there are no estimates of GMPEs for the IMR at this time. The DSHA here has been carried out using an in-house MATLAB© code ~~development~~, while for the PSHA the OpenQuake engine software was used (OQ v3.21) (Pagani et al., 2014; Silva et al., 2014).

2. Study area

The study area is characterized by a complex geodynamic context resulting from the interaction between the Nubia and the Iberian tectonic plates (Fig. 1) (e.g., Custódio et al., 2016; Neres et al., 2016). The plate boundary of the study area is usually divided into three main areas according to their stress regime: the SW as simple shear zone, the pure shear Gulf of Cádiz as the Eastern Betic, and the South Moroccan compressional arc. Tectonic models of NW-SE to WNW-ESE show oblique convergence between the Nubia and Iberian plates (Herraiz et al., 2000; Reilly et al., 1992) with displacements of 2 to 5 mm/yr (Fernandes et al., 2007; Nocquet, 2012) of the western Betic Cordilleras with respect to the Iberian Massif (Gonzalez-Castillo et al., 2015; Palano et al., 2013).

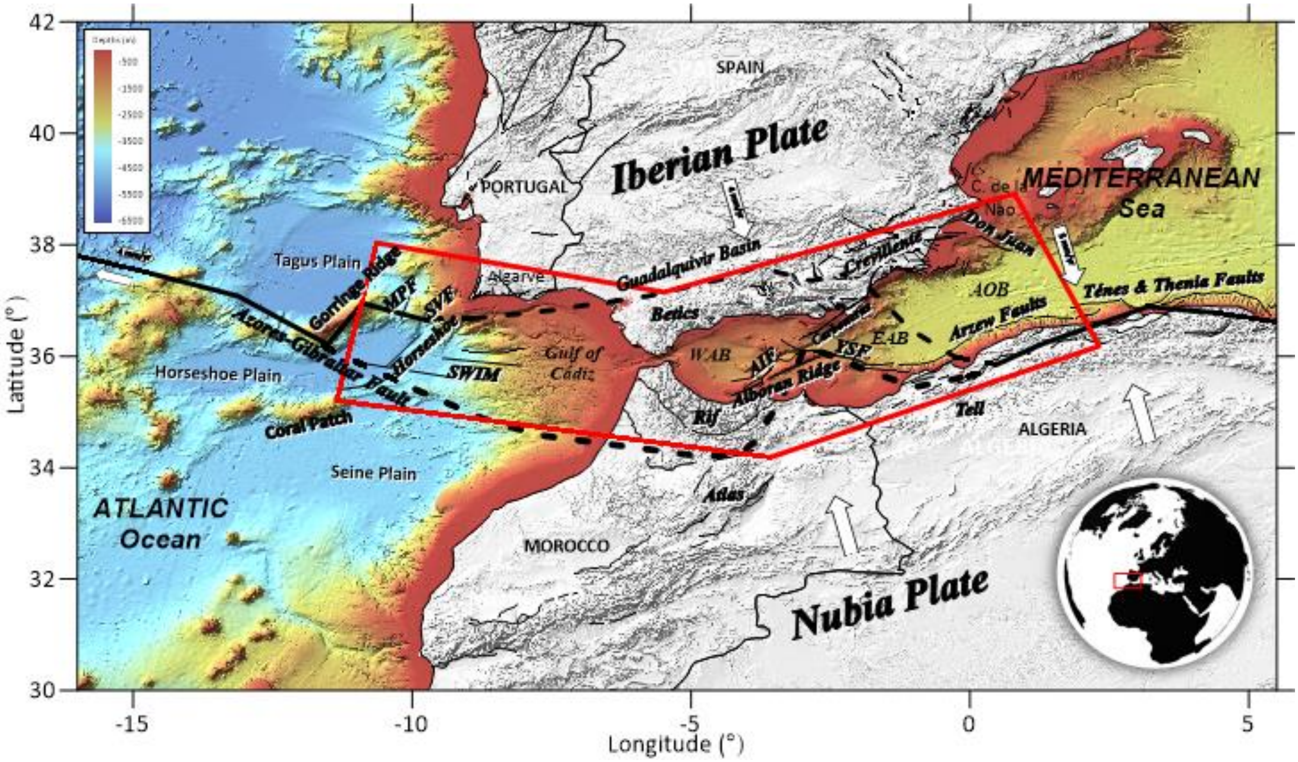

Figure 1. Location of the area of interest of this work in relation to the tectonic setting. Abbreviations are as follows: WAB: Western Alboran Basin, EAB: Eastern Alboran Basin, AOB: Algerian Oceanic Basin, SVF: Sao Vicente Fault, MPF: Marques de Pombal fault, SWIM: Southwest Iberian Margin lineaments (1, 2 and 3). AIF: Al Idrisi fault, YSF: Yusuf fault. Background: shadowed Digital Terrain Model (altimetry and coloured bathymetry) in the study area (extracted from EMODnet; https://emodnet.ec.europa.eu/en/bathymetry).

The Gulf of Cádiz (western sector of IMR) is located on the contact boundary between the Eurasian and African plates. It extends from the Azores Islands to the Strait of Gibraltar, through the Iberian massif and the Algarve region to the north, and, in the eastern part, through the orogenic arc of the Betic-Rifeña mountain range. It is characterised by a NW-SE oblique convergence regime, mainly controlled by the formation of the Betic-Rifeño Orogen and by the accommodation of post-orogenic compressional tectonic activity (IGN, 2025a). This tectonic configuration makes seismic activity in the Gulf of Cádiz significant, with moderately deep earthquakes (h < 40 - 60 km) (Custódio et al., 2016). Some moderate magnitude earthquakes have also been recorded (Martín-Dávila and Pazos, 2003). Most of the focal mechanisms in this area are reverse and rifting type. There is also historical and instrumental evidence of several high-magnitude earthquakes in the region. These include the earthquakes of 1755 (M_w 7.7 - 8.5; Chester, 2001; Fonseca, 2020; Mendes-Victor et al., 2009) and 1969 (M_w 7.8; López Arroyo and Udías, 1972), both causing tsunamis that affected the coasts of Morocco, Portugal, and Spain. The Gorringe Bank, the Sao Vicente submarine canyon (Sao Vicente fault), Horseshoe, Marqués de Pombal, and the Southwest Iberian Margin (SWIM) faults show the greatest magnitudes in the region (M_w 7.2 – 8.4; Grevemeyer et al., 2017; Martínez-Loriente et al., 2013) surrounded by the Gorringe Ridge, the Coral Patch, the Horseshoe and Seine abyssal plains.

The Alboran Sea is the westernmost part of the Mediterranean Sea and the oriental sector of IMR. It is bordered by the Alpine Mountain ranges of the Betic in the Iberian Peninsula and the Rif in the north of Africa. It is a contact zone between the converging Eurasia and Nubia tectonic plates. Among the tectonic structures, the submarine mountain ranges stand out, with a length of more than 50 km, oriented NE-SW and limited to the north and south by reverse faults with opposite dip. Several sets of conjugate directional faults are also found in this area: the NNE-SSW sinistral faults, such as the Al-Idrisi; the NE-SW sinistral faults, such as the Carboneras; and NW-ESE dextral faults, such as the Yusuf. Most of the seismic events recorded in the Alboran Sea have lower magnitudes ($M_w < 4$; IGN, 2025b). The seismic activity in the Alboran Sea is interconnected with the southern Iberian Peninsula through the tectonic system running E-W from the Rif and Alboran Ridge, Eastern Alboran Basin, to the Arzew faults and Tell Atlas (e.g., Mourabit et al., 2014; Leprêtre et al., 2018). Some relevant events in the Alboran Sea are the Adra earthquake in 1910 (M_w 6.1; Stich et al., 2003), and the Al Hoceima earthquakes of 1994 (M_w 6.0), 2004 (M_w 6.3) and 2016 (M_w 6.4) (Kariche et al., 2018).

The majority of Most recorded earthquakes in the IMR are between 0 and 30 km, although a considerable number of earthquakes are of intermediate depth ($30 \leq h \leq 180$ km), mostly located in the Gulf of Cádiz (IGN, 2025c). Deeper earthquakes ($h \geq 600$ km) are less frequent and located in the province of Granada (Buforn and Udías, 2007). About 90% of the registered seismicity in the IMR is located in the Gorringe Bank, High Atlas and the Granada-Malaga-W of Alboran Sea area. In the Alboran Sea, there is also significant shallow seismicity at depths of less than 30 km, especially in the active Betico-Alboran-Rif shear zone; to the W, earthquakes go deeper.

3. Materials

For seismic hazard estimation on the seabed, using the DSHA and PSHA methods, the following input parameters are required: a) a digital terrain model (DTM); ab) seismogenic sources and their associated seismic parameters; and c) GMPEs.

3.1 Ocean and land digital terrain models

The DTM used in this study was obtained from the EMODnet Bathymetry World Base Layer (EBWBL), composed of the bathymetric grid for Europe from the European Marine Observation and Data Network (EMODnet; https://emodnet.ec.europa.eu/en/bathymetry) (Martín Míguez et al., 2019), with spatial resolution of 4 arc seconds, and the raster for oceans and land from the General Bathymetric Chart of the Oceans (GEBCO; https://www.gebco.net/) (GEBCO Bathymetric Compilation Group 2024, 2024; Mayer et al., 2018), with a spatial resolution of 15 arc seconds.

3.2 Seismogenic source models and seismicity parameters

Considering the SHAs carried out in the emerged IMR zone, several seismogenic source models have been identified (Table 2). The one implemented in the ESHM20 (Danciu et al., 2021a, 2024) has been used for this work given it is the latest update. This zonation includes areal seismogenic sources (shallow and deep), active faults and background smoothed seismicity (Fig. 2). To achieve our SHA, all seismic sources influencing our study area were incorporated, together with their corresponding characteristic seismic parameters.

Table 2: Some seismogenic zonation models covering the study area.

Zonation model	Covered extension	Reference	Implementation
SA and SB	Portugal	Vilanova and Fonseca (2007)	Seismic hazard map of Portugal
ZESIS or COMMISSION	Iberian Peninsula	García Mayordomo (2015)	Seismic hazard map of Spain
NAF	North Africa	Poggi et al. (2020)	Seismic hazard map of North Africa
SHARE- ESHM13	Euro-Mediterranean region	Wössner et al. (2015)	Seismic hazard map for Europe
ESHM20	Euro-Mediterranean region	Danciu et al. (2024)	Seismic hazard map for Europe

The seismic parameters used for the DSHA (Fig. 2), were extracted from the ESHM20 model (Danciu et al., 2021a, b). The maximum magnitude $<MM_{max}>$ from the maximum magnitude distribution function, was adopted as the maximum credible earthquake (MCE) along with the predominant rupture mechanism assigned to each planar source ID at its depth (Tables S1 and S2 in supplementary material). The areal seismogenic sources are located at depths ranging from 12 to 60 km (Fig. 2 A1). Seismic features derived from Active Shallow Crustal Region (ASCR) seismogenic sources have magnitudes ranging from 6.6 to 8.8 (Fig. 2 A3). The predominant rupture mechanism is inverse in the band from the Gulf of Cádiz towards the Algerian Mediterranean coast, through the southern Rif and parallel to the Atlas chain (Fig. 2 A2, B2 and C2). This rupture mechanism transitions into strike-slip toward the Alboran Sea and the adjacent Iberian coastal zone, while evolving into normal faulting further inland within the Iberian Peninsula. The deep source beneath the Strait of Gibraltar (~150 km) was initially discarded in line with the original DSHA approach, since it is outperformed by shallower ASCR sources. However, this work includes the distribution of all seismic sources~~ even if their attenuation make them negligible at any given point~~. The active faults are located at depths ranging from 6 to 25 km (Fig. 2 B1) and magnitudes ranging from 6.9 to 8.5 (Fig. 2 B3). For the background smoothed seismicity, point sources have depths ranging from 12 to 60 km (Fig. 2 C1) and magnitudes ranging from 6.5 to 8.6 (Fig. 2 C3). For the PSHA, the same dataset used in the ESHM20 model has been used Danciu et al. (2021b, c). These files include all the seismogenic sources and their characteristic parameters, required to carry out the probabilistic calculation in our study area. Since we adopted the same calculation software (OQ Engine) used in the ESHM20 model for the seismic hazard calculation, it was not necessary to modify the seismogenic source files.

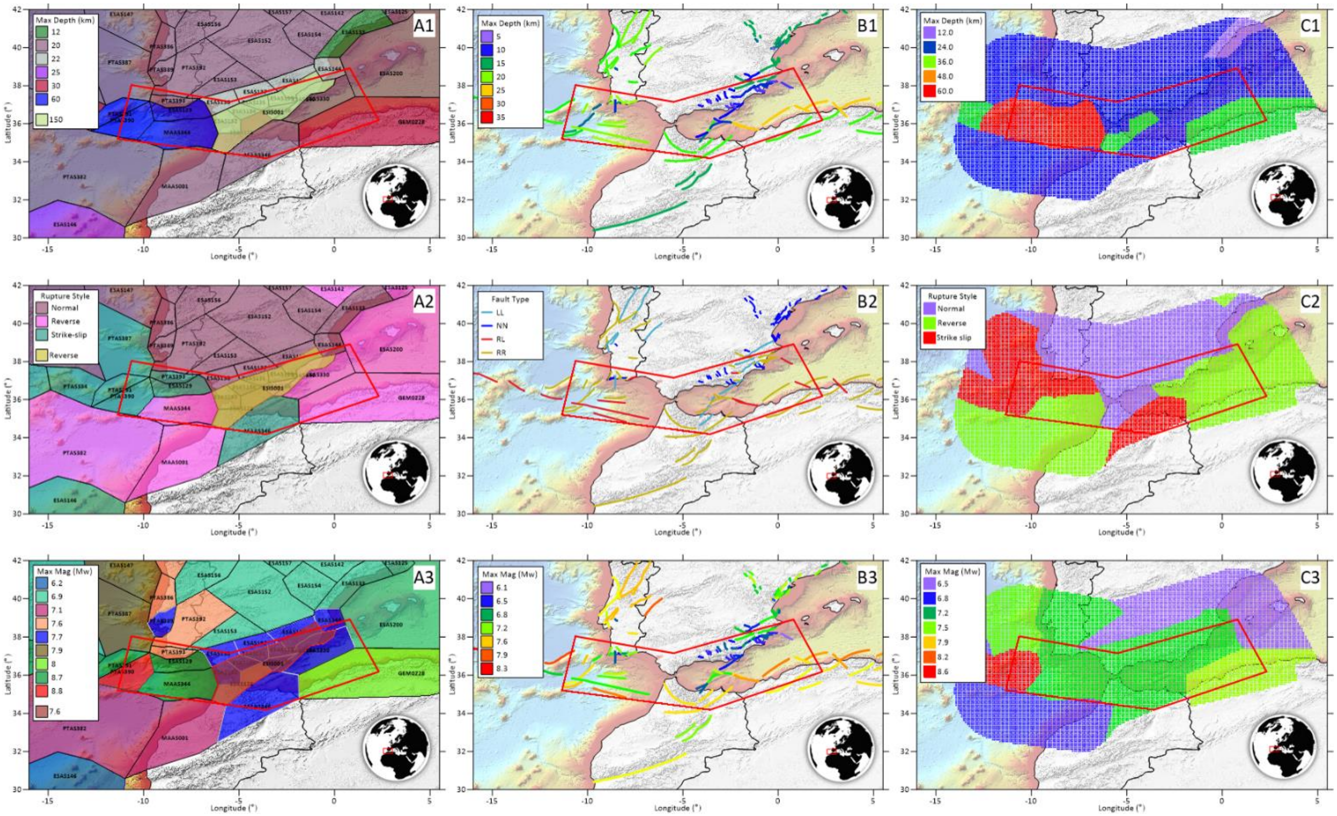

Figure 2. Seismogenic source models of ESHM20: (A~~a~~) areal seismogenic sources (shallow and deep); (B~~b~~) active faults and (C~~c~~) smoothed seismicity; in function of (1) Depth (km), (2) Predominant rupture mechanism for each seismogenic source, and (3) Magnitude of maximum credible earthquake (MCE). (Data from Basili et al., 2024; Danciu et al., 2021b, 2024).

3.3 Ground motion prediction equations (GMPEs)

GMPEs are essential in seismic hazard analysis, as they model how ground motion attenuates with distance. These equations estimate shaking intensity at a site based on factors like earthquake magnitude, distance to the source, faulting style, and local geological conditions (Barani et al., 2016). GMPEs are commonly derived from strong ground-motion records for an earthquake (e.g., Campbell and Bozorgnia, 2003). Functions relate the magnitude M and the distance R of the seismic scenario (M, R). With an appropriate set of quality records, it is possible to fit a parametric model $f(M,R,\phi_k)$ to estimate the intensity of strong motion (Y) for a given seismic scenario. The fitted parameters reflect the characteristics of elastic and anelastic energy attenuation through distance scaling, but also near and far-source, faulting mechanism, and hanging wall effects. The heterogeneous geological media causes a dispersion in the (M, R) sample pairs. Therefore, the correlation between variables can be strong, but never perfect, meaning there is an unavoidable uncertainty ε. If the expected seismic intensity at the project site Y is interpreted as a conditional random variable on the pair (M, R), the fitted model (Atik et al., 2010):

$$Y \sim f(M,R,\phi_k) + \varepsilon \qquad (1)$$

provide an estimate of the median ground motion and the residual ε (Akkar et al., 2013) identified by a Gaussian distributed random variable.

~~Most~~ GMPEs are commonly defined in terms of relative fault distance to the SHA site assuming a planar rupture geometry. The rupture trace is defined as the projection of the upper edge of the rupture onto the ground surface. The rupture plane, trace, and surface projection allow the definition of four finite fault distance metrics: R_{RUP}, R_{JB}, R_X, R_Y, Z_{TOR} (Fig. 3). R_{RUP} is the closest distance between the site and the rupture surface. R_{JB} is the Joyner and Boore distance or the closest distance between the site and the surface projection of the rupture. R_X is the horizontal and R_Y the vertical distance between the site and the top edge of the rupture. Finally, Z_{TOR} is the depth to the top edge of the rupture. These metrics are usually~~commonly~~ incorporated in GMPEs, as R in in the mathematical formulation of Eq. (1) (e.g., Douglas, 2020). Some of the GMPEs formulation Eq. (1) consider the distance R as a function of depth (e.g., R_{RUP}). In these cases, the estimation of the intensity of the motion is affected by the terrain relief where the site is located. Thus, the estimated shake motion Y in elevated areas will be lower than in marine abyssal plains because they are closer to seismogenic sources, and the results of Y estimation in regions with significant unevenness will be sensitive to the use of a DTM.

The wealth of available strong ground motion data has enabled the development of numerous GMPEs, the vast majority on the rocky ground inland (e.g., Douglas, 2020). However, in offshore regions, traditional rock-based models may not adequately capture the unique conditions of the sea floor (Chen et al., 2024; Tan and Hu, 2023; Wang et al., 2024). The growing importance of subsea structures and the associated risks of seabed instability have prompted the development of efforts to obtain GMPEs for offshore areas. Nevertheless, the limited availability of data and the scarcity of strong motion records have restricted their collection to very few offshore areas. A significant proportion of recent research has focused on the active area of the Japan Trench using the S-net and KiK-net stations data (Kanazawa et al., 2016), where several GMPEs have been recently developed (e.g., Dhakal et al., 2024; Hu et al., 2020, 2023; Nakanishi and Takemura, 2024).

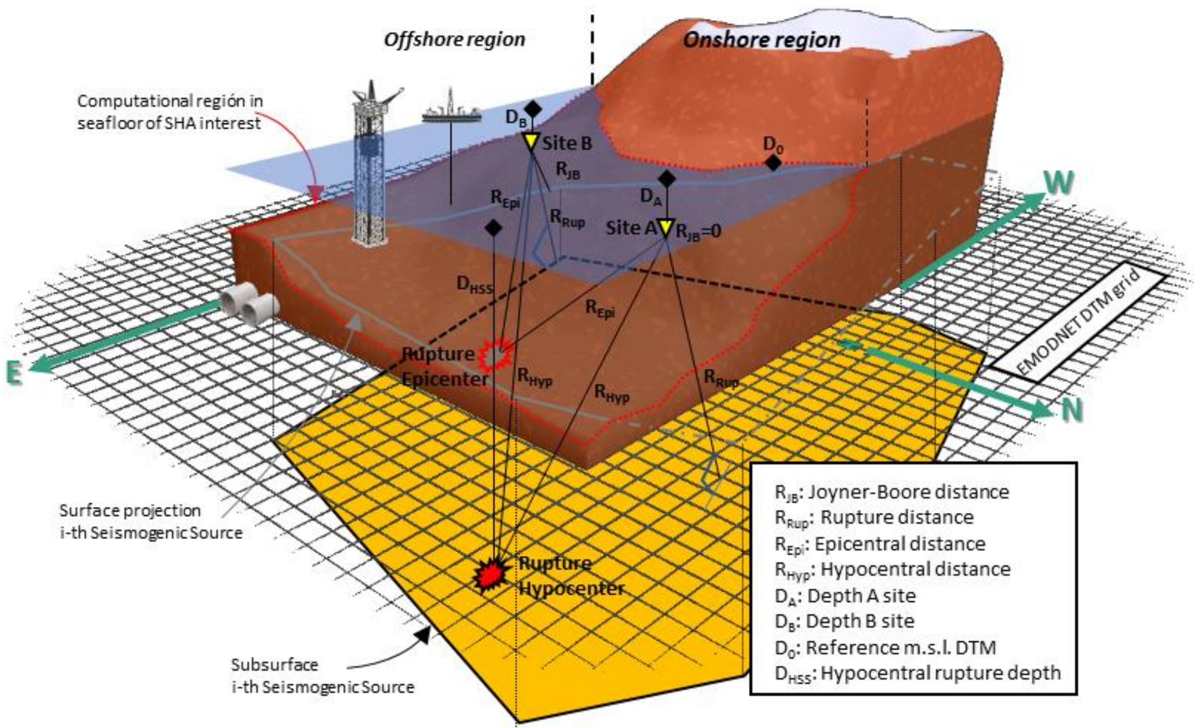
Offshore region
Onshore region
Computational región in seafloor of SHA interest
Site B
Site A
D_B
D_0
D_A
R_{JB}
R_{Epi}
R_{Rup}
$R_{JB}=0$
D_{HSS}
R_{Hyp}
Rupture Epicenter
Rupture Hypocenter
W
E
N
EMODNET DTM grid
Surface projection i-th Seismogenic Source
Subsurface i-th Seismogenic Source
R_{JB}: Joyner-Boore distance
R_{Rup}: Rupture distance
R_{Epi}: Epicentral distance
R_{Hyp}: Hypocentral distance
D_A: Depth A site
D_B: Depth B site
D_0: Reference m.s.l. DTM
D_{HSS}: Hypocentral rupture depth

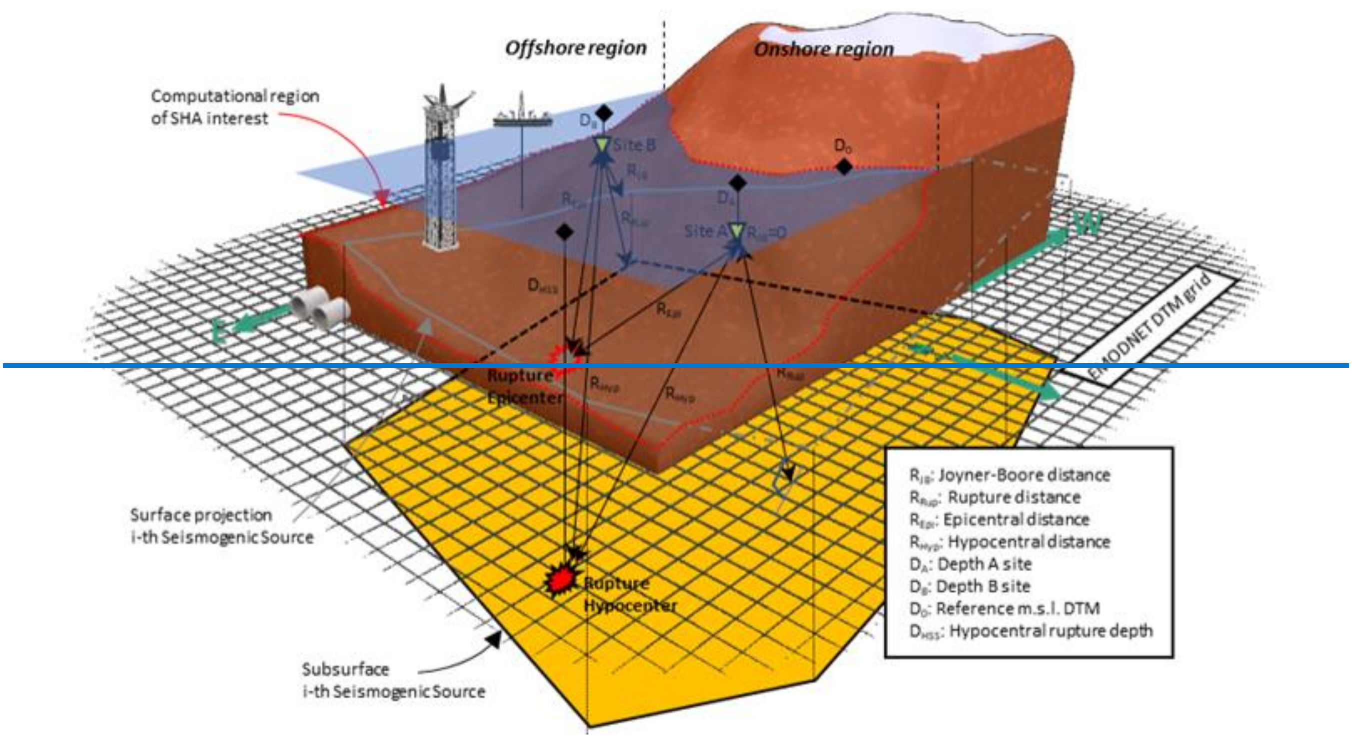
Offshore region
Onshore region
Computational region of SHA interest
Site B
Site A
Rupture Epicenter
Rupture Hypocenter
EMODNET DTM grid
Surface projection i-th Seismogenic Source
Subsurface i-th Seismogenic Source
R_{JB}: Joyner-Boore distance
R_{Rup}: Rupture distance
R_{Epi}: Epicentral distance
R_{Hyp}: Hypocentral distance
D_A: Depth A site
D_B: Depth B site
D_0: Reference m.s.l. DTM
D_{HSS}: Hypocentral rupture depth

Figure 3. Earthquake source and distance metrics from an offshore evaluation site in and out a seismogenic source area. Site A outside the ground projection of the seismogenic source, with (H≠0) and without surface altimetry or bathymetry (H=0). Site B inside the ground projection of the seismogenic source, without surface altimetry or bathymetry (H=0).

For soft soils, a GMPE model was already described by Idriss (1991) in the early 1990s (IDR91). The IDR91 model is suggested for the entire moment magnitude range and a distance of 0-100 km or more. The Joyner-Boore metric is used as the source-to-site distance (R_{JB}) to obtain Ln (Y), where Y is in g, and the uncertainty (ε) in Ln (Y) depends on the earthquake magnitude in the function described by Idriss (1991) if $M_w < 7.25$, otherwise the standard error term is constant ($\varepsilon = 0.38$). This model is suited for crustal earthquakes and it has been implemented in SHA for submarine zones in the Mediterranean Sea (e.g., D'Acremont et al., 2022; Lafuerza et al., 2012; Sultan et al., 2007). Therefore, IDR91 was also considered in this work to compare it with other recent approaches to offshore GMPEs. Recently, the HZ23 model (Hu et al., 2023), has been developed for offshore earthquakes in the Japan Trench area and derived from onshore model ZH06 (Zhao et al., 2006). HZ23 was developed for M_w between 4.0 and 7.1, and hypocentral distances of 20-300 km. This model uses R_{RUP} as distance metric in Eq. (1) for crustal, interface, and slab events to obtain Ln (Y) with a constant standard error ($\varepsilon = 0.7784$), where Y is in cm/s². Additionally, the averaged shear-wave velocity to 30 m depth (Vs30) was incorporated as a parameter in Eq. (1) for the definition of the site class. The NT24 model (Nakanishi and Takemura, 2024), was also developed for the Japan Trench area and derived from the onshore model MF13 (Morikawa and Fujiwara, 2013). It can assess PGAs for M_w between 5.5 and 7.4 for crustal, intraplate, and slab earthquakes ($M_w > 5.0$ for crustal events) and epicenter distances of 1 to 300 km. This model uses R_{RUP} to obtain $\log_{10}$ (Y) with a constant standard error ($\varepsilon = 0.326$). Finally, the DKK24 model (Dhakal et al., 2024) was developed for M_w between 5.5 and 7.4, and hypocentral distances of 1 to 300 km. This model uses R_{RUP} as distance metric in Eq. (1) for crustal, interplate and intraslab events to obtain $\log_{10}$ (Y) with a constant standard error ($\varepsilon = 0.25183$). Therefore, four GMPEs have been used in this work: IDR91, HZ23, NT24, and DKK24 (Fig. 4), considering both the seminal studies on soft soils and recent works proposing new GMPEs for submarine environments. In this study, the PGA (g) is the Y seismic intensity used in all of these selected attenuation functions. A unit weighting was assigned to each GMPE for the SHAs.

The predominantly offshore setting of the study area (at the intersection of oceanic, active continental, and stable continental crust) poses significant challenges for selecting appropriate GMPs. Recent tectonic classifications (Chen et al., 2018; Poggi et al., 2020) describe the study region as a Variscan-Hercynian zone in an Active Shallow Crustal Region (ASCR). In the case of the HZ23, NT24 and DKK24 models and their implementation in our study area, the IMR and the Japan Trench area share some geo-tectonical similarities. In the IMR, the African Plate is subducting beneath the Eurasian Plate (Gutscher et al., 2002), while in the Japan Trench area, the Pacific Plate is subducting beneath the Okhotsk Plate (Nishikawa et al., 2023). Both areas experience significant seismic activity due to the tectonic interactions. The IMR has a history of large earthquakes (Buforn et al., 2015), while the Japan Trench area is known for its frequent and intense earthquakes, including the devastating 2011 Tōhoku earthquake (Ritsema et al., 2012).

~~In addition, t~~The selected ~~performance of the~~ GMPEs were~~as~~ benchmarked~~evaluated~~ against horizontal PGAs ~~observed ground motions~~ fro~~rm~~ six regional offshore earthquakes in the IMR (Fig. 4), including five crustal and one intraslab event, using onshore/near-coastal accelerograms. This benchmark is a statistical plausibility check within~~in~~ overlapping M_w-R ranges,~~.~~ b~~B~~ut it does~~is~~ not constitute a validation nor recalibration of seabed GMPEs in the IMR. The primary evidence supporting seabed GMPEs (HZ23, NT24, DKK24) remains their calibration on ocean-bottom data (S-net/KiK-net) and the documented land-seafloor differences reported in the literature (e.g., Dhakal et al., 2021; Hu et al., 2023; Chen et al., 2015, 2024a). This approach follows previous IMR hazard studies (e.g., Molina Palacios, 1998; Vilanova and Fonseca, 2004; Perea et al., 2023; Olaiz et al., 2025), which also relied on inland proxies due to the absence of seabed recordings. Therefore, this comparison should be interpreted as an acceptability check within the GMPEs magnitude-distance validity ranges, rather than a direct GMPE re-calibration. The scarcity of offshore strong-motion data underscores the need for OBS deployments to enable future seabed-specific GMPE validation in the IMR. The~~A~~ comparative analysis of IDR91, HZ23, NT24, and DKK24 was conducted using the following events:

1) M_w 4.5 Alboran Sea earthquake, 31/01/2016 (Fig. 4A),
2) M_w 4.9 Alboran Sea earthquake, 04/01/1994 (Fig. 4B),
3) M_w 5.5 Oran earthquake, 06/06/2008 (Benfedda et al., 2020) (Fig. 4C),
4) M_w 6.1 SW Cape St. Vincent earthquake, 12/02/2007 (Fig. 4D)
5) M_w 6.3 Alboran Sea strike-slip earthquake, 25/01/2016 (Fig. 4E),
6) M_w 6.8 Boumerdès Earthquakes, 21/05/2003 (Khellafi et al., 2013) (Fig. 4F).

The acceleration data for earthquakes in Fig.4 (A), (B), (D), and (E) are sourced from IGN (https://www.ign.es/web/sis-catalogo-acelerogramas, last accessed 08/07/2025).

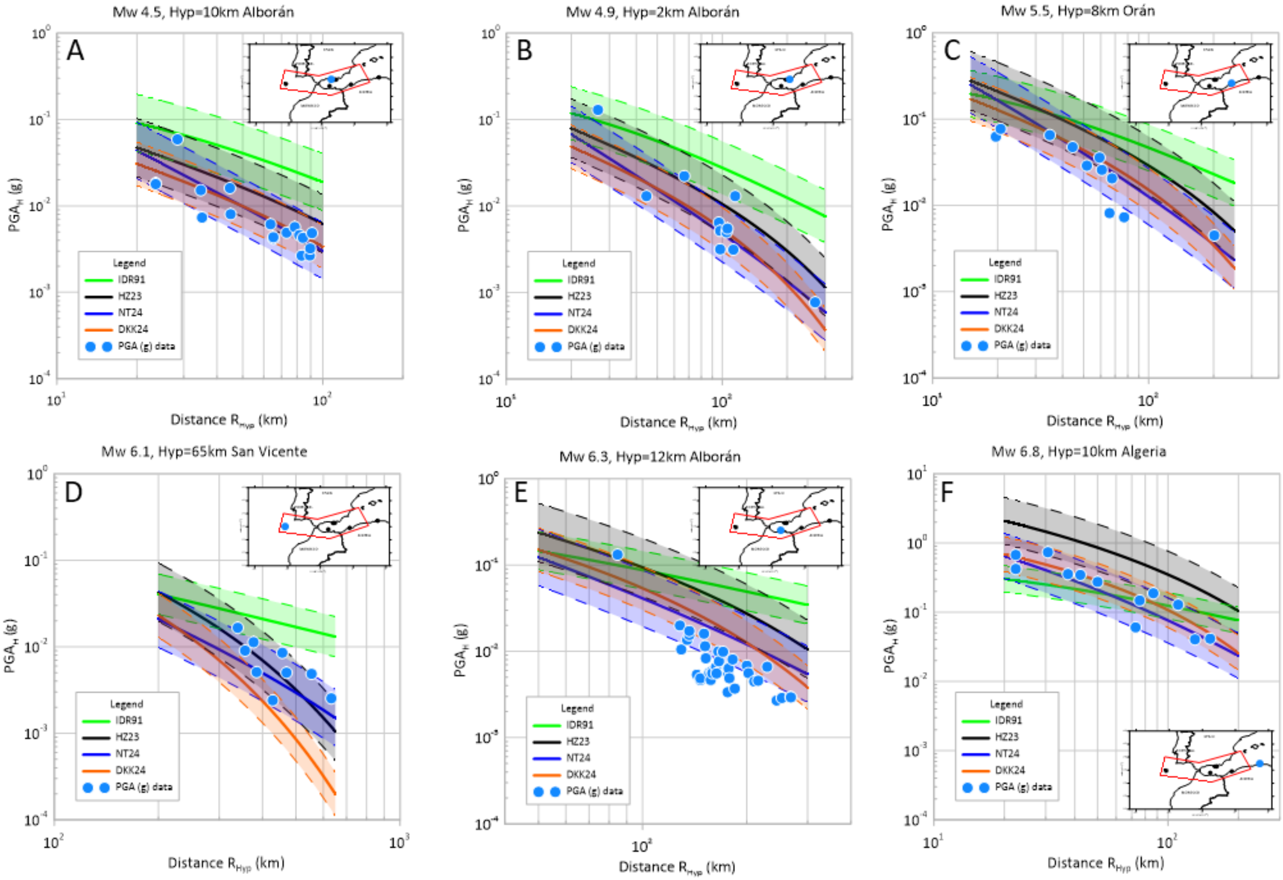
Mw 4.5, Hyp=10km Alborán
A
Mw 4.9, Hyp=2km Alborán
B
Mw 5.5, Hyp=8km Orán
C
Mw 6.1, Hyp=65km San Vicente
D
Mw 6.3, Hyp=12km Alborán
E
Mw 6.8, Hyp=10km Algeria
F
PGA_H (g)
Distance R_Hyp (km)
Legend
IDR91
HZ23
NT24
DKK24
PGA (g) data

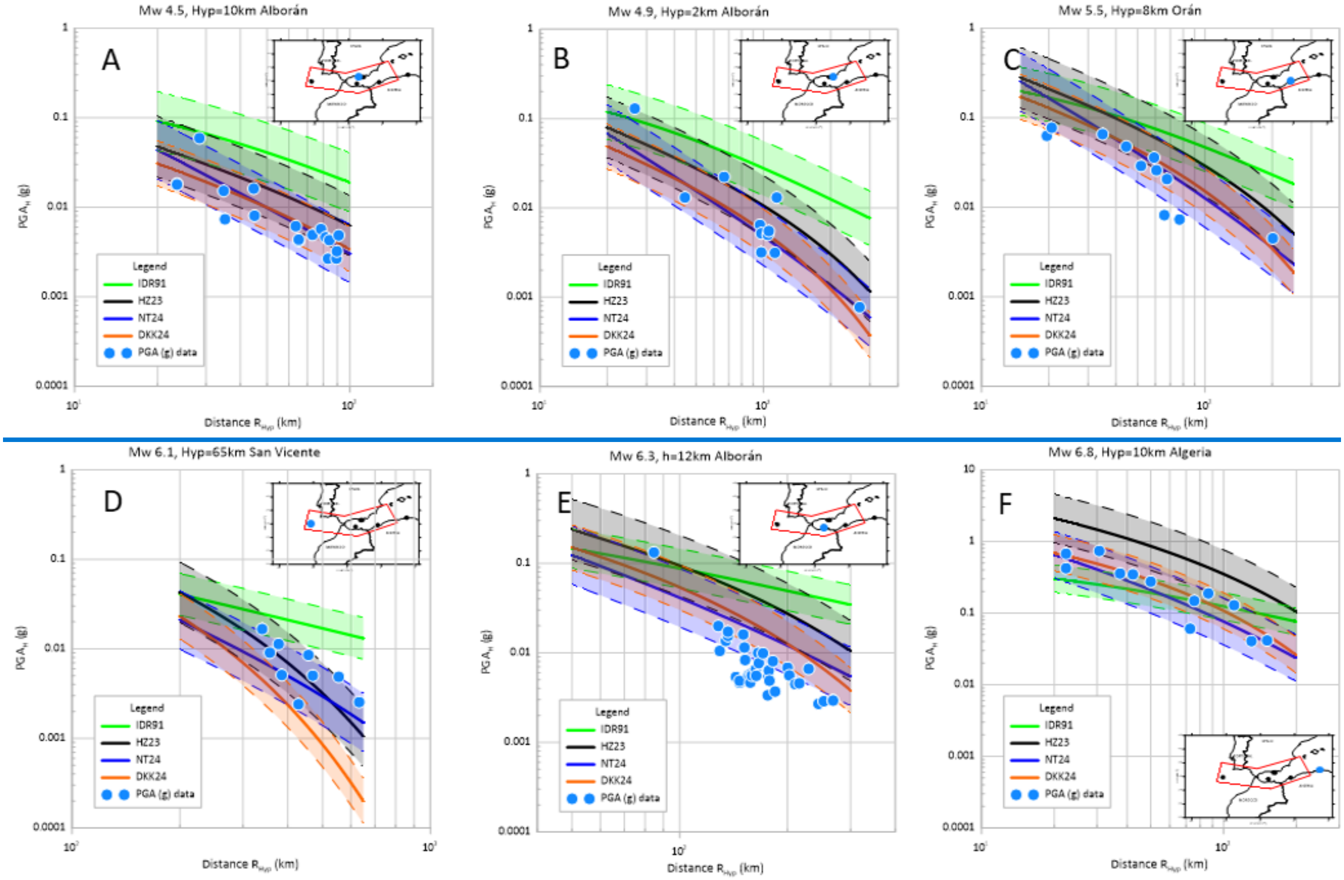

Figure 4. Relationship plots between PGA (g) and hypocentral distances (R_{Hyp}) of the selected GMPEs. Solid lines denote the median prediction curves for each earthquake, whereas the shadowed region between the dashed lines denote one standard deviation range ($\pm s_\varepsilon$).

The predicted PGAs, through the HZ23, NT24 and DKK24 models and their respective standard deviation bands around each curve are consistent with the observed ones from the six tested earthquakes (Fig. 4). Most of the observed PGAs are within $\pm s_\varepsilon$ bands. However, IDR91 behaves as an upper limit boundary of models in the majority of cases and, for M_w 6.3 Alboran Sea earthquake (Fig. 4 E), the observed PGAs are usually lower than the predicted values of the GMPEs for seabed. To evaluate the model's accuracy, residuals were obtained as the difference between the observed PGAs and the estimated PGA from the selected GMPE. As Fig. 5 shows, a near-zero tendency of residual distribution is found, with mean residual values presented in Table S3. Despite the oscillations discernible in the graphs (Fig. 5 A, C), residuals are situated between the curves (dashed lines in the graphs Fig. 5 A, C) that delineate the uncertainty bands ($\pm s_\varepsilon$). The residuals demonstrate bounded variance homoscedasticity, with standard deviations of about 0.077 g, 0.236 g, and 0.047 g for IDR91, HZ23, and NT24, respectively, with the M_w 6.8 earthquake exception. All four GMPEs benchmarked against nearby observed ground motions~~.~~ ~~evaluated~~

demonstrate adequate goodness of fit.~~;~~ H~~h~~owever, NT24 and values that exceed the observed ones, with the exception of the closest recorded PGAs. The GMPE that exhibits a reduced capacity to capture this variability is HZ23 (see Fig. 5 C, D), with the highest RMSE (Table S3) relative to the others, but predicting a higher seismic intensity, according to the observed residuals, primarily for the largest earthquake (M_w 6.8). Its prediction is, in this instance, limited by the lower boundary curve of the uncertainty band of one σ_ε.

The final step in the diagnosis undertaken here evaluates the properties of the prediction errors in the logarithms of the PGA (Fig. S1), as defined in Eq. (1). The averages of the epsilon values should be zero, where NT24 and DKK24 best fit the theoretical value (Fig. 6A). Their standard deviations are either below or very close to the values that the authors of the GMPEs provide for their models. Furthermore, it cannot be discarded that residuals in the logPGA have a normal distribution, as shown by the histogram for and the Q-Q plot (Fig. 6B, C) and indicated by the p-value for the Kolmogorov-Smirnov and the Saphiro-Wilk tests in NT24 (bold p-values in Table 3) at 95 % confidence.

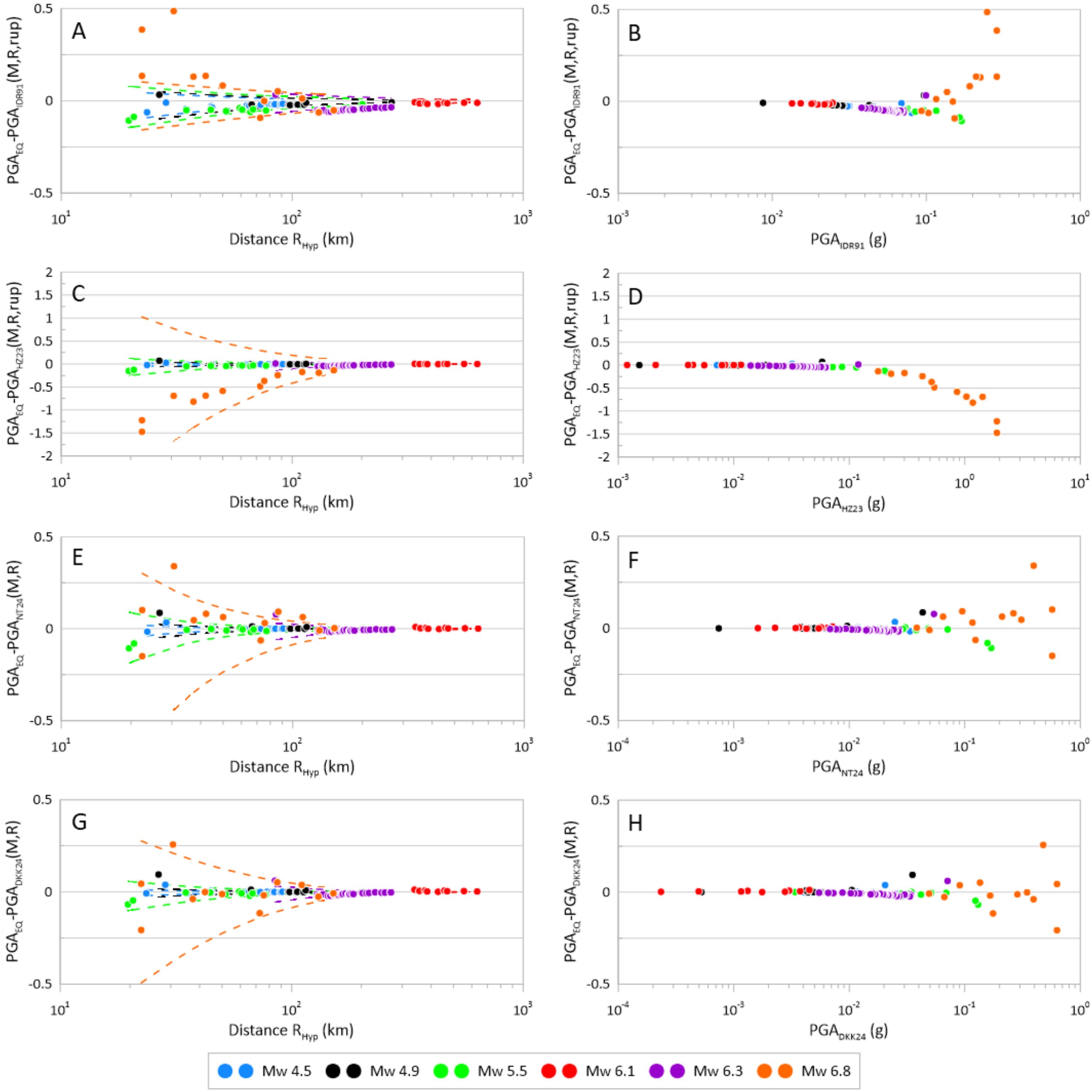
A
B
C
D
E
F
G
H
PGA_{EQ}-PGA_{IDR91}(M,R,rup)
PGA_{EQ}-PGA_{HZ23}(M,R,rup)
PGA_{EQ}-PGA_{NT24}(M,R)
PGA_{EQ}-PGA_{DKK24}(M,R)
Distance R_{Hyp} (km)
PGA_{IDR91} (g)
PGA_{HZ23} (g)
PGA_{NT24} (g)
PGA_{DKK24} (g)
Mw 4.5
Mw 4.9
Mw 5.5
Mw 6.1
Mw 6.3
Mw 6.8

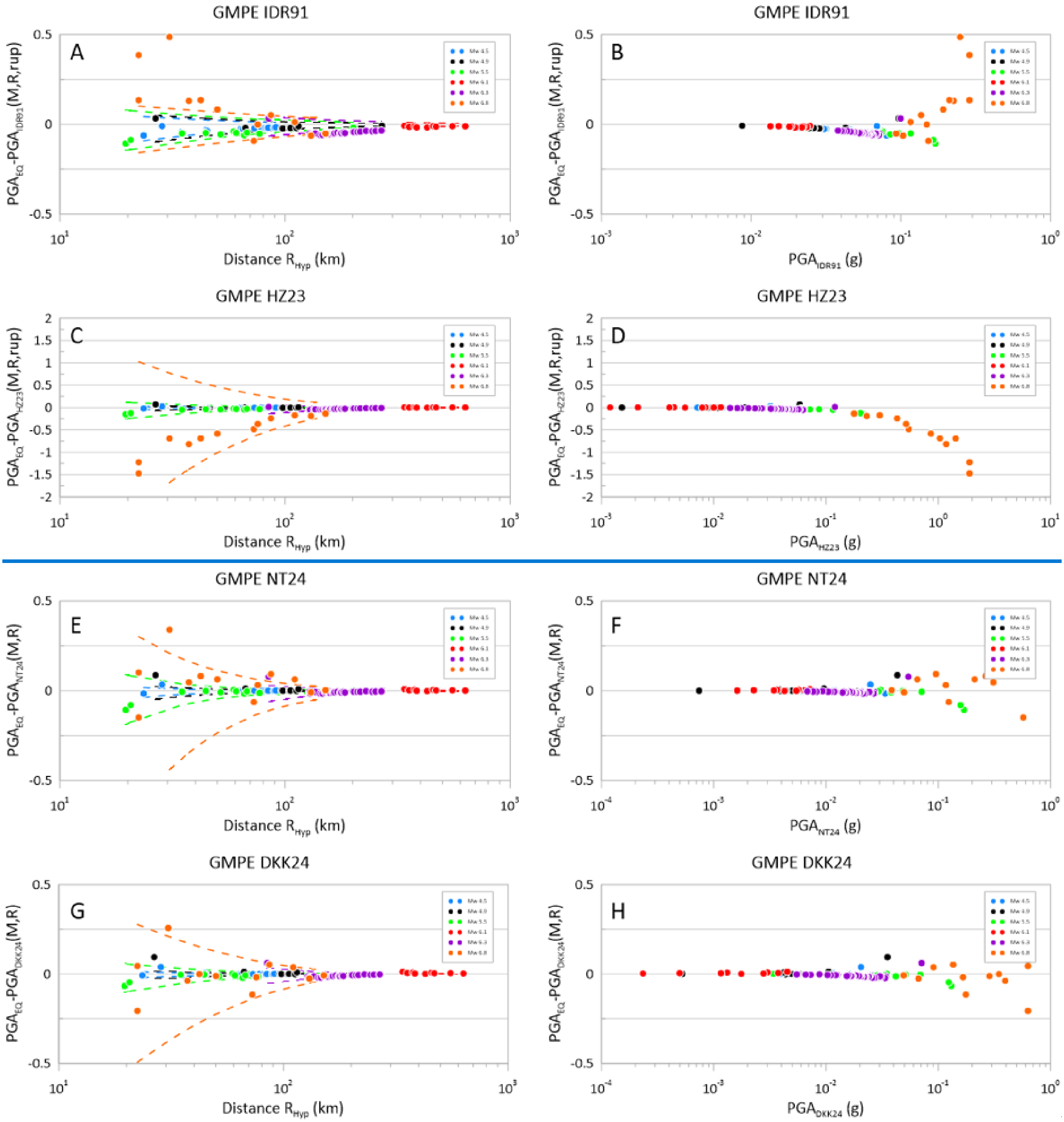

Figure 5. Residual plots of the goodness of fit for the predicted values by the selected GMPEs: IDR91, HZ23, NT24, and DKK24, against the registered data in the earthquakes used for diagnosis.

NT24 and values that exceed the observed ones, with the exception of the closest recorded PGAs. The GMPE that exhibits a reduced capacity to capture this variability is HZ23 (see Fig. 5 C, D), with the highest RMSE (Table 3) relative to the others, but predicting a higher seismic intensity, according to the observed residuals, primarily for the largest earthquake (M_w 6.8). Its prediction is, in this instance, limited by the lower boundary curve of the uncertainty band of one σ_ε.

Table 3: Diagnosis of selected GMPEs.

GMPE	RES_{PGA} = Residuals of PGAs PGA_{EQ}-PGA_{GMPE}(M,R,rup)		$\varepsilon = RES_{LogPGA}$ = Residuals of log PGAs Log(PGA_{EQ}-)-Log(PGA_{GMPE}(M,R,rup))		Standardised (RES_{LogPGA}) p-values – 95% confidence	
	Average	RMSE	Average ε	Std ε	Saphiro-Wilk	K-S
IDR91	-0.020	0.077	-1.4702	0.9012	0.00004	**0.09164**
HZ23	-0.090	0.236	-1.0494	0.7663 (0.723)	0.01057	**0.5848**
NT24	0.002	0.047	-0.1310	0.2855 (0.7784)	**0.21763**	**0.8160**
DKK24	-0.0043	0.040	-0.1267	0.3630 (0.377556)	0.000796	**0.2919**

The final step in the diagnosis undertaken here evaluates the properties of the prediction errors in the logarithms of the PGA (Fig. S1), as defined in Eq. (1). The averages of the epsilon values should be zero, where NT24 and DKK24 best fit the theoretical value (Fig. 6A). Their standard deviations are either below or very close to the values that the authors of the GMPEs provide for their models. Furthermore, it cannot be discarded that residuals in the logPGA have a normal distribution, as shown by the histogram for and the Q-Q plot (Fig. 6B, C) and indicated by the p-value for the Kolmogorov-Smirnov and the Saphiro-Wilk tests in NT24 (bold p-values in Table 3) at 95 % confidence.

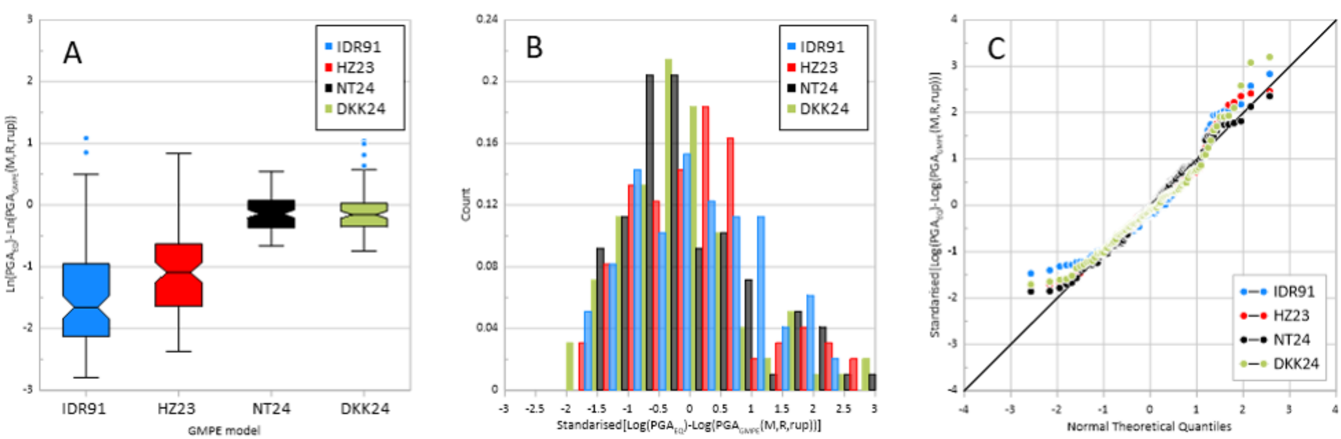

Figure 6. Diagnosis of the residuals in logarithms of PGA. A) Box-Whisker plot of residuals for each GMPE model used here. B) Stacked histogram in relative frequencies for the residuals in logarithms of PGA. C) Q-Q plot of the standardised residuals in logarithms of PGA.

4. Seismic hazard assessment

Seismic hazard refers to the probability of exceeding a certain earthquake intensity in a specific area within a given time period (Kijko, 2019; McGuire, 2004). Seismic hazard can be assessed using two main methods: Deterministic Seismic Hazard Analysis (DSHA) and Probabilistic Seismic Hazard Analysis (PSHA). In DSHA, hazard is defined as a specific percentile (such as the 50th, 84th, or 98th, as used in this study) of ground shaking intensity measured as peak ground acceleration (PGA) caused by one or several earthquakes. This method uses basic earthquake data and ground motion models based on a chosen earthquake scenario (Krinitzsky, 1995, 2002). Despite their deterministic character, the results obtained have frequently been used as a proxy for the upper limit of seismic intensity. Seismic hazard in PSHA is determined by calculating ground motion frequencies or exceedance rates using a mathematical model based on earthquake statistics and ground motion functions (McGuire, 2004, 2008). This model takes into account uncertainties related to earthquake size and moment (Kramer, 1996). PSHA methods can be categorized into parametric, using the total probability theorem (Cornell, 1968; Kramer, 1996), and nonparametric methods that utilize extreme value distribution functions (Epstein and Lomnitz, 1966). Other approaches, such as NDSHA, are often discussed together with DSHA and PSHA in relation to their representativeness for the largest events. Although both SHA methods use seismological and geological information, they define and calculate seismic hazard differently, which improves the understanding of seismic hazard forecasting at the studied site or region (Orozova and Suhadolc, 1999; Wang and Cobb, 2012).

4.1 Deterministic Seismic Hazard Assessment (DSHA)

In DSHA, the capable controlling source at a site is identified, ~~(~~typically a mapped fault segment and, where faults are diffuse, an areal/background sources~~) identified~~. The maximum credible earthquake (MCE) for that source and an appropriate GMPE are then used to compute a chosen percentile (e.g., 50th or 84th) of ground motion at the shortest source-to-site distance under the adopted distance metric (Reiter, 1990;~~ Kramer, 1996;~~ Krinitzsky,~~ 1995,~~ 2002)~~The main input parameters in the classic DSHA (Reiter, 1990) are the maximum magnitude associated with the characteristic earthquake as the MCE for each seismic source area and a set of attenuation relationship or GMPEs~~. DSHA does not explicitly incorporate probability and recurrence functions, the seismic hazard is obtained as a certain percentile of ground motion. The 50th percentile is mostly used in preliminary DSHA studies, as well as the 84th percentile when it is used for inland critical structures such as nuclear or hydraulic power plants. Thus, some DSHA use the second quartile PGA plus a standard deviation, which is equivalent to an exceedance probability of 16% (Ben-Zion et al., 2003), calculated from simple earthquake and ground motion statistics (Krinitzsky, 1995, 2002). To perform these calculations, this study adopts a DSHA approach, following the standard algorithmic workflow as used in Wang et al. (2012), Vipin (2013), Candia et al. (2019), and Ramkrishnan et al., (2021) which implement the classical deterministic hazard assessment procedure (Reiter, 1990). Deterministic ground motions are computed for areal seismic sources in regions lacking well-defined fault geometries. This method has precedent in offshore hazard studies and is particularly suitable for submarine environments where seismicity is diffuse and fault structures are unresolved. Similar approaches have been discussed (i.e., Krinitzsky, 2002, Kramer, 1996, Campbell, 2005) and are widely used in engineering applications where deterministic estimates are required for preliminarily infrastructure design. this work follows a series of steps as the classic DSHA scheme (Kramer, 1996; Krinitzsky, 1995; Reiter, 1990) that allow the deterministic derivation of the seismic hazard with a zone-based method:

OperationallyComputationally, the DSHA is implemented through the following steps:

(i) Build a catalogue of seismogenic sources (faults and, where needed, areal/background zones) $\{SS_j\}_{j=1 \ldots Nf}$.

(ii) Assign the seismic potential to each source SS_j with its MCE_j and the prevailing focal mechanism (normal, reverse or strike-slip).

(iii) Select the set $\{f^i\}$ of the empirical GMPEs or attenuation relationships $Y^i=f^i(M,R,\phi^i_k,\sigma^i_Y)$, with their corresponding parameters ϕ^i_k and the random uncertainties σ^i_Y for each i-th prediction equation.

(iv) Arbitrarily select the desired probability of exceedance $PR_{exed}=Pr[Y>=y_{max}/M,R]$, for a seismic scenario given by the (M,R) pair.

(v) Calculate the p-th percentile equivalent to the probability of exceedance:

$$PC_{Pr}= Pr[Y<y_p/M,R]=1- Pr[Y>=y_p/M,R] \quad (2)$$

(vi) Calculate the standard normal random variable Z_{01}, of mean 0 and variance 1, that matches the percentile PC_{Pr}.

(vii) Loop for each site P located at the geographic coordinate position (x,y,h) with latitude, longitude and hypsometry (height or depth above mean sea level) do,

(viii.a) Loop for each j-th seismic source SS_j ($j=1, \ldots N_F$), assuming that the worst-case scenario (M,R, focal mechanism) is selected, defined as the occurrence of an earthquake of magnitude M=MCEj from a point of the j-th seismogenic source at the shortest possible distance $R = R_{min} = \min\{d(P,SSj)\}$, based on the distance to be handled (R_{JB}, R_{ep}, R_{hip}, etc.) in the attenuation function (Fig. 3).

(viii.a.1) Calculate the median ground motion (50th percentile or GMPE treated as deterministic) of the seismic parameter $Y^i_{50,j}$ at the site, with each i-th GMPE: $Y^i_{50,j} = f^i(M,R,\phi^i_k)$.

(viii.a.2) Calculate the p-th percentile of the seismic parameter at the site with the i-th equation of motion:

$$\log Y^i_{p,j} = \log Y^i_{50,j} + Z_{01}\, \sigma^i_Y \quad (3)$$

(viii.a.3) Obtain the on-site seismic ground shaking parameter $Y_{p,j}$ on site P produced by each j-th earthquake source.

(viii.b) Deterministic evaluation of the th-percentile of the seismic hazard $Y_p(x,y,h)$ at the site located at (x,y,h) as the largest parameter of the intensity of ground shake obtained from each seismogenic source: $Y_p(x,y,h) = \max\{Y_{p,j}\}$

(ix) Write $Y_p(x,y,h)$ output to change to a new location of the P site to assess.

However, since in each GMPE the logY value is distributed as a normal random variable of mean logY with standard deviation σ (Kramer, 1996), and $Y_p(x,y,h) = \max\{Y_{p,j}\}$, both Y_p and $Y_{p,j}$ are random variables. The p-th percentile Y_p is accurately calculated as follows:

$$\Pr\left[Y_p <= \frac{y_p}{M,R}\right] = F\left(\frac{\log Y_p - \log y_{max/M,R}}{\sigma}\right) = \frac{p}{100} \tag{4}$$

in accordance with the classical scheme, with a single dominant seismic source, and where F denotes the cumulative density function of the standard normal distribution (e.g., mean μ = 0, and variance = 1). Now, considering the distribution of $Y_{p,NS}$ as the extreme value of a set of values (Ang and Tang, 2007; Coles, 2001), the above approximation is computed as:

$$\Pr\left[Y_{p,NS} <= \frac{y_p}{M,R}\right] = \Pr\left[Y_1 <= \frac{y_p}{M,R}\right] \text{ x } \Pr\left[Y_2 <= \frac{y_p}{M,R}\right] \text{x} \ldots \text{x } \Pr\left[Y_{NS} \leq \frac{y_p}{M,R}\right] = \frac{p}{100} \tag{5}$$

This implies incorporation of the effect of the remaining NS seismic sources in the hazard percentile estimation in the hazard assessment. The estimation is more complicated than in the case of a single source, as it is now necessary to solve the nonlinear equation:

$$\prod_{j=1}^{NS} F\left(\frac{\log Y_{p,NS} - \log y_{j/M,R}}{\sigma}\right) = \frac{p}{100} \tag{6}$$

As this paper uses an approach based on a logic tree scheme that weights the GMPEs to capture the epistemic uncertainties in the hazard estimation, the above equation is rewritten to solve for each i-th GMPE $f^i(M,R,\phi^i_k)$ used and its corresponding i-th random uncertainty σ^i:

$$\varphi^i\left(\log Y^i_{p,NS}\right) = \prod_{j=1}^{NS} F\left(\frac{\log Y^i_{p,NS} - \log y_{j/M,R}}{\sigma^i}\right) - \frac{p}{100} = 0 \tag{7}$$

from which each $Y^i_{p,NS}$ is obtained.

4.2 Probabilistic Seismic Hazard Assessment (PSHA)

The principles of PSHA find their roots in the work of Cornell (1968), and Cornell et al. (1971), andprogrammed in FORTRAN by McGuire (1976) at the USGS. To this end, Cornell uses the total probability theorem (Kramer, 1996) to consolidate information on various variables (magnitude, distance, source location) into a single measure of seismic hazard for a specific site. Once probability relationships are derived from the observed seismicity (locations, sizes, recurrence) in the area, exceedance probabilities of ground motion can be quantified (Kijko, 2019). It takes into consideration the seismicity of the area from the distribution of locations, sizes, recurrence times and energy attenuation (Benito and Jiménez, 1999), to integrate the probabilities of exceeding a certain level of ground motion from various seismic sources, at different distances and with different magnitudes, that may occur at a site.~~proposes a probabilistic method whereby, having established the probability relationships that govern seismic events in a seismogenic area (point, fault plane, or spatial region) regarding the distribution of locations, sizes, and recurrence times, and knowing the past seismicity of the area (Benito and Jiménez, 1999), it is possible to quantify the probability of exceeding a specific level of ground motion at least once in that area over a specific exposure time (Kijko, 2019) using the total probability theorem (Kramer, 1996).~~

The ~~technique~~ basis for carrying out PSHA is described in several steps (Kramer, 1996; McGuire, 2004; Reiter, 1990):

(i) identification and characterization of seismic sources;

(ii) determination of the recurrence distribution of each source, in time or magnitude;

(iii) establishing the response parameter based on magnitude, distance, and site conditions with its uncertainty; and

(iv) calculating the probability that the response parameter is exceeded over a time period and estimating the hazard at the studied site, resulting from the sum of the hazard probabilities of all seismic sources influencing it.

This method allows for obtaining the mean annual exceedance rate ($\lambda_{IM>x}$) for a given site and exposure time, defined as the probability that a specified level x of intensity measure (IM) of ground motion is exceeded at this site (McGuire, 2004):

$$\lambda_{IM>x} = \sum_{i=1}^{N_s} v_i \int_{r=0}^{\infty} \int_{m=M_{min}}^{M_{max}i} P[IM > x|m, r] f_{Mi}(m) f_{Ri}(r)\, dm\, dr \qquad (8)$$

Where:

- $\lambda_{IM>x}$ is the annual exceedance rate of a soft soil movement intensity IM that exceeds a threshold value x.
- $P[IM > x|m, r]$ is the probability that IM exceeds x given an earthquake of magnitude M= m at a distance R= r.
- $f_{Mi}(m)$ is the probability distribution of the earthquake magnitude.
- $f_{Ri}(r)$ is the probability distribution of the distance to the site.
- N_s is the total number of seismic sources considered.

And the mean annual occurrence rate of earthquakes from source i:

$$v_i = \exp(\alpha_i - \beta_i\, m_0) \qquad (9)$$

with $\alpha = a \ln(10)$ and $\beta = b \ln(10)$ being the parameters of the Gutenberg-Richter recurrence law:

$$\lambda_m = \exp(\alpha - \beta m) = 10^{a-bm}, \tag{10}$$

adjusted from the seismic catalog of the project using statistical techniques of~~ least squares or~~ maximum likelihood. The probability function in (8) is:

$$P[IM > x|m, r] = 1 - F_{IM}(x) = 1 - \Phi' \left(\frac{\ln x - \ln IM_{average}}{\sigma_{\ln_{IM}}} \right) \tag{11}$$

where the function $P[IM > x \mid m, r]$ indicates the IM ground motion parameter generated by a source i of magnitude (m), distance (r), and uncertainty epsilon (ε) in relation to the threshold value x. Finally, $f_{Mi}(m)$ and $f_{Ri}(r)$ are the parametric probability density functions for which a functional model is assumed, estimated from the magnitude and distance catalogue.

Results are expressed as seismic hazard curves (SHC), which can be obtained for different intensity measures, the most common being Peak Ground Acceleration (PGA), representing the exceedance probabilities over usually 50 years, and the ordinates of the acceleration spectrum $S_a(T)$. Another result is the response spectra, commonly referred to as uniform hazard spectra (UHS), derived from the SHC and obtained for each chosen return period.

4.3 Epistemic uncertainty treatment: logic tree scheme in DSHA and PSHA

There are numerous uncertainties in the DSHA and PSHA methodologies that arise from limited comprehension of the seismic process. The random nature of earthquakes and their occurrence generates variations in the spatial, temporal, and magnitude distribution when defining and characterizing seismic sources. In addition, the way seismic waves attenuate as they propagate from the source to the site of interest can be uncertain, generating uncertainties about the attenuation models or GMPEs, whose statistical adjustment of their coefficients incorporates an estimation error. Moreover, the arbitrary choice of GMPEs by users is itself an unsure process. All these uncertainties can be classified as random and epistemic (Kiureghian and Ditlevsen, 2009; McGuire and Shedlock, 1981).

In this work, the logic tree method has been used ~~as a practical method~~ to incorporate and analyse the inherent uncertainties both for DSHA and PSHA analysis. Its formulation uses weighting factors, assigned to seismic source models and GMPEs based on their likelihood (Coppersmith and Youngs, 1986; EPRI, 1987). The logic tree is constructed from a series of branches connected through nodes, from which the computational process twigs according to a possibility or appropriate weighting factors $\{w^i\}$. These factors are assigned based on expert judgment (Budnitz et al., 1997), depending on the suitability and importance of each seismic source model and GMPE used. The treatment of uncertainties by the logic tree scheme is made mathematically explicit in the calculation process in the equations to obtain $Y_{p,j}$ at site P produced by each j-th seismic source:

$$Y_{p,j} = \Sigma_i w^i Y^i_{p,j} \tag{12}$$

And also, to obtain $Y_{p,Ns}$ at each site P:

$$Y_{p,Ns} = \Sigma_i w^i Y^i_{p,Ns} \tag{13}$$

which includes the effects of the N_S seismic sources. The logic tree scheme shown here is used both for the estimation of the PGA based on a single control source, with the most unfavourable seismic scenario, and for the PGA estimation based on all seismogenic sources with their particular seismic scenario.

The logic trees used in this study incorporate a combination of three seismic source models and four~~three~~ GMPEs, selected to estimate the PGA in our study area. In the logic trees used in the DSHA (Fig. 7a) and PSHA (Fig. 7b), the weights assigned to each seismic source model were those used in the ESHM20 (Danciu et al., 2024). The GMPEs weights in this study are based on statistical performance and regional relevance, in order to properly address epistemic uncertainty. At each node, branch weights are normalized so that $\sum w = 1$.~~In contrast, each GMPE was implemented independently in this study, so the weighting assigned to each GMPE in the logic tree was unitary, generating three different seismic hazard results.~~

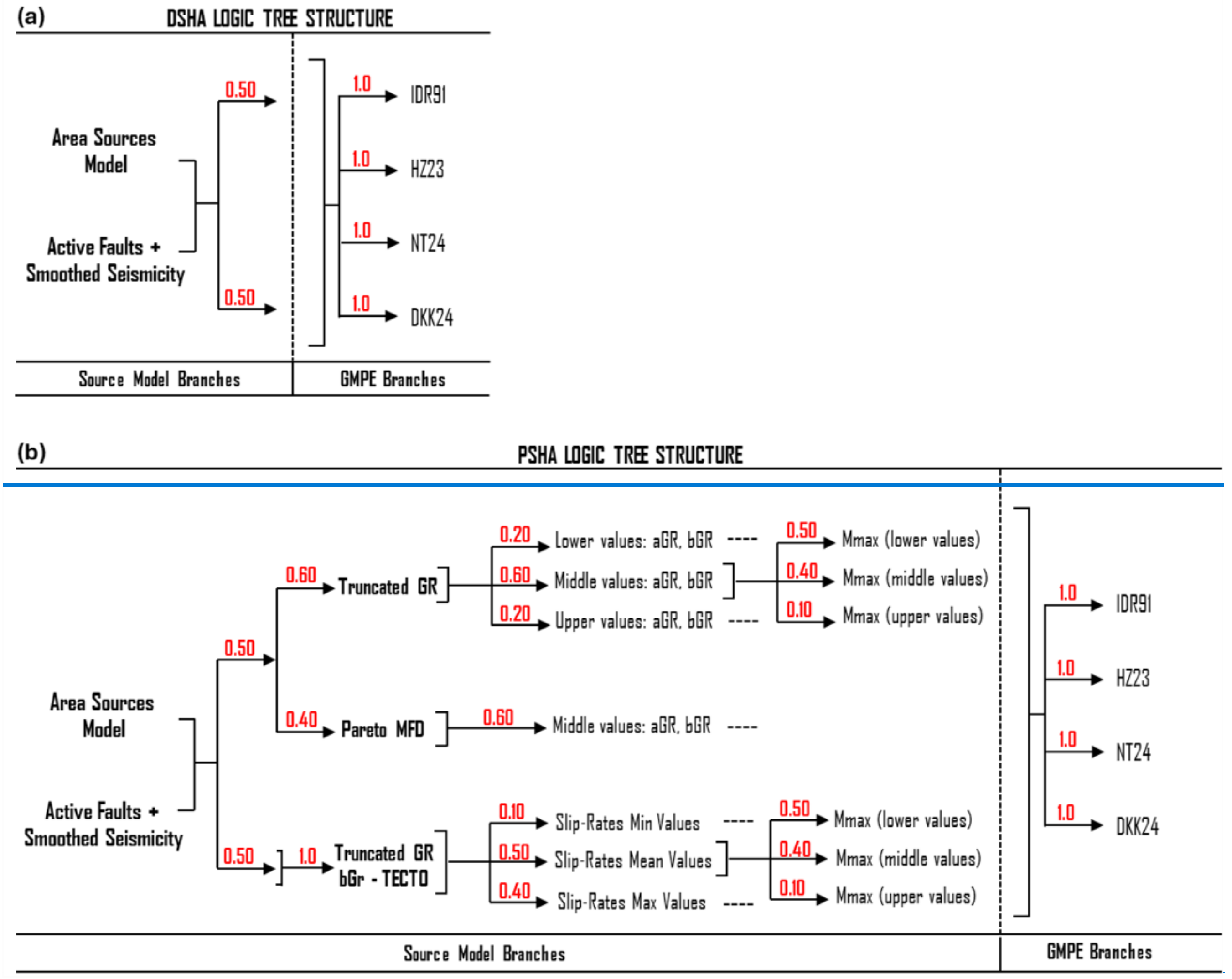
(a)
DSHA LOGIC TREE STRUCTURE
Area Sources Model
Active Faults + Smoothed Seismicity
0.50
0.50
1.0
IDR91
1.0
HZ23
1.0
NT24
1.0
DKK24
Source Model Branches
GMPE Branches
(b)
PSHA LOGIC TREE STRUCTURE
Area Sources Model
Active Faults + Smoothed Seismicity
0.50
0.60
Truncated GR
0.20
Lower values: aGR, bGR ----
0.60
Middle values: aGR, bGR
0.20
Upper values: aGR, bGR ----
0.50
Mmax (lower values)
0.40
Mmax (middle values)
0.10
Mmax (upper values)
0.40
Pareto MFD
0.60
Middle values: aGR, bGR ----
0.50
1.0
Truncated GR bGr - TECTO
0.10
Slip-Rates Min Values ----
0.50
Slip-Rates Mean Values
0.40
Slip-Rates Max Values ----
0.50
Mmax (lower values)
0.40
Mmax (middle values)
0.10
Mmax (upper values)
1.0
IDR91
1.0
HZ23
1.0
NT24
1.0
DKK24
Source Model Branches
GMPE Branches

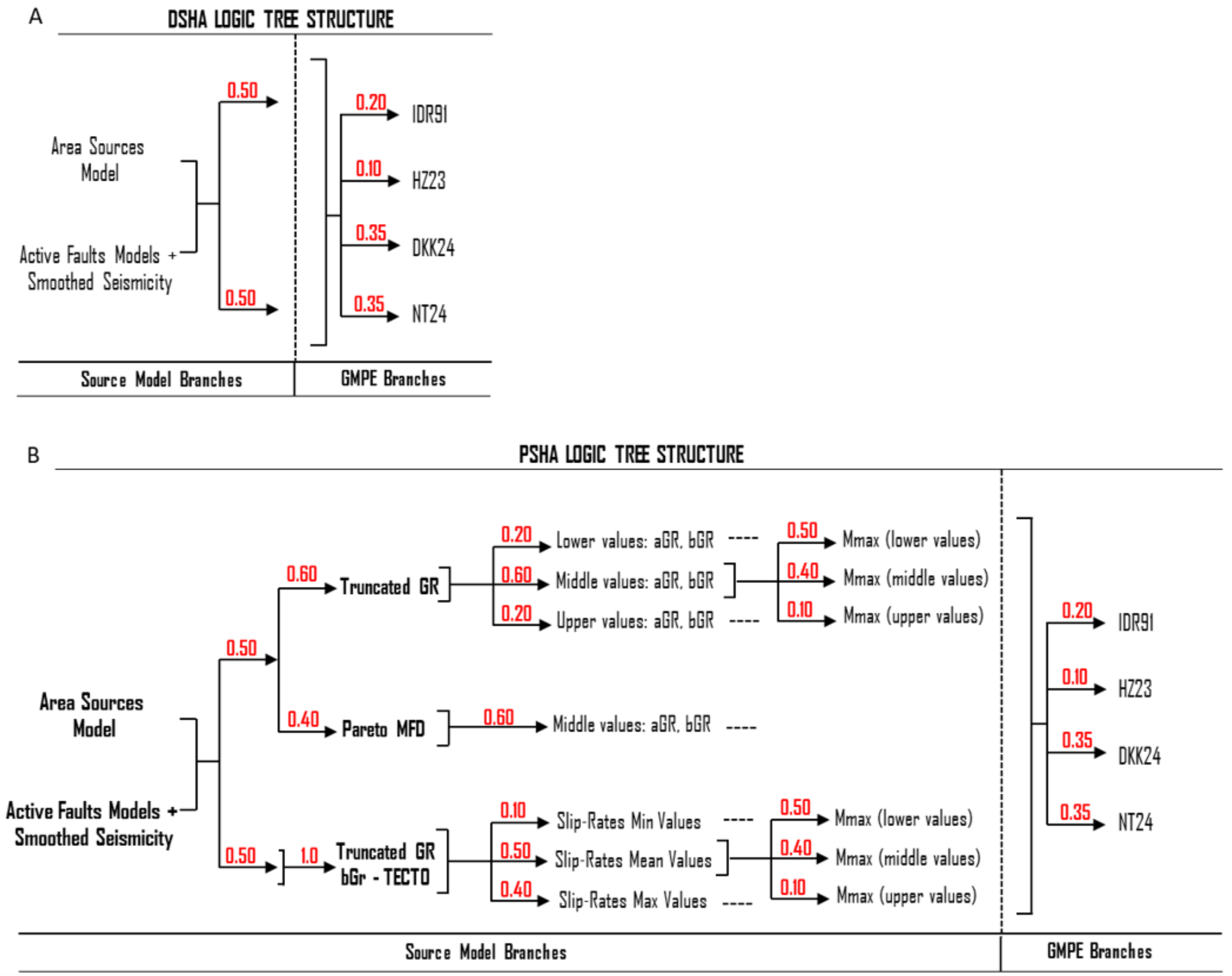

Figure 7. Schematic representation of the logical tree structure of the seismic hazard models: (Aa) DSHA and (Bb) PSHA. The weights assigned for each branch are shown in red. (modified from Danciu et al., 2024).

4.4 DSHA and PSHA calculation specifications

The open source DTM downloaded from EMODnet website (Fig. 1) has been used to generate the computational grid in the seismic hazard calculations of this work. The DTM was resampled to generate grid points spaced at 0.1 degrees (approximately the standard error in earthquake epicentre determination; Panza et al., 1990). In addition to its geographical coordinates, each point was assigned its respective bathymetric or topographic elevation. This mesh size, commonly used in the region (e.g., Danciu et al., 2024; IGN-UPM, 2017; Poggi et al., 2020), was chosen for its balance between computational efficiency and spatial resolution. This allowed capturing the variations in seismic hazard in this study while keeping a manageable computational load. Thus, computationally, SHA calculations, using DSHA and PSHA, were performed on a grid of 3,854 sites (Fig. S2). The elevation of~~vertical component that~~ the DTM~~ incorporates~~ is used in the estimation of the relative geographical distances, from the site to the seismogenic source, used by~~ some of ~~the GMPEs.

For DSHA calculations, a computational routine was~~a MATLAB© code has been~~ developed to calculate the seismic intensity with a selected GMPE, from different seismic source types, incorporating the extreme value distribution into the DSHA as the scenario in which all seismic sources contribute (maximum Y distribution in Eq. (5)), and to account for the logical tree with them. Since the extreme value distribution must be determined at each site where the hazard is estimated, the convergence characteristics of this algorithm allow it to be repeated for up to 100 iterations. This number is sufficient to achieve an admissible error, |Xo - X*| in the root X* solution of Eq. (7) (Burden et al., 2015). T~~Moreover, t~~o ~~notably~~ reduce the computational time compared with earlier ~~older~~ DSHA implementations~~versions~~ (e.g., Wang et al., 2012), the~~-~~ routine was optimized through parallel processing~~algorithm has been improved to reduce computing time by its parallelization~~ in MATLAB© (R2024a, Update 6, available at https://www.mathworks.com, last accessed: 08/07/2025). The routine is publicly available at https://es.mathworks.com/matlabcentral/fileexchange/183034-dsha.

PSHA calculations where performed~~rovided~~ for the mean values of PGA (in g) and four annual probabilities of exceedance (APEs), i.e., 0.01, 0.002105, 0.000404, and 0.0002, which correspond to the return periods of 100, 475, 2475, and 5000 years, respectively. These hazard maps are prescribed in the European seismic-resistant standards. Here, the OQ Engine configuration and the input files used are publicly available from ESHM20 (Danciu et al., 2021b, c), but the calculations were performed under soft soil conditions, with a Vs30 = 200 m/s, corresponding to class E according to the Eurocode 8 classification (CEN, 2004) and the National Earthquake Hazards Reduction Program (NEHRP) (BSSC, 2004). The DTM was incorporated into the calculations. For epistemic uncertainty representation in this study, a total of 100,000 logic trees end-branches were sampled using the OQ random technique. The programming of the new GMPEs, as well as all PSHA calculations in this study, was carried out using OpenQuake (OQ) engine (Pagani et al., 2014) version 3.21.0 in development mode (available at https://docs.openquake.org/oq-engine/manual/3.19/getting-started/installation-instructions/universal.html#devel-installation, last accessed: 08/07/2025).

5. Seismic hazard assessment results and discussion.

The findings of this study demonstrate the effectiveness of using both DSHA and PSHA methodologies to generate seabed seismic hazard maps in~~within~~ the IMR. The spatial hazard patterns in these maps are mainly controlled by the seismogenic source model and its parameters. The selected offshore oriented GMPEs are statistically consistent with the onshore/near coastal data used for benchmarking.~~seismicity. Similarlythe most recent GMPEs specifically tailored for offshore environments and show statistically robust compatibility with the available seismic data~~. This advancement represents a significant improvement over previous results in this field. In particular, this study extends and updates the only published maps (i.e., Molina Palacios, 1998) in the IMR.

The seismic hazard maps presented in the results obtained with either DSHA or PSHA suggest that the highest PGA values are concentrated in deep seafloor areas, where areal seismogenic sources of medium and high activity and faults are found. It has been demonstrated in previous studies that PGA maps depict the areas of highest seismic intensity as being limited to coastal and inland regions of the Iberian Peninsula and northern Africa or zones characterized by high seismic activity along major tectonic fault line (e.g., Danciu et al., 2024; IGN-UPM, 2017; Poggi et al., 2020). However, the present results expand the geographical coverage of previous studies by highlighting the overlapping influence of the Gorringe and Horseshoe active zones with the SVF, MPF, and SWIM faults (distributed across the western IMR) and by emphasizing the significant role of the Arzew, AIF, and YSF faults in shaping the diffuse seismicity sources in the Alboran Sea. This is of great interest in the design of offshore infrastructures and their current and future deployment on the ocean floor, as vulnerable infrastructures may be affected by significant seismic effects not previously considered (Karthigeyan, 2022; Kee et al., 2023). The seismic intensity of these effects varies according to the approach used for the SHA and the soft ground attenuation function applied. However, a discernible amplification is evident in all cases when compared to equivalent PGA maps on comparable rock formations in emerged zones bordering the IMR of this study or in seafloor zones.

5.1 Probabilistic approach

The seismic hazard maps for the area between the western Gulf of Cádiz and the eastern Alboran Sea, with return periods of 100, 475, 2475, and 5000 years are shown in Figure 8. The maximum expected PGA values vary according to the analysed return perioddepend significantly on each GMPE used, thus generating four different seismic hazard scenarios in the IMR. For the 100-year return period (Fig. 8A)Using IDR91, the mean horizontal PGA are between 0.17 and 0.60 gvalues reach 0.39 g, 0.60 g, 0.91 g and 1.06 g, for each the analysed return period. For 475-year (Fig. 8B)With NT24, these values are betweenreach 0.2672 g, 1.78 g, 2.43 g and 12.906 g. It is considered that the results obtained with HZ23 model should be disregarded, considering the obtained PGA is greater than 3 g for most of the return periods; hence, suggesting numerical saturation of the model. In the case of 2475-year (Fig. 8C)the DKK24, maximum the PGA values range from 0.38 g to 2.59 g. Finally, for a 5000-year return period (Fig. 8D), the PGA values are around 0.44 - 3 are around 0.51 g, 0.78 g, 1.06 g, and 1.17 g, respectively. As commented, the range of PGA values in Figure 8, for the four seismic hazard scenarios presented, falls within the maximum values indicated for each return period. For each map shown, the highest PGA values are found in geographic areas over deep submarine zones of the IMR that exhibit the highest levels of seismic activity and intensity. Consequently, the highest seismic hazard values in the IMR are observed across most of the studied extent of the Gulf of Cádiz. This pattern is primarily attributed to deep seismic sources, located at approximately 60 km depth, which are associated with more intense reverse or strike-slip faulting ruptures. Notable examples include the among these areal sources PTAS390, ESAS129, and MASS344 (identified in the ESHM20 catalogue) within the Gorringe and Horseshoe regions. Shallower right-lateral (RL) and reverse (RR) faults, including the SVF, MPF, and SWIM, also contribute to the observed hazard levels. In the Alboran Sea, the highest PGA values are mainly organised in accordance with the most active shallow fault systems, Arzew, AIF and YSF, forming a pattern of strike-slip oriented regions. It is evident that these values exhibit a reduced sensitivity to the selected GMPEs, in comparison to those obtained in the western sector of the Gulf of Cádiz. The PGA values, attributable to the AIF surface faults, are located over a SW-NE band that traverses the Alboran Basin and extends northwards, accompanied by a band of more attenuated intensities NW-SE, as a consequence of the YSF faults' orientation. At the easternmost point of the IMR, the Arzew Faults, which are characterised by elevated levels of activity, delineate a high-hazard zone along the Algerian coast that extends in an east-west direction, reaching almost the centre of the Alboran Basin. This phenomenon is attributable to the geometrical configuration of these semi-deep faults.

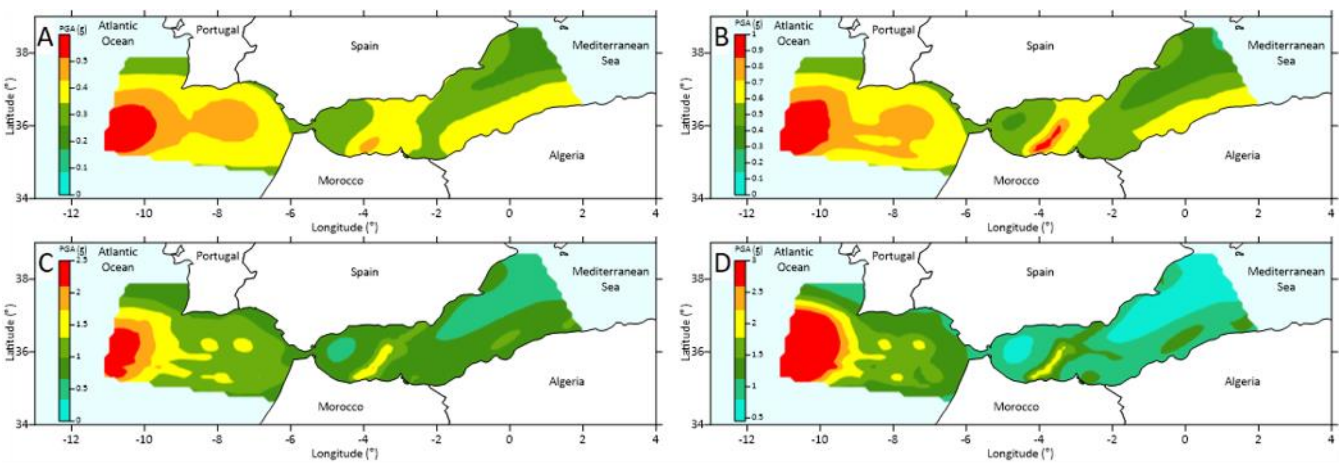

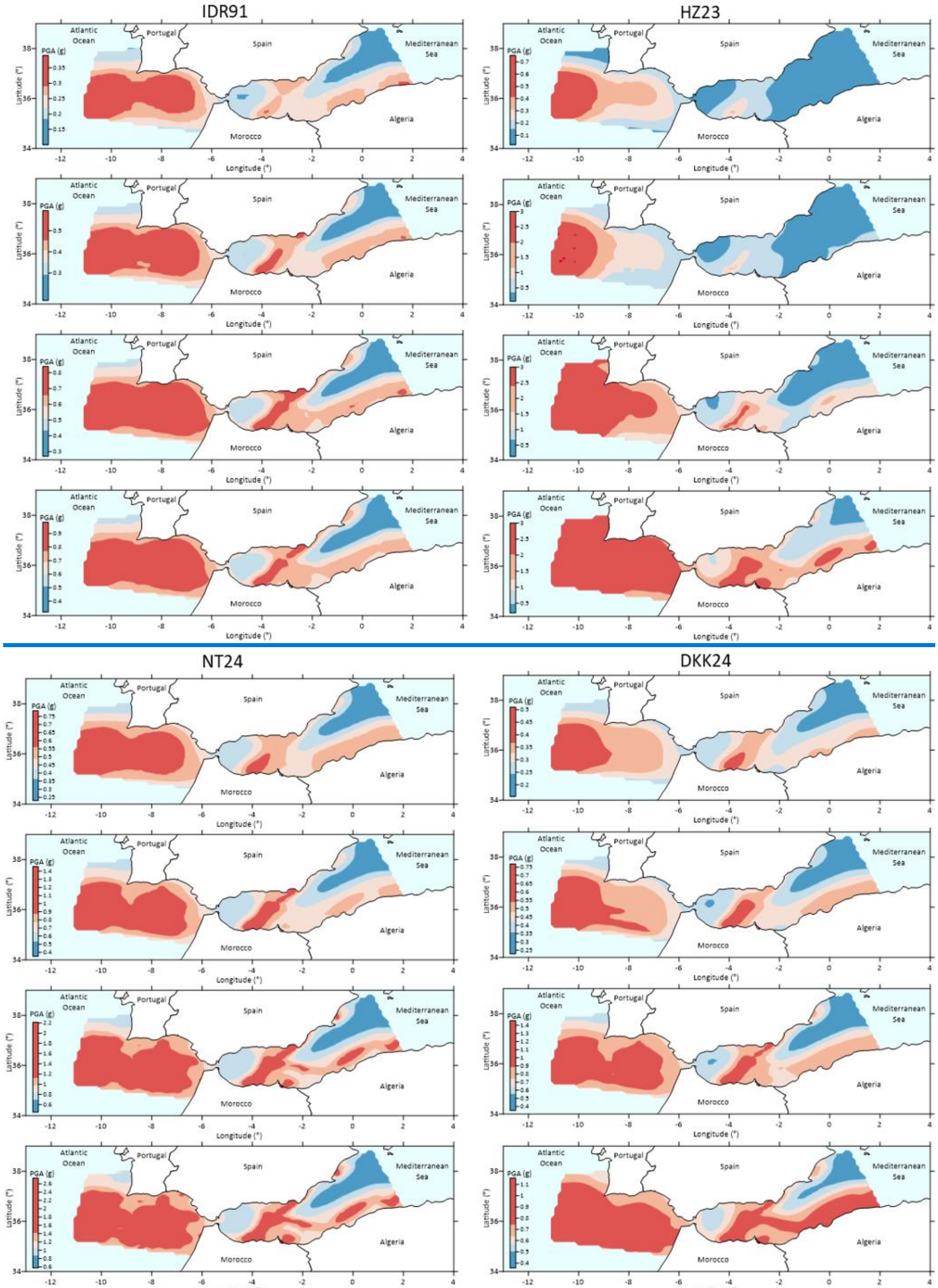

Figure 8. Probabilistic seismic hazard maps for the mean horizontal PGA (g) at APEs of (A) 1/100, (B) 1/475, (C) 1/2475, and (D) 1/5000~~, according to each GMPE used in this study~~. All values are estimated under soft soil conditions with Vs30 = 200 m/s.

Regarding the locally~~anomalously~~ high PGA values (approaching the upper bound of ~~~>~~3g) that appear in the longest return-period map (Fig. 8D) and, to a lesser extent, in the 2475-year map (Fig. 8C) should be interpreted with particular caution because long return periods are increasingly controlled by rare, large-magnitude scenarios and by the upper tail of the ground-motion variability~~after the HZ23 model,~~. I~~i~~t is likely that these results stem from extrapolating the HZ23 model beyond its intended range of applicability. Although HZ23 contributes only 10% of the total weighting scheme, it has comparatively large aleatory variability (ε = 0.7784). Therefore, when the IMR hazard calculation requires evaluating scenarios that may exceed the GMPE calibration ranges, the HZ23 branch can disproportionately influence the high-end tail of the combined hazard estimate. This effect is amplified at very low annual exceedance probabilities (2475 - 5000 years), where extrapolation beyond validated magnitude ranges and model variability have greater leverage on the final PGA levels. Consequently, the highest PGA patches in Figs. 8C–D should be regarded as reflecting increased epistemic uncertainty associated with GMPEs extrapolation and variability. ~~This extrapolation may lead to unrealistic ground motion estimates, especially when compounded by the relatively high standard deviation of the model (ε = 0.7784), and the absence of empirical calibration for the unique seismotectonic and geomechanical conditions of the IMR.~~ ~~–~~The overprediction observed in the ~~HZ23~~ results of~~in~~ the probabilistic seismic ~~and deterministic~~ hazard maps suggests that, while the HZ23 model may offer valuable insights within its original context, its use in the IMR should be approached with caution. Although the hazard results remain consistent with the prevailing seismicity of the study region, this limitation should be taken into account, and priority should be given to the future development of regionally calibrated offshore GMPEs for the tectonic context of the IMR to reduce uncertainty in the large magnitude range.

Results show significant differences compared to previous PSHA studies in the IMR (e.g., Molina Palacios, 1998), particularly in marine zones. These results not only refine previous assessments in IMR but also improve the understanding of the tectonic influence on offshore seismicity. More recent SHAs typically highlight the higher seismic intensity in the coastal areas of the Iberian Peninsula and North Africa (e.g., Danciu et al., 2024; IGN-UPM, 2017; Poggi et al., 2020). However, these new results extend the geographical scope of seismic hazard studies in the region by demonstrating considerable seismic activity in the marine areas of the IMR. This emphasizes the need to consider seabed seismic dynamics in regional SHA studies.

The resulting seismic hazard maps could be highly valuable for offshore infrastructure design, as they highlight the potential vulnerability of current and future subsea facilities in the region. Hazard results are presented in terms of seabed PGAs, which enables first-order screening of offshore shaking demand. Spectral acceleration Sa(T) hazard maps, which are more directly linked to structural response at different periods, are not provided because the selected offshore GMPEs that have been implemented are currently developed for PGA (and, in some cases, PGV) (e.g., Dhakal et al., 2024; Nakanishi and Takemura, 2024).

5.2 Deterministic approach

The obtained mean PGA (g) seismic hazard map~~s~~ (Fig. 9), considering the distribution of maximum control scenarios at each of the 3,854 study sites (Fig. S2), were generated by incorporating the DTM into the calculation, as well as the specific rupture mode of each fault and seismogenic source (Tables S1 and S2) and the GMPEs considered in this study: IDR91, HZ23, NT24, and DKK24. As illustrated in the applied logic tree (Fig. 7A), the weighted implementation of each GMPE has resulted in a consolidated~~different~~ seismic hazard scenario, which has been weighted according to Eq. (13).~~. Figure 9A shows the seismic hazard map considering IDR91. In this scenario, maximum PGA reaches around 0.91 g. With HZ23 (Fig. 9B), the maximum estimated PGA values exceed 3 g; hence HZ23 was disregarded. With NT24 (Fig. 9C), maximum PGA are of about 1.4 g. In contrast, when using DKK24 (Fig. 9D), maximum PGA values hover around 1.8 g.~~

~~For the four scenarios presented~~ The expected PGA values in the deterministic seismic hazard scenario are between 0.58 and 2.55 g. T~~, t~~he spatial distribution of accelerations shows ~~relative similarities. T~~the that highest PGA values are found in the Gorringe seafloor and extend to the Horseshoe Plain~~ in all four resulting maps~~. These abyssal areas are influenced by seismogenic sources and faults with moderate to strong seismicity, generating PGA outliers in the area, ranging approximately between 1.2~~0.65~~ g and 2.55~~1.8~~ g~~, excluding the previously discarded HZ23 results~~. To the ~~w~~east, PGA values range from 0.4~~6~~5 g to 1.8~~2~~ g. This relates to a sequence of moderate seismicity sources along the Algerian coastal zone, together with the Arzew faults. Notably, the use of a DTM to determine the three-dimensional location of each calculation site, may result in amplified PGA values in areas where the site depth is closer to the seismic source, particularly in the deeper oceanic regions of the IMR. In general terms, the PGA (g) map~~s~~ obtained show a geographical distribution of the maximum values over the Atlantic areas of Gorringe, Horseshoe and Coral Patch, as well as off the Algerian coast, in the Mediterranean Basin of the Alboran Sea. This coincides with the areas of highest seismogenic potential in the IMR.

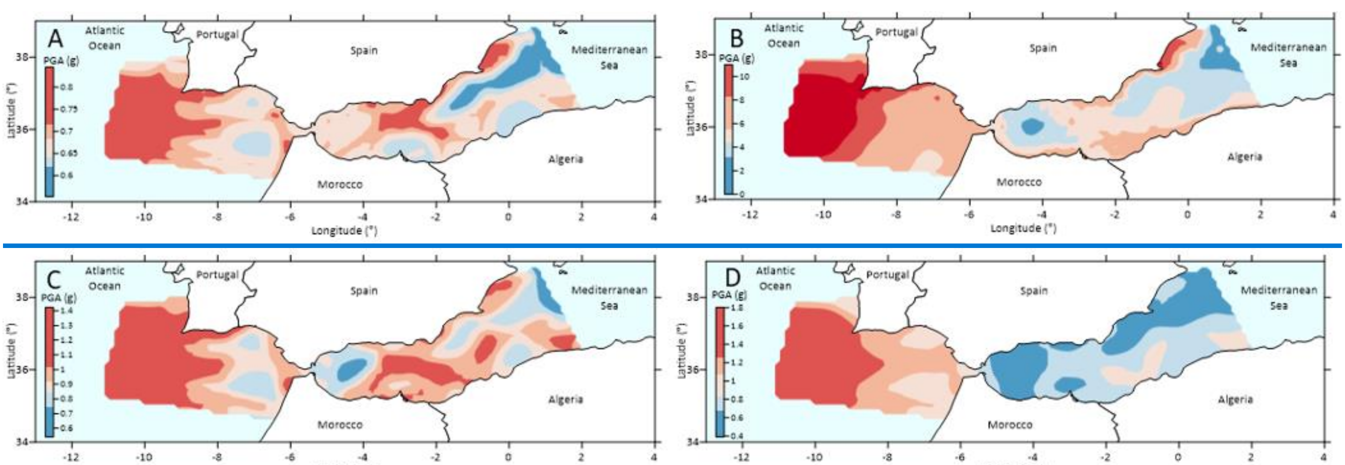

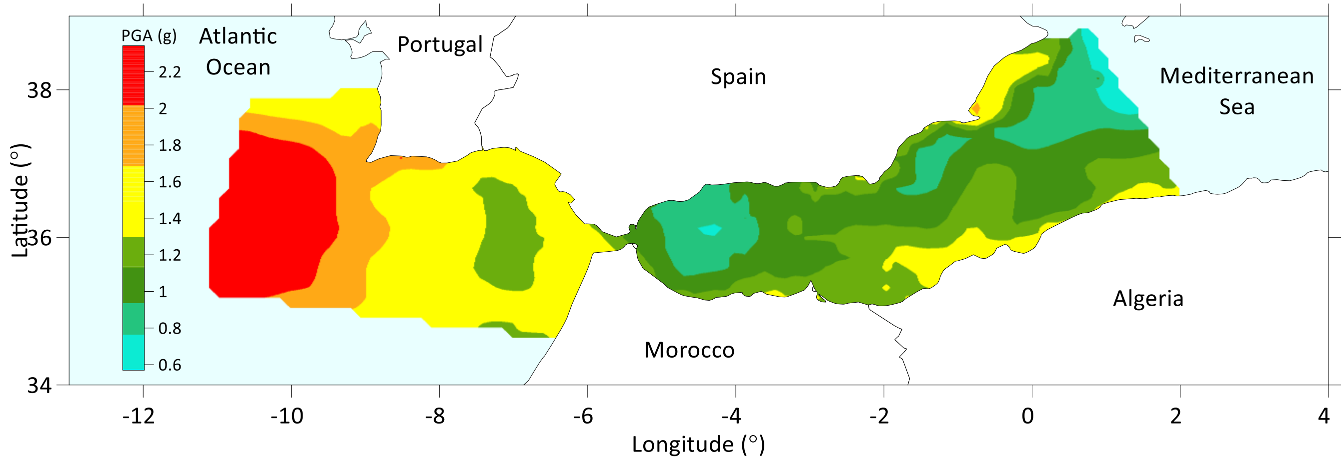

Figure 9. Deterministic seismic hazard maps in terms of mean PGA (g) under soft soil conditions.~~, for the GMPEs used in this study: A) IDR91, B) HZ23, C) NT24, and D) DKK24.~~

~~The geographic distribution of the maximum expected PGA values obtained with the PSHA is very similar to the results obtained with the DSHA.~~ As Reiter (1990) points out, the DSHA does not contemplate the inherent uncertainty in the estimation of seismic hazard, since the frequency of occurrence and magnitudes are not explicitly considered. So, a less accurate version, distributing the uncertainty due to randomness in the attenuation functions over a large region, is preferable, even though it provides larger values as in this work. These PGA values can be used as preliminary upper bounds of those that can be achieved, for different exceedance probabilities, rather than working with more precise, but less accurate PGAs.

The decision for the SHA method is based on its suitability for assessing earthquake hazards, as earthquakes are inherently random and unpredictable. It is important to acknowledge that hazard estimates cannot be fully verified due to the nature of seismic events (Musson, 2012a, b; Wang, 2012). Therefore, the use of DSHA could be recommended for critical industrial facilities of socioeconomic relevance.

~~5.3 Convergence in return period~~

~~The hazard maps obtained from deterministic and probabilistic estimations demonstrate a clear correlation: as the return period increases, PGA values calculated by PSHA increase and approach those obtained via DSHA. This finding corroborates the preliminary supposition that the results derived from the application of deterministic methodologies can be utilised as an upper limit on those derived from probabilistic methodologies. reinforcing the idea that DSHA may well be considered a 'worst-case' estimate of ground motion for a given earthquake scenario (Wang, 2011). Nevertheless, this assertion is supported by evidence to a certain degree. For lower exceedance probabilities, the hazard curve exhibits a monotonically increasing, quasi-asymptotic trend. As a result, beyond a certain return period, estimates using DSHA are surpassed. In the IMR, for 2475~~

years return period, a prominent 1:1 correlation is observed between the deterministically and probabilistically obtained PGA values (Fig. 10). The correlation structure between the two PGA values is dependent on depth, with the shallowest depths, i.e., those below 2500 m, exhibiting the poorest correlation and greatest dispersion. The correlation is most evident when using NT24 (Fig. 10 C), followed by IDR91 (Fig. 10 A) and finally DKK24 (Fig. 10 D). HZ23 (Fig. 10 B) has been excluded due to model saturation. For each GMPE, the correlations are more significant and show lower dispersion around 1:1 at the highest PGAs and over points at medium and high depths, above 2,500 to 3,000 m. The DSHA may underestimate or overestimate seismic hazard, causing this dispersion, in regions with complex or poorly understood seismic sources. In areas where there are multiple faults or where the seismic source zone or the maximum credible earthquake is uncertain (as is the case in this submarine area with scarce direct seismic data), the method may fail to account for all possible earthquake scenarios (Wang, 2011). The dispersion in PSHA is due to this method is highly dependent on the quality of the seismic catalogue, the GMPEs used, and the seismicity parameters (Peresan et al., 2013).

The correlation can be enhanced by combining expert knowledge with specific seismic intensity data from the region. This approach involves fine-tuning weights in the logic tree, which leads to an asymptotic quasi-equivalence between the results obtained with PSHA at larger return periods and those of DSHA. The efficiency and speed of DSHA calculations can serve as a preliminary approximation to SHA in scarce strong shake data areas. However, it is important to note that this claim cannot be made for all the GMPEs used, and it is not the aim of this paper to identify how the maximum correlation between the DSHA and PSHA approximations used here is achieved. With regard to the selection of the attenuation model, while the evaluation of the models in use does not provide statistical justifications for their rejection, the utilisation of solely the available recorded data from six significant offshore earthquakes did not adequately represent the anticipated behaviour across the entire IMR. In particular, it has been determined that HZ23, despite a favourable statistical diagnosis, yields PGA values that are considered too high (PGA > 3g) in comparison to those that would be observed in the area for a return period of 2475 year. Consequently, the PSHA calculations result in overestimated PGA values in certain regions of the IMR, despite these areas were not excluded during the preceding statistical validation tests.

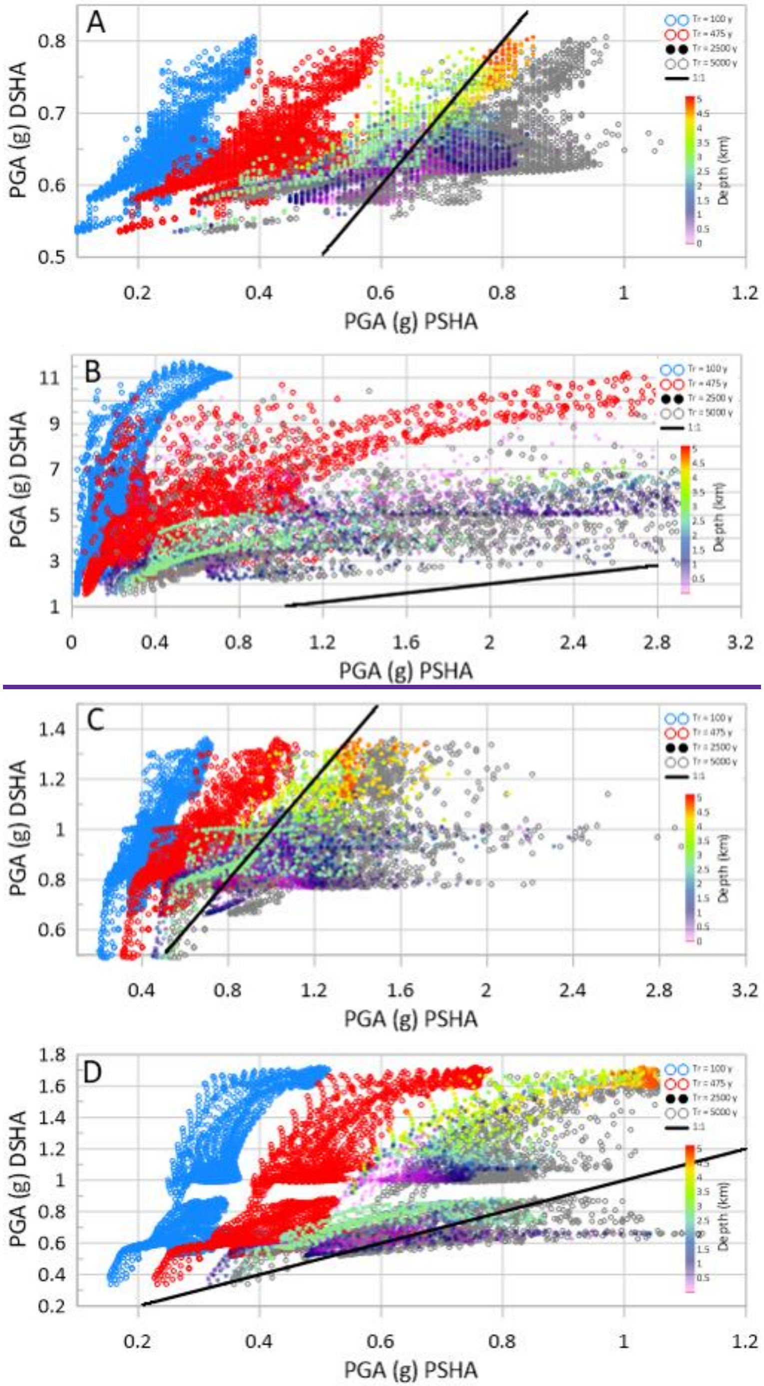

~~**Figure 10. Scatter plots of PGA by DSHA vs. PGA by PSHA for the 100, 475, 2475, and 5000-year return periods for the GMPEs used in this work: A) IDR91, B) HZ23, C) NT24, and D) DKK24. Dots representing the 2475-year return period were colour-coded according to DTM depth.**~~

5.3~~4~~ Distribution of PGAs amplification ~~in the ocean floor~~relative to a baseline PSHA using the ESHM20 model (rock, onshore).

A baseline PSHA seismic hazard maps were~~as~~ computed using the published ESHM20 source model and GMPE logic tree exactly as released (rock, ~~/~~onshore site conditions) (Danciu et al., 2021a, b, c, 2024), clipped to our study zone in the IMR, to provide a reference for how the hazard results obtained, by incorporating seabed-specific GMPEs and bathymetry, alter PGA valuess~~s~~. These baseline results are not part of the official ESHM20 products and are used here strictly as a methodological contrast~~The PGA values obtained using DSHA and PSHA with the GMPEs selected in this study, are higher than those obtained using input data files containing the information of the seismogenic sources (accessible via https://doi.org/10.12686/ESHM20-MAIN-DATASETS) and the OQ Engine configuration and input files (accessible via https://doi.org/10.12686/ESHM20-OQ-INPUT). These were used to calculate the ESHM20 hazard mapping scheme (Danciu et al., 2021a, 2024) in the IMR, as recorded in several ocean floor areas (Boore and Smith, 1999; Dhakal et al., 2021)~~. The distribution of PGA values obtained by baseline PSHA (ESHM20 model; rock) is increased throughout all its ~~spectrum~~ range (Fig. 10~~1~~ A and B)~~ and with very similar rates for IDR91 and DKK24, and much higher for NT24~~. Incorporating the relief of the ocean floor through bathymetry has an effect, although not as significant as the amplification of the attenuation curves. The deeper the seismic intensity increases, the closer the control point is to the seismogenic sources in relation to inshore territory or mean sea level.

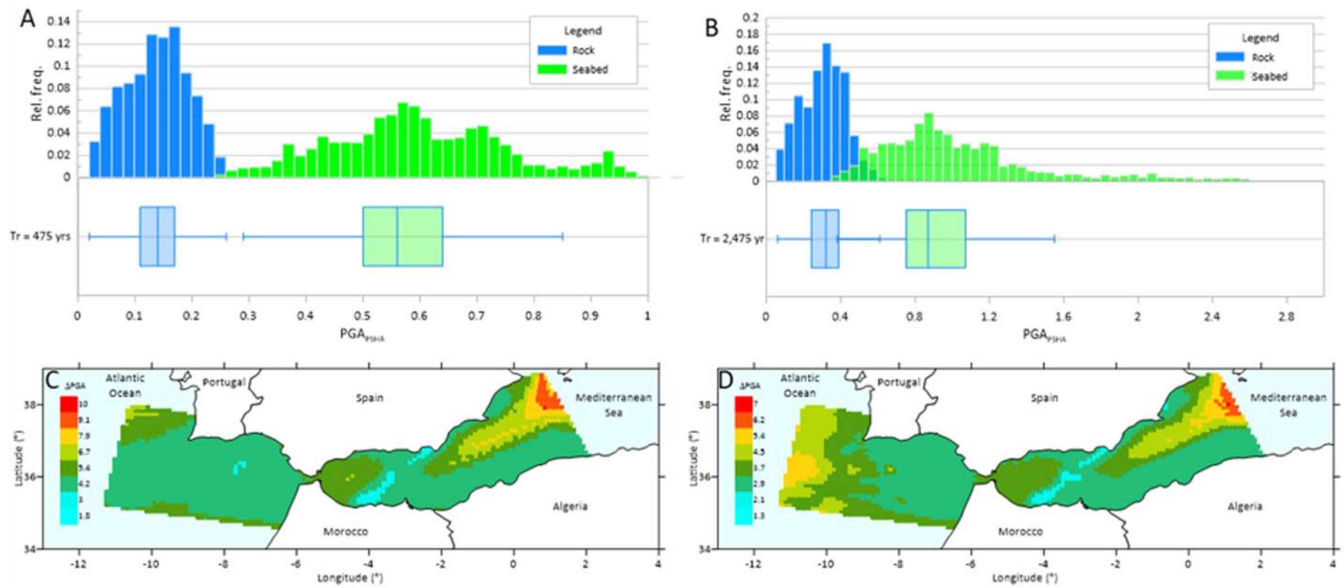

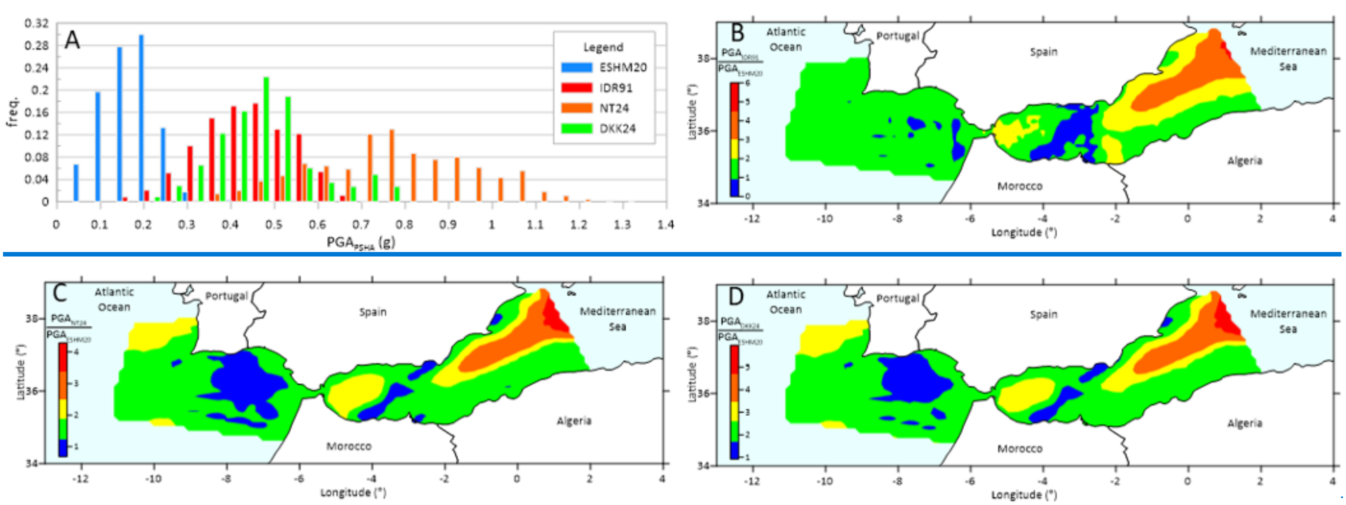

~~**Figure 11. A) Histogram of the PGA values estimated by PSHA for a 475-year return period, from ESHM20, from different GMPEs and seismic models indicated in the legend. Relative amplification maps showing the percentage increment in estimated PGA values based on PSHA for each GMPE used in this work: B) IDR91, C) NT24, and D) DKK24.**~~ **Figure 10. Distributions and relative-change maps of PSHA (in terms of PGA) at the seabed. (A–B) Histograms (in relative frequency) and box–whisker plots of estimated PGA values for return periods of 475 years (A) and 2475 years (B), comparing baseline PSHA results under rock/onshore site conditions (PGArock; blue) with the seabed PSHA results obtained in this work (PGAseabed; green) within the study area in the IMR. Baseline PSHA (ESHM20 model; rock) results were computed by the authors using the published ESHM20 seismogenic source model and GMPE logic tree exactly as released, clipped to the study area. They are not official ESHM20 products and must not be interpreted as an offshore extension of ESHM20. (C–D) Relative-change maps are shown expressed as the ratio ΔPGA = PGAseabed / PGArock for return periods of 475 years (C) and 2475 years (D).**

The combination of GMPEs, bathymetry and the spatial distribution of seismogenic sources in this study has provided a new geographical pattern of amplification rates ΔPGA$_{GMPE}$~~/PGA~~$_{ESHM20}$ (see Figs~~s~~. 10~~1~~ C and D~~B D~~) close similar for different return periods. As demonstrated in the literature (see Dhakal et al., 2021; Hu et al., 2020), offshore sites exhibit differing distance attenuation when compared to inshore sites. This discrepancy is due to the incorporation of modifications to offshore zones as specified by the authors of the GMPEs within the model. It is acknowledged that some of the offshore GMPEs used (HZ23 and NT24) are derived from onshore GMPEs. The maximum amplification reaches approximately about 7 to 9~~6~~ times ~~PGA$_{ESHM20}$ with IDR91 (Fig. 11 B), 4.5 times with NT24 (Fig. 11 C) and about 5.5 times with DKK24 (Fig. 11D~~ in deepest areas of the IMR eastern limits~~)~~, all very specifically located in AOB. In the remaining zones, the rate of increase of the PGA is within the medium ranges in comparison to the reference PGA$_{rock}$~~$_{ESHM20}$~~ values in rock and emerged terrain (PGA ~~at 475 years,~~ calculated using the ESHM20 seismic model with the PSHA approach). It is observed that, in most of the studied area, the amplification rates were found to be less than ~~double~~ five times in all seismic hazard scenarios. The site effect is primarily attributable to the attenuation characteristics of soft seafloor soils and their depth found in WAB and AOB (Chen et al., 2023; Diao et al., 2014), which are incorporated through the GMPEs used.

Regarding ~~There are notable similarities in~~ the spatial distribution of PGAs amplification rates, ~~tregardless of the GMPE used. T~~he highest amplification rates (represented by ~~red~~ yellow, ~~and~~ orange and red colors), exceeding five to ~~six~~ nine times max the PGA values from the baseline PSHA (ESHM20 model; rock), are concentrated in regions where the expected PGA values are relatively low, such as the Argelo-Balearic Basin. Mid-range amplifications rates (~~green~~ blue, ~~and yellow~~ green and olive colors) are distributed across the entire study area. In this case, regions where the PGA values are already high, such as the Gorringe Ridge, Horseshoe Abyssal Plain, and the Algerian margin, the amplification rates tend to be moderate, typically ranging between 2~~1.5~~ and 4~~2.5~~ times the PGA$_{rock}$~~$_{ESHM20}$~~. On the other hand, the lowest amplification rates (blue color) are observed in the West Alboran Basin (WAB), following the Alboran Ridge and Channel, as well as in the Gulf of Cádiz. As illustrated in these amplification maps, the phenomenon is most evident in the West Alboran WAB and the Algerian Ocean Basin (AOB), extending to the west in the Gorringe Ridge and Tagus Plain. In such instances, the site effect assumes a heightened significance, particularly in the context of basin bottoms characterised by the accumulation of substantial sedimentary deposits.

Within IMR geographical framework, no discernible spatial correlation is identified between the amplification outcomes resulting from the GMPEs used in this study. Areas exhibiting low seismic intensity, such as AOB, demonstrate a substantial amplification effect, while regions characterised by higher PGA values exhibit average amplifications, as observed in the Gorringe Ridge area, or even attenuations to the west of Gorringe Bank and in the AIF and YSF fields. Excluding these areas where the PGA values are highest or lowest, the study area shows an amplification rate of less than ~~double~~three times, despite the variations in the PGA values obtained with the GMPEs used and with the baseline ESHM20.

Due to the absence of data concerning strong motion events within the IMR, there exists inadequate empirical data within the magnitude-distance range to directly develop a GMPE using empirical regression techniques. The authors of this study argue that there is a significant need for underwater seismic observation stations. This need arises from the considerable uncertainty and limited understanding of attenuation processes within the IMR. This is ~~despite~~regardless of the extensive knowledge already available on amplification and attenuation processes caused by the substantial water column and the rheological characteristics of the ocean floor. To address this gap, the authors recommend implementing underwater seismic stations similar to those used in the United States (Boore and Smith, 1999) and the S-Net network in Japan (Kanazawa, 2013).

This approach would enable two key advancements: 1) calibration and empirical modification of existing GMPE, as demonstrated in HZ23; 2) r~~R~~eformulation of a regionally adjustable backbone attenuation function, or a system of ergodic functions, to better capture ground motion variability. Such methods have already been successfully applied in seismotectonic settings, as shown in the ESHM20 model (Kotha et al., 2020; Weatherill and Cotton, 2020). These improvements would be tailored to the specific Vs30 and D14 distribution characteristics of the IMR as recently detailed by Hu et al. (2024).

6. Conclusions

This study addresses the critical need for a comprehensive seismic hazard assessment in the IMR, particularly in the marine domain between the Gulf of Cádiz and the Alboran Sea. Despite the well-documented historical and instrumental seismicity of the region, previous hazard studies have largely focused on terrestrial zones, leaving a considerable gap in our understanding of undersea seismic hazard, especially in terms of PGA at the seabed level. This work contributes to filling that gap by applying both probabilistic (PSHA) and deterministic (DSHA) methodologies, adapted to offshore conditions and integrated with recent developments in seismogenic zonation (ESHM20) and GMPEs. This study has demonstrated that PGA estimation for seabed conditions is both feasible and meaningful, providing crucial insight for hazard mitigation planning in marine environments.

Key findings show that significant PGA values are present across deep marine zones of the IMR, particularly over the Gorringe Ridge, Horseshoe Plain, and along active fault zones near the Algerian margin. The results confirm a consistent spatial distribution of hazard for both DSHA and PSHA approaches, with maximum values occurring over regions characterised by dense seismogenic activity and structural complexity.~~ Notably, the probabilistic results for long return periods (e.g., 2475 years) show convergence with deterministic outcomes, validating the use of DSHA as a robust upper-bound proxy in the absence of long-term probabilistic data, which may be particularly handy for infrastructures.~~ The incorporation of four GMPEs (IDR91, NT24, HZ23, and DKK24) allowed a comparative analysis of offshore attenuation behaviour. Among these, NT24 and DKK24 provided the best statistical fit to observed regional ground motion data, while HZ23 exhibited overestimation tendencies beyond its intended magnitude range, indicating potential constraints in its application to this region. The logic-tree framework adopted in both DSHA and PSHA enabled the epistemic uncertainty to be systematically incorporated into the hazard modelling. The overestimation observed with HZ23 highlights the importance of developing or calibrating GMPEs specifically for the IMR, particularly for large magnitude, short distance offshore events. Given the extrapolation beyond the validated model range, we recommend that future SHA applications in the IMR down-weight HZ23 in the logic tree or exclude it of the analyses to avoid potential overestimation of PGAs in the region.

The findings have significant implications for the seismic design and risk management of subsea structures, such as pipelines, cables, wind farms, and potential transcontinental tunnels. Current hazard assessments based solely on terrestrial models may significantly underestimate seabed accelerations and associated risks in the IMR. Moreover, the results underscore the importance of incorporating seabed-specific GMPEs and digital terrain models in offshore SHA, as bathymetry demonstrably affects source-to-site distances and thus ground motion predictions. In this context, the PGA-based hazard maps provide first-order screening of seabed shaking for offshore infrastructures. However, because subsea assets exhibit a wide range of fundamental periods, a complete design-oriented hazard characterization ideally includes spectral acceleration Sa(T) at representative periods. The Sa(T) characterization remains a necessary next step for detailed structural design of subsea structures with longer natural periods in the. Future work will extend the framework to Sa(T) hazard and uniform hazard spectra once suitable offshore spectral GMPEs and/or regionally calibrated models for the IMR become available.

However, some limitations remain to be addressed. The scarcity of direct offshore strong-motion records and the use of a uniform Vs30 proxy to represent soft soils in the IMR required the adoption of GMPEs derived from analogue seismotectonic contexts, such as the Japan Trench. While this approach was statistically validated, it introduces uncertainties that should be addressed in future studies through the expansion of OBS monitoring networks in the region and region-specific GMPE calibration. Similarly, the DTM resolution, though consistent with regional studies, may benefit from refinement in areas of steep bathymetric gradients to improve hazard detail, accordingly, to include possible site-effects. Moreover, the potential interaction between earthquakes and co-seismic hazards (such as landslides and tsunamis) requires further research. This could be approached through integrated, multihazard assessment frameworks to better understand and manage these complex interdependencies.

The integration of Neo-deterministic SHA (NDSHA) method and machine-learning approaches for source characterisation are promising avenues. Under the adopted modelling choices, both DSHA and PSHA yield consistent spatial patterns of high hazard over major offshore structures in the IMR. ~~The demonstrated alignment between DSHA and PSHA under appropriate modelling choices underlines the robustness of the results, offering a scientifically grounded tool for enhancing resilience in the face of submarine seismic risks in the IMR.~~

Code availability

All MATLAB© ~~code~~ scripts and configuration files used to perform the DSHA calculations in this study are publicly available at https://es.mathworks.com/matlabcentral/fileexchange/183034-dsha.~~from the corresponding author upon reasonable request.~~ OpenQuake (OQ) engine code is publicly available at~~in~~ https://www.globalquakemodel.org/product/openquake-engine.

Data availability

This work used publicly available ESHM20 datasets (accessible via https://doi.org/10.12686/ESHM20-MAIN-DATASETS and https://doi.org/10.12686/ESHM20-OQ-INPUT).

Author contributions

AJRB, CPB and M~~L~~LI: investigation. AJRB and CPB: conceptualization. AJRB and CPB: data preparation. AJRB and CPB: methodology. AJRB and CPB: software. AJRB and CPB: formal analysis. AJRB: writing (original draft). AJRB, CPB and ML~~L~~I: writing (review and editing). AJRB, CPB and ML~~L~~I: visualization. CPB and ML~~L~~I: supervision. ML~~L~~I: validation.

Competing interests

The authors have no relevant competitive or financial interests to disclose.

Acknowledgements

The authors would like to express their gratitude to João Fonseca and Alexandra Carvalho, whose suggestions helped improve and clarify this manuscript. We would also like to thank Dr. Laurentiu Danciu and Professor Giuliano Panza for their comments. The Open Access publishing for this study has been covered thanks to a CSIC agreement with Copernicus Publications. Thanks to the EMODnet Bathymetry Consortium (2020), EMODnet Digital Bathymetry (DTM) (https://doi.org/10.12770/bb6a87dd-e579-4036-abe1-e649cea9881a) to allow the download and use of the current EMODnet DTM version of December 2020, which has a resolution of 1/16 * 1/16 arc minutes.

References

AEIS-IGN: Seminario sobre criterios sísmicos para centrales nucleares y obras públicas: Madrid, 29-30 de marzo de 1978, Asoc. Esp. Ing. Sísmica AEIS Inst. Geográfico Nac. IGN, 1979.

Ang, A. H. and Tang, W. H.: Probability Concepts in Engineering Planning: Emphasis on Applications to Civil and Environmental Engineering, John Wiley and Sons, 2007.

Submarine Cable Map: https://www.submarinecablemap.com/, last access: 11 February 2025.

Atik, L. A., Abrahamson, N., Bommer, J. J., Scherbaum, F., Cotton, F., and Kuehn, N.: The Variability of Ground-Motion Prediction Models and Its Components, Seismol. Res. Lett., 81, 794–801, https://doi.org/10.1785/gssrl.81.5.794, 2010.

Ayadi, A. and Bezzeghoud, M.: Seismicity of Algeria from 1365 to 2013: Maximum Observed Intensity Map (MOI2014), Seismol. Res. Lett., 86, 236–244, https://doi.org/10.1785/0220140075, 2014.

Báez, J. C., Vázquez, J.-T., Camiñas, J. A., and Malouli Idrissi, M. (Eds.): Alboran Sea - Ecosystems and Marine Resources, Springer International Publishing, Cham, https://doi.org/10.1007/978-3-030-65516-7, 2021.

Barani, S., Albarello, D., Massa, M., and Spallarossa, D.: Influence of Twenty Years of Research on Ground-Motion Prediction Equations on Probabilistic Seismic Hazard in Italy, Bull. Seismol. Soc. Am., 107, 240–255, https://doi.org/10.1785/0120150276, 2016.

Basili, R., Danciu, L., Beauval, C., Sesetyan, K., Vilanova, S. P., Adamia, S., Arroucau, P., Atanackov, J., Baize, S., Canora, C., Caputo, R., Carafa, M. M. C., Cushing, E. M., Custódio, S., Demircioglu Tumsa, M. B., Duarte, J. C., Ganas, A., García-Mayordomo, J., Gómez de la Peña, L., Gràcia, E., Jamšek Rupnik, P., Jomard, H., Kastelic, V., Maesano, F. E., Martín-Banda, R., Martínez-Loriente, S., Neres, M., Perea, H., Šket Motnikar, B., Tiberti, M. M., Tsereteli, N., Tsironi, V., Vallone, R., Vanneste, K., Zupančič, P., and Giardini, D.: The European Fault-Source Model 2020 (EFSM20): geologic input data for the European Seismic Hazard Model 2020, Nat. Hazards Earth Syst. Sci., 24, 3945–3976, https://doi.org/10.5194/nhess-24-3945-2024, 2024.

Benfedda, A., Bouhadad, Y., Boughacha, M. S., Guessoum, N., Abbes, K., and Bezzeghoud, M.: The Oran January 9th (Mw 4.7) and June 6th, 2008 (Mw 5.4) earthquakes: Seismological study and seismotectonic implication, J. Afr. Earth Sci., 169, 103896, https://doi.org/10.1016/j.jafrearsci.2020.103896, 2020.

Benito, B. and Jiménez, E.: Peligrosidad sísmica, Física Tierra, 11, 13–47, 1999.

Ben-Zion, Y., Lee, W. H. K., Kanamori, H., Jennings, P. C., and Kisslinger, C.: Key formulas in earthquake seismology, Int. Handb. Earthq. Eng. Seismol., 81, 1857–1875, 2003.

Boore, D. M. and Smith, C. E.: Analysis of earthquake recordings obtained from the Seafloor Earthquake Measurement System (SEMS) instruments deployed off the coast of southern California, Bull. Seismol. Soc. Am., 89, 260–274, https://doi.org/10.1785/BSSA0890010260, 1999.

BSSC: NEHRP recommended provisions for seismic regulations for new buildings and other structures (FEMA 450). Part 1: Provisions., Build. Seism. Saf. Counc. BSSC Natl. Inst. Build. Sci. Wash. DC USA, 2004.

Budnitz, R. J., Apostolakis, G., and Boore, D. M.: Recommendations for probabilistic seismic hazard analysis: Guidance on uncertainty and use of experts, US Nuclear Regulatory Commission (NRC), Washington, DC (United States). Div. of Engineering Technology; Lawrence Livermore National Lab. (LLNL), Livermore, CA (United States); Electric Power Research Inst. (EPRI), Palo Alto, CA (United States); US Department of Energy (USDOE), Washington DC (United States), https://doi.org/10.2172/479072, 1997.

Buforn, E. and Udías, A.: Sismicidad y mecanismo focal de los terremotos de la región Cabo de San Vicente-Argelia, Rev. Soc. Geológica Esp., 20, 301–310, 2007.

Buforn, E., Sanz de Galdeano, C., and Udías, A.: Seismotectonics of the Ibero-Maghrebian region, Tectonophysics, 248, 247–261, https://doi.org/10.1016/0040-1951(94)00276-F, 1995.

Buforn, E., Udías, A., and Pro, C.: Large Earthquakes at the Ibero-Maghrebian Region: Basis for an EEWS, Pure Appl. Geophys., 172, 2387–2396, https://doi.org/10.1007/s00024-014-0954-0, 2015.

Buforn, E., Udías, A., and Pro, C.: Source mechanism studies of earthquakes in the Ibero-Maghrebian region and their tectonic implications, J. Seismol., 20, 1075–1088, https://doi.org/10.1007/s10950-015-9551-7, 2016.

Burden, R. L., Faires, J. D., and Burden, A. M.: Numerical Analysis, Cengage Learning, 918 pp., 2015.

Campbell, K. W. and Bozorgnia, Y.: Updated Near-Source Ground-Motion (Attenuation) Relations for the Horizontal and Vertical Components of Peak Ground Acceleration and Acceleration Response Spectra, Bull. Seismol. Soc. Am., 93, 314–331, https://doi.org/10.1785/0120020029, 2003.

Candia, G., Macedo, J., Jaimes, M. A., and Magna-Verdugo, C.: A New State-of-the-Art Platform for Probabilistic and Deterministic Seismic Hazard Assessment, Seismol. Res. Lett., 90, 2262–2275, https://doi.org/10.1785/0220190025, 2019.

CEN: Eurocode 8: design of structures for earthquake resistance—part 1: general rules, seismic actions and rules for buildings., Eur. Comm. Stand. CEN Bruss., BS EN 1998–1:2004: E, 219, 2004.

Chen, B., Wang, D., Li, H., Sun, Z., and Shi, Y.: Characteristics of Earthquake Ground Motion on the Seafloor, Journal of Earthquake Engineering, 19, 874–904, https://doi.org/10.1080/13632469.2015.1006344, 2015.

Chen, B., Wang, B., Ma, Z., Du, Y., and Li, C.: Influence of seawater depth on offshore ground motion characteristics and seismic responses of sea-crossing cable-stayed bridges, Ocean Eng., 280, 114853, https://doi.org/10.1016/j.oceaneng.2023.114853, 2023.

Chen, B., Wang, B., Hu, S., and Bi, K.: The influence of seabed on offshore ground motion, Soil Dyn. Earthq. Eng., 179, 108567, https://doi.org/10.1016/j.soildyn.2024.108567, 2024a.

Chen, W., Lin, J., Zheng, Y., Su, L., Chen, G., and Huang, L.: Nonlinear seismic response of seabed with terrain variation and seawater-seabed coupling, Soil Dyn. Earthq. Eng., 180, 108579, https://doi.org/10.1016/j.soildyn.2024.108579, 2024b.

Chen, Y.-S., Weatherill, G., Pagani, M., and Cotton, F.: A transparent and data-driven global tectonic regionalization model for seismic hazard assessment, Geophys. J. Int., 213, 1263–1280, https://doi.org/10.1093/gji/ggy005, 2018.

Chester, D. K.: The 1755 Lisbon earthquake, Prog. Phys. Geogr. Earth Environ., 25, 363–383, https://doi.org/10.1177/030913330102500304, 2001.

Coles, S.: An Introduction to Statistical Modeling of Extreme Values, Springer, London, https://doi.org/10.1007/978-1-4471-3675-0, 2001.

Coppersmith, K. J. and Youngs, R. R.: Capturing uncertainty in probabilistic seismic hazard assessments within intraplate tectonic environments, in: Proceedings of the Third US national conference on earthquake engineering, 301–312, 1986.

Cornell, C. A.: Engineering seismic risk analysis, Bull. Seismol. Soc. Am., 58, 1583–1606, https://doi.org/10.1785/BSSA0580051583, 1968.

Cornell, C. A., Howells, D. A., Haigh, I. P., and Taylor, C.: Probabilistic analysis of damage to structures under seismic loads, Dyn. Waves Civ. Eng., 473–488, 1971.

Crespo, M. J., Martínez, F., and Martí, J.: Seismic hazard of the Iberian Peninsula: evaluation with kernel functions, Nat. Hazards Earth Syst. Sci., 14, 1309–1323, https://doi.org/10.5194/nhess-14-1309-2014, 2014.

Custódio, S., Lima, V., Vales, D., Cesca, S., and Carrilho, F.: Imaging active faulting in a region of distributed deformation from the joint clustering of focal mechanisms and hypocentres: Application to the Azores–western Mediterranean region, Tectonophysics, 676, 70–89, https://doi.org/10.1016/j.tecto.2016.03.013, 2016.

D'Acremont, E., Lafuerza, S., Rabaute, A., Lafosse, M., Jollivet Castelot, M., Gorini, C., Alonso, B., Ercilla, G., Vazquez, J. T., Vandorpe, T., Juan, C., Migeon, S., Ceramicola, S., Lopez-Gonzalez, N., Rodriguez, M., El Moumni, B., Benmarha, O., and Ammar, A.: Distribution and origin of submarine landslides in the active margin of the southern Alboran Sea (Western Mediterranean Sea), Mar. Geol., 445, 106739, https://doi.org/10.1016/j.margeo.2022.106739, 2022.

Danciu, L., Nandan, S., Reyes, C. G., Basili, R., Weatherill, G., Beauval, C., Rovida, A., Vilanova, S., Sesetyan, K., and Bard, P.-Y.: The 2020 update of the European Seismic Hazard Model-ESHM20: Model Overview, EFEHR Tech. Rep., 1, https://doi.org/10.3929/ethz-b-000590386, 2021a.

Danciu, L., Nandan, S., Reyes, C., Basili, R., Weatherill, G., Beauval, C., Rovida, A., Vilanova, S., Şeşetyan, K., Bard, P.-Y., Cotton, F., Wiemer, S., and Giardini, D.: Main Datasets of the 2020 Update of the European Seismic Hazard Model (ESHM20) [Data set], EFEHR Eur. Facil. Earthq. Hazard Risk, https://doi.org/10.12686/ESHM20-MAIN-DATASETS, 2021b.

Danciu, L., Nandan, S., Reyes, C., Wiemer, S., and Giardini, D.: OpenQuake Input Files for the 2020 Update of the European Seismic Hazard Model (ESHM20) [Data set], EFEHR Eur. Facil. Earthq. Hazard Risk, https://doi.org/10.12686/ESHM20-OQ-INPUT, 2021c.

Danciu, L., Giardini, D., Weatherill, G., Basili, R., Nandan, S., Rovida, A., Beauval, C., Bard, P.-Y., Pagani, M., Reyes, C. G., Sesetyan, K., Vilanova, S., Cotton, F., and Wiemer, S.: The 2020 European Seismic Hazard Model: overview and results, Nat. Hazards Earth Syst. Sci., 24, 3049–3073, https://doi.org/10.5194/nhess-24-3049-2024, 2024.

Dhakal, Y. P. and Kunugi, T.: Preliminary analysis of nonlinear site response at the S-net seafloor sites during three Mw 7 class earthquakes, Front. Earth Sci., 11, https://doi.org/10.3389/feart.2023.1180289, 2023.

Dhakal, Y. P., Kunugi, T., Suzuki, W., Kimura, T., Morikawa, N., and Aoi, S.: Strong Motions on Land and Ocean Bottom: Comparison of Horizontal PGA, PGV, and 5% Damped Acceleration Response Spectra in Northeast Japan and the Japan Trench Area, Bull. Seismol. Soc. Am., 111, 3237–3260, https://doi.org/10.1785/0120200368, 2021.

Dhakal, Y. P., Kubo, H., and Kunugi, T.: Prediction Equations for Peak-Ground Accelerations and Velocities in Northeast Japan Using the S-net Data, J. Disaster Res., 19, 760–771, https://doi.org/10.20965/jdr.2024.p0760, 2024.

Diao, H., Hu, J., and Xie, L.: Effect of seawater on incident plane P and SV waves at ocean bottom and engineering characteristics of offshore ground motion records off the coast of southern California, USA, Earthq. Eng. Eng. Vib., 13, 181–194, https://doi.org/10.1007/s11803-014-0222-4, 2014.

Douglas, J.: Ground motion prediction equations 1964–2020, Dept Civ. Env. Eng Univ Strathclyde Glas. UK, 670, 2020.

EPRI: Seismic hazard methodology for the central and eastern United States, Seysmicity Own. Group Electr. Power Res. Inst. EPRI, P101-38-45–46, 2256–14, Report NP-472, 1987.

Epstein, B. and Lomnitz, C.: A Model for the Occurrence of Large Earthquakes, Nature, 211, 954–956, https://doi.org/10.1038/211954b0, 1966.

Ercilla, G., Casas, D., Alonso, B., Casalbore, D., Galindo-Zaldívar, J., García-Gil, S., Martorelli, E., Vázquez, J.-T., Azpiroz-Zabala, M., DoCouto, D., Estrada, F., Fernández-Puga, M. C., González-Castillo, L., González-Vida, J. M., Idárraga-García, J., Juan, C., Macías, J., Madarieta-Txurruka, A., Nespereira, J., Palomino, D., Sánchez-Guillamón, O., Tendero-Salmerón, V., Teixeira, M., Valencia, J., and Yenes, M.: Offshore Geological Hazards: Charting the Course of Progress and Future Directions, Oceans, 2, 393–428, https://doi.org/10.3390/oceans2020023, 2021.

Fernandes, R. M. S., Miranda, J. M., Meijninger, B. M. L., Bos, M. S., Noomen, R., Bastos, L., Ambrosius, B. A. C., and Riva, R. E. M.: Surface velocity field of the Ibero-Maghrebian segment of the Eurasia-Nubia plate boundary, Geophys. J. Int., 169, 315–324, https://doi.org/10.1111/j.1365-246X.2006.03252.x, 2007.

Fonseca, J. F. B. D.: A Reassessment of the Magnitude of the 1755 Lisbon Earthquake, Bull. Seismol. Soc. Am., 110, 1–17, https://doi.org/10.1785/0120190198, 2020.

García Mayordomo, J.: Creación de un modelo de zonas sismogénicas para el cálculo del Mapa de Peligrosidad Sísmica de España, CSIC - Instituto Geológico y Minero de España (IGME), 2015.

García-Fernández, M., Vaccari, F., Jiménez, M.-J., Magrin, A., Romanelli, F., and Panza, G. F.: Chapter 24 - Regional application of the NDSHA approach for continental seismogenic sources in the Iberian Peninsula, in: Earthquakes and Sustainable Infrastructure, edited by: Panza, G. F., Kossobokov, V. G., Laor, E., and De Vivo, B., Elsevier, 491–514, https://doi.org/10.1016/B978-0-12-823503-4.00006-3, 2022.

GEBCO Bathymetric Compilation Group 2024: The GEBCO_2024 Grid - a continuous terrain model of the global oceans and land. NERC EDS British Oceanographic Data Centre NOC., https://doi.org/10.5285/1c44ce99-0a0d-5f4f-e063-7086abc0ea0f, 2024.

Goded, T., Buforn, E., and Muñoz, D.: The 1494 and 1680 Málaga (Southern Spain) Earthquakes, Seismol. Res. Lett., 79, 707–715, https://doi.org/10.1785/gssrl.79.5.707, 2008.

Gonzalez-Castillo, L., Galindo-Zaldivar, J., de Lacy, M. C., Borque, M. J., Martinez-Moreno, F. J., García-Armenteros, J. A., and Gil, A. J.: Active rollback in the Gibraltar Arc: Evidences from CGPS data in the western Betic Cordillera, Tectonophysics, 663, 310–321, https://doi.org/10.1016/j.tecto.2015.03.010, 2015.

Grasso, S. and Maugeri, M.: The Seismic Microzonation of the City of Catania (Italy) for the Etna Scenario Earthquake (M = 6.2) of 20 February 1818, Earthq. Spectra, 28, 573–594, https://doi.org/10.1193/1.4000013, 2012.

Grevemeyer, I., Lange, D., Villinger, H., Custódio, S., and Matias, L.: Seismotectonics of the Horseshoe Abyssal Plain and Gorringe Bank, eastern Atlantic Ocean: Constraints from ocean bottom seismometer data, J. Geophys. Res. Solid Earth, 122, 63–78, https://doi.org/10.1002/2016JB013586, 2017.

Guo, Z., Hong, Y., and Jeng, D.-S.: Structure–Seabed Interactions in Marine Environments, J. Mar. Sci. Eng., 9, 972, https://doi.org/10.3390/jmse9090972, 2021.

Gutscher, M.-A., Malod, J., Rehault, J.-P., Contrucci, I., Klingelhoefer, F., Mendes-Victor, L., and Spakman, W.: Evidence for active subduction beneath Gibraltar, Geology, 30, 1071–1074, https://doi.org/10.1130/0091-7613(2002)030<1071:EFASBG>2.0.CO;2, 2002.

Hamidatou, M., Hallal, N., Lebdioui, S., Agius, M. R., and Sawires, R.: Probabilistic and Deterministic Seismic Hazard Assessments for Northeast Algeria: Insights into the Damaging Impact of the August 7, 2020 (Mw 5.0) Mila Earthquake, Pure Appl. Geophys., https://doi.org/10.1007/s00024-024-03593-y, 2024.

Herraiz, M., De Vicente, G., Lindo-Ñaupari, R., Giner, J., Simón, J. L., González-Casado, J. M., Vadillo, O., Rodríguez-Pascua, M. A., Cicuéndez, J. I., Casas, A., Cabañas, L., Rincón, P., Cortés, A. L., Ramírez, M., and Lucini, M.: The recent (upper Miocene to Quaternary) and present tectonic stress distributions in the Iberian Peninsula, Tectonics, 19, 762–786, https://doi.org/10.1029/2000TC900006, 2000.

Hu, J., Tan, J., and Zhao, J. X.: New GMPEs for the Sagami Bay Region in Japan for Moderate Magnitude Events with Emphasis on Differences on Site Amplifications at the Seafloor and Land Seismic Stations of K-NET, Bull. Seismol. Soc. Am., 110, 2577–2597, https://doi.org/10.1785/0120190305, 2020.

Hu, J., Zhang, W., Hu, L., Ding, L., and Tan, J.: Regional offshore ground motion prediction model from a referenced empirical approach: A case study in the Japan Trench area, Soil Dyn. Earthq. Eng., 174, 108196, https://doi.org/10.1016/j.soildyn.2023.108196, 2023.

Hu, L., Li, Y., and Ji, S.: An offshore non-ergodic ground motion model for subduction earthquakes in Japan Trench area, Earthq. Spectra, 40, 379–419, https://doi.org/10.1177/87552930231207118, 2024.

Idriss, I.: Earthquake Ground Motions at Soft Soil Sites, Int. Conf. Recent Adv. Geotech. Earthq. Eng. Soil Dyn., 1991.

IGN: National Geographic Institute (IGN). Geology and tectonics of Gulf of Cadiz, https://www.ign.es/web/resources/sismologia/tproximos/sismotectonica/pag_sismotectonicas/golfocadiz.html, 2025a.

IGN: National Geographic Institute (IGN). Geology and tectonics of Alboran basin, https://www.ign.es/web/resources/sismologia/tproximos/sismotectonica/pag_sismotectonicas/alboran.html, 2025b.

IGN: National Geographic Institute (IGN). Spanish Seismic Catalogue., https://doi.org/10.7419/162.03.2022, 2025c.

IGN-UPM: Actualización de mapas de peligrosidad sísmica de España 2012, Inst. Geográfico Nac. IGN, 267, https://doi.org/10.7419/162.05.2017, 2017.

Kanazawa, T.: Japan Trench earthquake and tsunami monitoring network of cable-linked 150 ocean bottom observatories and its impact to earth disaster science, in: 2013 IEEE International Underwater Technology Symposium (UT), 2013 IEEE International Underwater Technology Symposium (UT), 1–5, https://doi.org/10.1109/UT.2013.6519911, 2013.

Kanazawa, T., Uehira, K., Mochizuki, M., Shinbo, T., Fujimoto, H., Noguchi, S., Kunugi, T., Shiomi, K., Aoi, S., and Matsumoto, T.: S-net project, cabled observation network for earthquakes and tsunamis, Abstract WE2B–3 presented at SubOptic 2016, Suboptic, Dubai, 18–21 April, 2016.

Kariche, J., Meghraoui, M., Timoulali, Y., Cetin, E., and Toussaint, R.: The Al Hoceima earthquake sequence of 1994, 2004 and 2016: Stress transfer and poroelasticity in the Rif and Alboran Sea region, Geophys. J. Int., 212, 42–53, https://doi.org/10.1093/gji/ggx385, 2018.

Karthigeyan, V.: A review of current practice and future trends in the design of offshore installations to withstand seismic hazard, in: Seismic Design and Practice into the Next Century, Routledge, London, 2022.

Kee, T. K., Cheok, C. J., Kamarudin, M. A., Ahmad, S. W., and Suryanti, R.: Seismic Effect of the Offshore Structure Under Different Earthquake Loadings, Int. J. Integr. Eng., 15, 256–262, https://doi.org/10.30880/ijie.2023.15.02.025, 2023.

Khellafi, A. M., Harichane, Z., Afra, H., and Sadouki, A.: A Case Study of Accelerometric Records Analysis of May 21st, 2003, Boumerdes (Algeria) Earthquake, Int. J. Geotech. Earthq. Eng. IJGEE, 4, 34–52, https://doi.org/10.4018/ijgee.2013070103, 2013.

Kijko, A.: Seismic Hazard, in: Encyclopedia of Solid Earth Geophysics, edited by: Gupta, H. K., Springer International Publishing, Cham, 1–14, https://doi.org/10.1007/978-3-030-10475-7_10-1, 2019.

Kiureghian, A. D. and Ditlevsen, O.: Aleatory or epistemic? Does it matter?, Struct. Saf., 31, 105–112, https://doi.org/10.1016/j.strusafe.2008.06.020, 2009.

Kossobokov, V. and Panza, G.: Seismic roulette: Hazards and risks, Terra Nova, 34, 475–494, https://doi.org/10.1111/ter.12617, 2022.

Kotha, S. R., Weatherill, G., Bindi, D., and Cotton, F.: A regionally-adaptable ground-motion model for shallow crustal earthquakes in Europe, Bull. Earthq. Eng., 18, 4091–4125, https://doi.org/10.1007/s10518-020-00869-1, 2020.

Kramer, S. L.: Geotechnical Earthquake Engineering, Prentice-Hall Civ. Eng. Eng. Mech. Ser. Prentice Hall Up. Saddle River, 653, 1996.

Krinitzsky, E. L.: Deterministic versus probabilistic seismic hazard analysis for critical structures, Eng. Geol., 40, 1–7, https://doi.org/10.1016/0013-7952(95)00031-3, 1995.

Krinitzsky, E. L.: How to obtain earthquake ground motions for engineering design, Eng. Geol., 65, 1–16, https://doi.org/10.1016/S0013-7952(01)00098-9, 2002.

Kumar, V., Khan, P. K., Sarkar, R., and Pal, S. K.: Seismic hazard assessment of Faizabad region of Uttar Pradesh, India, utilizing deterministic and probabilistic approaches, J. Earth Syst. Sci., 134, 8, https://doi.org/10.1007/s12040-024-02451-8, 2024.

Lafuerza, S., Sultan, N., Canals, M., Lastras, G., Cattaneo, A., Frigola, J., Costa, S., and Berndt, C.: Failure mechanisms of Ana Slide from geotechnical evidence, Eivissa Channel, Western Mediterranean Sea, Mar. Geol., 307–310, 1–21, https://doi.org/10.1016/j.margeo.2012.02.010, 2012.

Lan, J., Liu, J., and Song, X.: Study on the influence of the seafloor soft soil layer on seismic ground motion, Nat. Hazards Earth Syst. Sci., 21, 577–585, https://doi.org/10.5194/nhess-21-577-2021, 2021.

Leprêtre, R., Frizon de Lamotte, D., Combier, V., Gimeno-Vives, O., Mohn, G., and Eschard, R.: The Tell-Rif orogenic system (Morocco, Algeria, Tunisia) and the structural heritage of the southern Tethys margin, BSGF-Earth Sci. Bull., 189, 10, https://doi.org/10.1051/bsgf/2018009, 2018.

Li, C., Diao, Y.-C., Li, R.-H., Pan, H.-Y., Han, Q., and Li, H.-N.: Effect of soil spatial variability on characteristics of depth-varying multi-support seismic motions at offshore sites, Soil Dyn. Earthq. Eng., 174, 108195, https://doi.org/10.1016/j.soildyn.2023.108195, 2023.

Liu, H., Yang, Y., and Peng, J.: A Unified Model for Analyzing Comprehensive Behaviors of Deepwater Anchors, J. Mar. Sci. Eng., 9, 913, https://doi.org/10.3390/jmse9080913, 2021.

López Arroyo, A. and Udías, A.: Aftershock sequence and focal parameters of the February 28, 1969 earthquake of the Azores-Gibraltar fracture zone, Bull. Seismol. Soc. Am., 62, 699–719, https://doi.org/10.1785/BSSA0620030699, 1972.

Martín Míguez, B., Novellino, A., Vinci, M., Claus, S., Calewaert, J.-B., Vallius, H., Schmitt, T., Pititto, A., Giorgetti, A., Askew, N., Iona, S., Schaap, D., Pinardi, N., Harpham, Q., Kater, B. J., Populus, J., She, J., Palazov, A. V., McMeel, O., Oset, P., Lear, D., Manzella, G. M. R., Gorringe, P., Simoncelli, S., Larkin, K., Holdsworth, N., Arvanitidis, C. D., Molina Jack, M. E., Chaves Montero, M. del M., Herman, P. M. J., and Hernandez, F.: The European Marine Observation and Data Network

(EMODnet): Visions and Roles of the Gateway to Marine Data in Europe, Front. Mar. Sci., 6, https://doi.org/10.3389/fmars.2019.00313, 2019.

Martín-Dávila, J. and Pazos, A.: Sismicidad del Golfo de Cadiz y zonas adyacentes, Física Tierra ISSN 0214-4557 Nº 15 2003 Pags 189-210, 2003.

Martínez-Loriente, S., Gràcia, E., Bartolome, R., Sallarès, V., Connors, C., Perea, H., Lo Iacono, C., Klaeschen, D., Terrinha, P., Dañobeitia, J. J., and Zitellini, N.: Active deformation in old oceanic lithosphere and significance for earthquake hazard: Seismic imaging of the Coral Patch Ridge area and neighboring abyssal plains (SW Iberian Margin), Geochem. Geophys. Geosystems, 14, 2206–2231, https://doi.org/10.1002/ggge.20173, 2013.

Mayer, L., Jakobsson, M., Allen, G., Dorschel, B., Falconer, R., Ferrini, V., Lamarche, G., Snaith, H., and Weatherall, P.: The Nippon Foundation—GEBCO Seabed 2030 Project: The Quest to See the World's Oceans Completely Mapped by 2030, Geosciences, 8, 63, https://doi.org/10.3390/geosciences8020063, 2018.

McGuire, R. K.: FORTRAN computer program for seismic risk analysis, US Geological Survey, 1976.

McGuire, R. K.: Seismic hazard and risk analysis, Earthquake Engineering Research Institute, Berkeley, 2004.

McGuire, R. K.: Probabilistic seismic hazard analysis: Early history, Earthq. Eng. Struct. Dyn., 37, 329–338, https://doi.org/10.1002/eqe.765, 2008.

McGuire, R. K. and Shedlock, K. M.: Statistical uncertainties in seismic hazard evaluations in the United States, Bull. Seismol. Soc. Am., 71, 1287–1308, https://doi.org/10.1785/BSSA0710041287, 1981.

Mendes-Victor, L. A., Oliveira, C. S., Azevedo, J., and Ribeiro, A.: The 1755 Lisbon Earthquake: Revisited, Springer Netherlands, Dordrecht, https://doi.org/10.1007/978-1-4020-8609-0, 2009.

Molina Palacios, S.: Sismotectónica y peligrosidad sísmica del área de contacto entre Iberia y África, http://purl.org/dc/dcmitype/Text, Universidad de Granada, 1998.

Morikawa, N. and Fujiwara, H.: A New Ground Motion Prediction Equation for Japan Applicable up to M9 Mega-Earthquake, J. Disaster Res., 8, 878–888, https://doi.org/10.20965/jdr.2013.p0878, 2013.

Mostafa, S. I., Abdelhafiez, H. E., and Abd el-aal, A. el-aziz K.: Deterministic scenarios for seismic hazard assessment in Egypt, J. Afr. Earth Sci., 160, 103655, https://doi.org/10.1016/j.jafrearsci.2019.103655, 2019.

Mourabit, T., Abou Elenean, K. M., Ayadi, A., Benouar, D., Ben Suleman, A., Bezzeghoud, M., Cheddadi, A., Chourak, M., ElGabry, M. N., Harbi, A., Hfaiedh, M., Hussein, H. M., Kacem, J., Ksentini, A., Jabour, N., Magrin, A., Maouche, S., Meghraoui, M., Ousadou, F., Panza, G. F., Peresan, A., Romdhane, N., Vaccari, F., and Zuccolo, E.: Neo-deterministic seismic hazard assessment in North Africa, J. Seismol., 18, 301–318, https://doi.org/10.1007/s10950-013-9375-2, 2014.

Musson, R. M. W.: Probability in PSHA: Reply to "Comment on 'PSHA Validated by Quasi-Observational Means' by Z. Wang," Seismol. Res. Lett., 83, 717–719, https://doi.org/10.1785/0220120036, 2012a.

Musson, R. M. W.: PSHA Validated by Quasi Observational Means, Seismol. Res. Lett., 83, 130–134, https://doi.org/10.1785/gssrl.83.1.130, 2012b.

Nakamura, T., Takenaka, H., Okamoto, T., Ohori, M., and Tsuboi, S.: Long-period ocean-bottom motions in the source areas of large subduction earthquakes, Sci. Rep., 5, 16648, https://doi.org/10.1038/srep16648, 2015.

Nakanishi, R. and Takemura, S.: Development of an offshore ground motion prediction equation for peak ground acceleration considering path effects based on S-net data, Earth Planets Space, 76, 146, https://doi.org/10.1186/s40623-024-02078-5, 2024.

Neres, M., Carafa, M. M. C., Fernandes, R. M. S., Matias, L., Duarte, J. C., Barba, S., and Terrinha, P.: Lithospheric deformation in the Africa-Iberia plate boundary: Improved neotectonic modeling testing a basal-driven Alboran plate, J. Geophys. Res. Solid Earth, 121, 6566–6596, https://doi.org/10.1002/2016JB013012, 2016.

Nishikawa, T., Ide, S., and Nishimura, T.: A review on slow earthquakes in the Japan Trench, Prog. Earth Planet. Sci., 10, 1, https://doi.org/10.1186/s40645-022-00528-w, 2023.

Nocquet, J.-M.: Present-day kinematics of the Mediterranean: A comprehensive overview of GPS results, Tectonophysics, 579, 220–242, https://doi.org/10.1016/j.tecto.2012.03.037, 2012.

NRC: Reactor site criteria. Appendix a: seismic and geology siting criteria for nuclear power plants, US Nucl. Regul. Comm. NRC Regul. Guide 10CFR100, 1973.

Olaiz, A., Álvarez Gómez, J. A., de Vicente, G., Muñoz-Martín, A., Cantavella, J. V., Custódio, S., Vales, D., and Heidbach, O.: Onshore and offshore seismotectonics of Iberia: an updated review, Solid Earth, 16, 947–1024, https://doi.org/10.5194/se-16-947-2025, 2025.

Orozova, I. M. and Suhadolc, P.: A deterministic–probabilistic approach for seismic hazard assessment, Tectonophysics, 312, 191–202, https://doi.org/10.1016/S0040-1951(99)00162-6, 1999.

Pagani, M., Monelli, D., Weatherill, G., Danciu, L., Crowley, H., Silva, V., Henshaw, P., Butler, L., Nastasi, M., Panzeri, L., Simionato, M., and Vigano, D.: OpenQuake Engine: An Open Hazard (and Risk) Software for the Global Earthquake Model, Seismol. Res. Lett., 85, 692–702, https://doi.org/10.1785/0220130087, 2014.

Palano, M., González, P. J., and Fernández, J.: Strain and stress fields along the Gibraltar Orogenic Arc: Constraints on active geodynamics, Gondwana Res., 23, 1071–1088, https://doi.org/10.1016/j.gr.2012.05.021, 2013.

Panza, G. F., Prozorov, A. G., and Suhadolc, P.: Lithosphere structure and statistical properties of seismicity in Italy and surrounding regions, J. Geodyn., 12, 189–215, https://doi.org/10.1016/0264-3707(90)90007-H, 1990.

Peresan, A., Magrin, A., Nekrasova, A., Kossobokov, V. G., and Panza, G. F.: Earthquake recurrence and seismic hazard assessment: a comparative analysis over the Italian territory, in: Proceedings of the ERES 2013 Conference. WIT transactions on the built environment, 23–34, https://doi.org/10.2495/ERES130031, 2013.

Poggi, V., Garcia-Peláez, J., Styron, R., Pagani, M., and Gee, R.: A probabilistic seismic hazard model for North Africa, Bull. Earthq. Eng., 18, 2917–2951, https://doi.org/10.1007/s10518-020-00820-4, 2020.

Ramkrishnan, R., Kolathayar, S., and Sitharam, T. G.: Probabilistic seismic hazard analysis of North and Central Himalayas using regional ground motion prediction equations, Bull. Eng. Geol. Environ., 80, 8137–8157, https://doi.org/10.1007/s10064-021-02434-9, 2021.

Randolph, M. and Gourvenec, S.: Offshore Geotechnical Engineering, CRC Press, London, 560 pp., https://doi.org/10.1201/9781315272474, 2017.

Reilly, W. I., Fredrich, G., Hein, G. W., Landau, H., Almazán, J. L., and Caturla, J. L.: Geodetic determination of crustal deformation across the Strait of Gibraltar, Geophys. J. Int., 111, 391–398, https://doi.org/10.1111/j.1365-246X.1992.tb00585.x, 1992.

Reiter, L.: Earthquake Hazard Analysis: Issues and Insights, Columbia University Press, 254 pp., 1990.

Ritsema, J., Lay, T., and Kanamori, H.: The 2011 Tohoku Earthquake, Elements, 8, 183–188, https://doi.org/10.2113/gselements.8.3.183, 2012.

Rodriguez, M., Maleuvre, C., Jollivet-Castelot, M., d'Acremont, E., Rabaute, A., Lafosse, M., Ercilla, G., Vázquez, J.-T., Alonso, B., Ammar, A., and Gorini, C.: Tsunamigenic submarine landslides along the Xauen–Tofiño banks in the Alboran Sea (Western Mediterranean Sea), Geophys. J. Int., 209, 266–281, https://doi.org/10.1093/gji/ggx028, 2017.

Román-de la Sancha, A., Silva, R., Areu-Rangel, O. S., Verduzco-Zapata, M. G., Mendoza, E., López-Acosta, N. P., Ossa, A., and García, S.: Modelling the sequential earthquake–tsunami response of coastal road embankment infrastructure, Nat. Hazards Earth Syst. Sci., 22, 2589–2609, https://doi.org/10.5194/nhess-22-2589-2022, 2022.

Rui, S., Zhang, H., Xu, H., Zha, X., Xu, M., and Shen, K.: Seabed structures and foundations related to deep-sea resource development: A review based on design and research, Deep Undergr. Sci. Eng., 3, 131–148, https://doi.org/10.1002/dug2.12042, 2024.

Sá, L. F., Morales-Esteban, A., and Neyra, P. D.: A deterministic seismic risk macrozonation of Seville, Arab. J. Geosci., 14, 2392, https://doi.org/10.1007/s12517-021-08626-7, 2021.

Salgado Gálvez, M. A., Cardona Arboleda, O. D., Carreño Tibaduiza, M. L., and Barbat Barbat, H. A.: Probabilistic seismic hazard and risk assessment in Spain: national and local level case studies, Centre Internacional de Mètodes Numèrics en Enginyeria (CIMNE), 2015.

Shan, Z., Wu, H., Ni, W., Sun, M., Wang, K., Zhao, L., Lou, Y., Liu, A., Xie, W., Zheng, X., and Guo, X.: Recent Technological and Methodological Advances for the Investigation of Submarine Landslides, J. Mar. Sci. Eng., 10, 1728, https://doi.org/10.3390/jmse10111728, 2022.

Silva, P. G., Elez, J., Giner-Robles, J., Perez-Lopez, R., Roquero, E., Rodriguez-Pascua, M., Azcárate, T., and Martínez-Graña, A.: ANÁLISIS GEOLÓGICO DEL TERREMOTO DE TORREVIEJA DE 1829 (ALICANTE, SE ESPAÑA), 2019.

Silva, V., Crowley, H., Pagani, M., Monelli, D., and Pinho, R.: Development of the OpenQuake engine, the Global Earthquake Model's open-source software for seismic risk assessment, Nat. Hazards, 72, 1409–1427, https://doi.org/10.1007/s11069-013-0618-x, 2014.

Stich, D., Batlló, J., Morales, J., Macià, R., and Dineva, S.: Source parameters of the MW= 6.1 1910 Adra earthquake (southern Spain), Geophys. J. Int., 155, 539–546, https://doi.org/10.1046/j.1365-246X.2003.02059.x, 2003.

Sultan, N., Gaudin, M., Berne, S., Canals, M., Urgeles, R., and Lafuerza, S.: Analysis of slope failures in submarine canyon heads: An example from the Gulf of Lions, J. Geophys. Res. Earth Surf., 112, https://doi.org/10.1029/2005JF000408, 2007.

Tan, J. and Hu, J.: Offshore ground motion characteristics on the horizontal PGA, spectral acceleration, frequency content and significant duration from the 2021 Mw 7.1 and 2022 Mw 7.4 offshore earthquakes near the Japan Trench area, Soil Dyn. Earthq. Eng., 164, 107646, https://doi.org/10.1016/j.soildyn.2022.107646, 2023.

Terrinha, P., Matias, L., Vicente, J., Duarte, J., Luís, J., Pinheiro, L., Lourenço, N., Diez, S., Rosas, F., Magalhães, V., Valadares, V., Zitellini, N., Roque, C., and Víctor, L. M.: Morphotectonics and strain partitioning at the Iberia–Africa plate boundary from multibeam and seismic reflection data, Mar. Geol., 267, 156–174, https://doi.org/10.1016/j.margeo.2009.09.012, 2009.

Udias, A. and Muñoz, D.: The Andalusian earthquake of 25 December 1884, Tectonophysics, 53, 291–299, https://doi.org/10.1016/0040-1951(79)90074-X, 1979.

Vázquez, J.-T., Ercilla, G., Alonso, B., Peláez, J. A., Palomino, D., León, R., Bárcenas, P., Casas, D., Estrada, F., Fernández-Puga, M. C., Galindo-Zaldívar, J., Henares, J., Llorente, M., Sánchez-Guillamón, O., d'Acremont, E., Ammar, A., Chourak, M., Fernández-Salas, L. M., López-González, N., and Lafuerza, S.: Triggering Mechanisms of Tsunamis in the Gulf of Cadiz and the Alboran Sea: An Overview, in: Historical Earthquakes, Tsunamis and Archaeology in the Iberian Peninsula, edited by: Álvarez-Martí-Aguilar, M. and Machuca Prieto, F., Springer Nature, Singapore, 65–104, https://doi.org/10.1007/978-981-19-1979-4_4, 2022.

Veiskarami, M., Neshaei, M. A. L., Karimpour Fard, M., and Pourramezan, T.: Numerical study on static and seismic stability of breakwaters on soft granular marine deposits against deep failure, Mar. Georesources Geotechnol., 35, 42–51, https://doi.org/10.1080/1064119X.2015.1099063, 2017.

Vilanova, S. P. and Fonseca, J. F. B. D.: Seismic hazard impact of the Lower Tagus Valley Fault Zone (SW Iberia), J. Seismol., 8, 331–345, https://doi.org/10.1023/B:JOSE.0000038457.01879.b0, 2004.

Vipin, K. S.: Assessment Of Seismic Hazard With Local Site Effects : Deterministic And Probabilistic Approaches, Thesis, 2013.

Wang, B., Hu, S., Song, G., and Chen, B.: The Influences of the Offshore Ground Motion and Site Factors on the Seismic Response of Immersed Tunnels, Int. J. Struct. Stab. Dyn., 24, 2450276, https://doi.org/10.1142/S0219455424502766, 2024.

Wang, J.-P., Huang, D., and Yang, Z.: Deterministic seismic hazard map for Taiwan developed using an in-house Excel-based program, Comput. Geosci., 48, 111–116, https://doi.org/10.1016/j.cageo.2012.05.014, 2012.

Wang, Z.: Seismic Hazard Assessment: Issues and Alternatives, Pure Appl. Geophys., 168, 11–25, https://doi.org/10.1007/s00024-010-0148-3, 2011.

Wang, Z.: Comment on "PSHA Validated by Quasi Observational Means" by R. M. W. Musson, Seismol. Res. Lett., 83, 714–716, https://doi.org/10.1785/0220120016, 2012.

Wang, Z. and Cobb, J. C.: A critique of probabilistic versus deterministic seismic hazard analysis with special reference to the New Madrid seismic zone, Recent Adv. North Am. Paleoseismology Neotectonics East Rock., 2012.

Weatherill, G. and Cotton, F.: A ground motion logic tree for seismic hazard analysis in the stable cratonic region of Europe: regionalisation, model selection and development of a scaled backbone approach, Bull. Earthq. Eng., 18, 6119–6148, https://doi.org/10.1007/s10518-020-00940-x, 2020.

Wössner, J., Laurentiu, D., Giardini, D., Crowley, H., Cotton, F., Grünthal, G., Valensise, G., Arvidsson, R., Basili, R., Demircioglu, M. B., Hiemer, S., Meletti, C., Musson, R. W., Rovida, A. N., Sesetyan, K., Stucchi, M., and The SHARE Consortium: The 2013 European Seismic Hazard Model: key components and results, Bull. Earthq. Eng., 13, 3553–3596, https://doi.org/10.1007/s10518-015-9795-1, 2015.

Zhang, Q. and Zheng, X. Y.: Temporal and spectral characteristics of seismic ground motions: Offshore versus onshore, Mar. Struct., 74, 102812, https://doi.org/10.1016/j.marstruc.2020.102812, 2020.

Zhao, J. X., Zhang, J., Asano, A., Ohno, Y., Oouchi, T., Takahashi, T., Ogawa, H., Irikura, K., Thio, H. K., Somerville, P. G., Fukushima, Y., and Fukushima, Y.: Attenuation Relations of Strong Ground Motion in Japan Using Site Classification Based on Predominant Period, Bull. Seismol. Soc. Am., 96, 898–913, https://doi.org/10.1785/0120050122, 2006.

Revised Manuscript (with changes marked)

Old version (nhess-2023-52)

~~Review article:~~ Deterministic seismic hazard assessment of the area comprised between west Gulf of Cádiz and east Alborán Sea

Adrián José Rosario Beltré[1,2], Carlos Paredes Bartolomé[1], Miguel Llorente Isidro[3]

[1] Department of Geological and Mining Engineering, Higher Technical School of Mines and Energy, Universidad Politécnica de Madrid (UPM), Ríos Rosas 21, 28003 Madrid, Spain
[2] Department of Geological Resources for the Ecological Transition, Geological Survey of Spain (IGME), Spanish National Research Council (CSIC), La Calera 1, 28760 Tres Cantos (Madrid), Spain
[3] Department of Geological Risk and Climatic Change, Geological Survey of Spain (IGME), Spanish National Research Council (CSIC), Rios Rosas 23, 28003 Madrid, Spain

Correspondence to: Adrián José Rosario Beltré (aj.rosario@igme.es) Carlos Paredes Bartolomé (carlos.paredes@upm.es)

Abstract. The convergence zone of the NE-SW complex at the Eurasian-Nubian plate boundary~~, comprising the Gulf of Cadiz and the Alboran Sea,~~ is frequently affected by seismic activity~~, caused by submarine long-strike fault systems and arcuate fold-thrust systems found in the region~~. This activity has caused moderate to high magnitude earthquakes and that may have triggered tsunamis either directly due to seabed elastic deformation or indirectly by triggering~~led to several tsunamigenic sources, mainly: seismogenic faults and~~ submarine landslides~~. The Spanish National Safety Strategy has identified tsunamis as a risk to National Safety~~. Tsumani~~he current~~ risk~~ is higher than~~ in the area is significant and increasing mainly because of the growing economic and social pressure on the coasts. Although seabed deformation after earthquakes in tsunami hazard has a de facto standard study approach, seismicity and submarine landslides are not well considered amongst different initiatives~~past due to increased socioeconomic development along the southern Iberian Peninsula and North African coastlines. The current revisions of tsunamis in the area includes seismic faults and submarine landslides. European initiatives have identified areas prone to submarine landslides based on seabed morphometry, but they have not considered seismic factors~~. To understand tsunamis caused by landslides, we need to consider both geomechanical properties and the spatial distribution of ~~PGA (~~Peak Ground Acceleration (PGA)~~)~~ as a triggering mechanism~~. This information is currently lacking in the seismic hazard studies conducted in the area. This study carries out a Seismic Hazard Analysis, for bedrock conditions, of the marine area between the W of the Gulf of Cadiz and the E of the Alboran Sea in the Ibero-Maghrebian region, based on a deterministic approach (DSHA), considering areal seismogenic sources. For the estimation of the deterministic seismic hazard, and to incorporate the different requirements in which the calculation must be implemented, the core of an Excel-based Visual Basic script has been used~~. This paper is the first of a series of papers to follow, showing our stepwise approach towards better understanding seismic triggers of landslides that may cause tsunamis. In this paper we present a deterministic seismic hazard approach (DSHA) preceding other approaches to be presented soon after. The idea behind testing different methods is to assess

the advantages and disadvantages of each approach to be considered as an input in landslide susceptibility. The improvements made on the script allow the 3D calculation of the DSHA on the surface of a digital terrain model (DTM), to use a logic tree type strategy with several ground motion estimation functions (GMPEs) and their uncertainties, and to solve the non-linear problem to use all the seismogenic sources in addition to the control one in the evaluation of the Peak Ground Acceleration (PGA). Our main contribution to the DSHA approach is to include a full 3D model to estimate peak ground acceleration (PGA). The results obtained show significant accelerations can be expected in the marine area along with a notable varied spatial distribution. Hence it proves the need to further and better study the seismic effects on the seabed, which are usually blanked out in seismic hazard maps. This information is essential in the assessment of slope instabilities that may cause tsunamis. that the most probable PGA ranges from 0.2 to 0.4 g, although it can reach up to 1.0 g in certain areas. These results highlight the need for a detailed study of the distribution of PGA in submarine areas, given the significant values of accelerations that can occur. This work is the first deterministic seismic hazard assessment carried out in the Ibero-Maghrebian region and aims to take a first step to promote seismic hazard studies in marine areas, whose results can provide relevant information given the implications of earthquakes in the genesis of other natural hazards such as tsunamis and submarine landslides.

1. Introduction

The areas between the Gulf of Cadiz and the Alboran Sea, or the (Ibero-Maghrebian region) is located on the Eurasian-Nubian plate boundary (Buforn et al., 2016) (Buforn et al., 1995). which It comprises the southern Iberian Peninsula and the Maghreb or (western part of North Africa) and it is characterized by active tectonics is medium to moderate active with frequent seismicity, due to the continental collision tectonic contact, where the convergence of the African and Eurasian plates converge. Major and devastating earthquakes he also been registered in the area (Buforn et al., 2015) such as This region has been the scene of several major and devastating historical earthquakes (López Casado et al., 2000). such as the Malaga earthquake of 1680 (Mw 9; Goded et al., 2008), the Torrevieja earthquake of 1829 (Mw 6.8-6.9; Silva et al., 2019), the Arenas del Rey earthquake of 1884 (Mw 6.5-6.7) and those that occurred in Adra (in 1910), Motril in 1804 (Morales et al., 2003), and the 1755 Lisbon earthquake of 1755and tsunami (Table 1). (Mw 7. 7; Fonseca, 2020) considered this as tsunamigenic. Also, there are records of Mw 6.7 and Mw 7.3 earthquakes occurred in Asnam, North Africa, in 1954 and 1980 (Bezzeghoud et al., 2017), which triggered submarine landslides and tsunamis (Papadopoulos et al., 2014).

Table 1: Location, date and magnitude of some large earthquakes in the Ibero-Maghrebian region.

Region	Location	Date	Magnitude	Casualties	Reference
Southern Iberian Peninsula	Málaga	10.09.1680	6.8	70	Goded et al. (2008)
	Lisbon	11.01.1755	7.7	100,000	Chester (2001), Fonseca (2020)
	Torrevieja, Alicante	03.21.1829	6.8 - 6.9	389	Silva et al. (2019)
	Andalusian	12.25.1884	6.5 - 6.7	839	Udias and Muñoz (1979)
	Adra, Almería	06.16.1910	6.1	-	Stich et al. (2003)
	Cape St. Vincent, Portugal	02.28.1969	7.8	19	López Arroyo and Udías (1972)
Nort Africa	Orán, Algeria	09.10.1790	6.0 - 6.5	2,000	Ayadi and Bezzeghoud (2014)
	El-Asnam, Algeria	10.10.1980	7.3	2,633	Ayadi and Bezzeghoud (2014)
	Zemmouri, Algeria	05.21.2003	6.8	2,278	Ayadi and Bezzeghoud (2014)
	El-Hoceima, Morocco	02.24.2004	6.4	629	Tahayt et al. (2009)

NowadaysTo date, the most used method is Seismic Hazard Analysis (SHA) to estimate plausible ground motions and mitigate seismic hazard and associated risks (Reiter, 1990). Currently, the two broad standard approaches to seismic hazard analysis (SHA) are Deterministic Seismic Hazard Analysis (DSHA) and Probabilistic Seismic Hazard Analysis (PSHA) (Reiter, 1990). The DSHA uses "deterministic" information during the analysis (Reiter, 1990; Kramer, 1996; Campbell, 2005), in which the largest individual earthquake defined as the maximum credible (MCE), expected or characteristic earthquake is considered; while PSHA combines probabilistic distributions of location, magnitude, recurrence, of a set of earthquakes or seismic catalogue, and the attenuation ratio (Cornell, 1968), to manage and incorporate the seismic uncertainty of the earthquake space-time-size events. These sometimes-questioned methods (Castaños and Lomnitz, 2002; Krinitzsky, 1993a, b, 2002, Kossobokov et al., 2022) remain the most widely used in regional seismic hazard assessments worldwide (Loi et al., 2018; Sinha and Sarkar, 2020) although they have also been criticised (Castaños and Lomnitz, 2002; Kossobokov and Panza, 2022). Although, the approach offered by a probabilistic assessment PSHA is currently the most widely implemented by the scientific community and seismic risk assessment and mitigation plans, the DSHA is still considered useful in "worst-case" scenario modeling situations (Grasso and Maugeri, 2012; Mostafa et al., 2019). The latter is anis type of scenario is standard procedure in emergency planning due to its conservative approach to hazardrisk estimation commonly used by civil protection systems. DSHA was the first methodology proposed in the late 1960s to assess seismic hazard in nuclear power plant design and engineering projects and was later applied to large industrial infrastructures (NRC, 1973; AEIS-IGN, 1979). This method assumes that seismicity behaves stationary by assuming that future earthquakes will occur in a similar way as they did in the past. The simplicity of its application is based on the fact that the seismic information required for its implementation uses geology and seismic history to identify earthquake sources and interpret the strongest earthquake that each source is capable of producing, regardless of time, or maximum credible or capable earthquake (MCE) (Krinitzsky, 2005). Therefore, the DSHA is a method that does not provide information on the return period of the MCE. The MCE earthquake is the largest possible occurrence along a recognised fault under currently known or assumed tectonic activity (USCOLD, 1995). However, it should be noted that DSHA and PSHA can complement each other, providing more information about the existing seismic hazard at the site under study (Wang et al., 2012).

The ~~marine zone proposed~~ test area in this work~~, comprised between the western end of the Gulf of Cadiz and the eastern end of the Alboran Sea,~~ has not been ~~specifically~~ addressed in seismic hazard studies recently~~,~~ despite its significant record of ~~the importance of the region as a generating source of~~ earthquakes, submarine landslides and tsunamis (~~Papadopoulos et al., 2014;~~ Rodríguez et al., 2017; Vázquez et al., 2022). ~~The~~Moreover, ~~-~~the first and only ~~recorded~~ attempt to assess the seismic hazard in this area was made by Molina Palacios (1998), in which the seismic hazard of the Iberia-Africa contact area was ~~assessed~~ based on a probabilistic approach. However, no DSHA ~~application~~ approaches ~~is~~ have been carried ~~available~~ out in this submarine region. The study area ~~also~~ includes some emerged ~~areas~~ land~~on its borders, ; to~~ the coastal areas of the ~~north on the~~ southern ~~coast of the~~ Iberian Peninsula and ~~to the south, on the~~ North Africa~~n coast~~. These~~, being habitable areas,~~ emerged sites do have exhaustive seismic hazard studies, using both deterministic and probabilistic approaches. Several ~~In the Iberian part, multiple probabilistic~~ studies have been conducted in the Iberian region~~arried out~~ (e.g., Crespo et al., 2014;~~ Rivas Medina, 2014;~~ Salgado Gálvez et al., 2015; IGN-UPM, 2017; Rivas-Medina et al., 2018) to assess seismic hazard using PSHA method~~date~~. Recently~~ Similarly~~, the ~~seismic hazard of the city of Seville was evaluated by Sá et al. (2021) based on a deterministic approach and a~~ Neo-deterministic Seismic Hazard Assessment (NDSHA) ~~(Panza et al., 2001; Panza and Bela, 2020)~~ has been applied ~~was recently performed~~ for the Iberian Peninsula ~~by~~ (García-Fernández et al., ~~(~~2022) and for Sevilla city (Sá et al., 2021)~~, being the first study of this type in the peninsula~~. In the North African part, ~~the most recent PSHA was performed by~~ Poggi et al. (2020) performed a PSHA, and ~~being one of the works used in this study as a data source. Regarding the SHA by deterministic approach, an NDSHA was performed by~~ Mourabit et al. (2014) also conducted an NDSHA approach in this region.

The main goal of this paper is to ~~perform a SHA, for bedrock conditions,~~ fill the gap of studying the marine area between the W of the Gulf of Cádiz and the E of the Alborán Sea, ~~based on~~ using a DSHA approach~~, considering areal seismogenic sources~~. To carry out this analysis, we have used an improved and upgraded ~~Excel-based Visual Basic script for DSHA (original simple version~~ the model from Wang et al., 2012~~)~~. ~~Also, a~~ To test the reliability of the outcomes, we have ~~comparison with studies presented on the geography of the emerged terrain within the study area,~~ compared our results in the emerged land with previous work carried out in those areas with other seismic hazard analysis techniques (e.g., NDSHA, PSHA)~~, is provided to verify and validate the results obtained in the submarine zone. This work is the first comprehensive DSHA performed in the Ibero-Maghrebian region and aims to take a first step to promote the assessment of seismic hazard in submerged areas, whose results may yield relevant information for the identification of possible seismic sources that could be tsunamigenic or triggers of submarine landslides.~~. This work is the first DSHA carried out in the Ibero-Maghrebian submarine region.

2. Seismotectonic setting of the study area

The study region ~~in this paper~~ ~~comprises the Ibero-Maghrebian band of the Gulf of Cadiz-Alboran Sea arc, located at the present-day boundary between the Eurasian and Nubian tectonic plates (West Africa). Geographically, from west to east, the region of interest (outlined with a red polygon line in~~ ~~(Fig. 1)~~ extends from ~~the Gorringe Ridge and the Horseshoe Abyssal Plain (longitude~~ 11.5ºW ~~) in the west up to the Algerian compression belt (longitude~~ to 2ºE~~)~~; from the Gorringe Ridge and the Horseshoe Abyssal plain to the Algerian compression belt (Fig. 1) ~~in the east (Fig. 1), with the Gibraltar Arc, the deformation front of the Betico-Rif orogenic belt and related structures in the centre~~ ~~(Vázquez and Vegas Martínez, 1999)~~. The northern edge is bounded from WNW to ESE at latitude 38ºN, by the Algarve region to the Guadalquivir basin~~,~~. ~~where~~ This limit ~~it~~ runs parallel to the ENE-WSW Cenozoic reverse fault line, along the southern boundary of the Guadalquivir depression with the B~~a~~etic, parallel to the Crevillente fault, ~~-~~and its extension to Cabo de la Nao, close to the Don Juan fault, the beginning of the Valencia trough. To the south, it follows the trace of the Gibraltar transform fault WNW-ESE at latitude 34ºN to the Rif~~t~~ region and from there it takes an ENE-WSW direction parallel to the Algeria's~~n~~ Mediterranean C~~c~~oast along the southern boundary of the Atlas Mountains, parallel to ~~the~~ Arzew faults, to the Algerian ~~compression belt~~Ténes and Thenia faults systems. ~~(Buforn et al., 1995).~~

The ~~structures that tectonically compose~~tectonic structures of this region are still active today as proven with seismic records. This activity also demonstrated after~~As shown by~~ geodetic data and geodynamic studies that have been carried out for decades (e.g., Buforn et al., 1995; ~~Negredo et al., 2002;~~ Soumaya et al., 2018).~~,~~ T~~t~~ectonic models of NW-SE to WNW-ESE show oblique convergence between the Nubia and Iberian plates (Reilly et al., 1992; Herraiz et al., 2000) with~~present~~ displacements of 2 to 5 mm/yr (Nocquet, 2012) of the western Betic Cordilleras with respect to the Iberian Massif (~~Koulali et al., 2011;~~ Palano et al., 2013; Gonzalez-Castillo et al., 2015). The Gulf of Cádiz and Alborán Sea basins are characterized by a complex geodynamic context resulting from the interaction between tectonic plates (Custódio et al., 2016; Neres et al., 2016). This area is highly active~~The complex geodynamic context of interaction between the Eurasian and Nubian plates characterises the tectonics affecting the seafloor of the Gulf of Cádiz (Medialdea et al., 2004; Custódio et al., 2016; Neres et al., 2016) and Alborán Sea regions, and makes it the most~~ geologically~~, active area in the~~ with~~western Mediterranean, affected by some offshore geological hazards, triggered by ground shakings, given its~~ moderate to low-moderate seismic activity.~~, as attested by~~ H~~h~~istorical cases have demonstrated the occurrence of such hazards in the region (Vázquez et al., 2022a). The plate boundary of the study area is usially divided into four main areas acording to their stress regime: the SW as simple shear zone, the pure shear Gulf of Cadiz as the Eastern Betic, and the South Moroccan compressional arc.

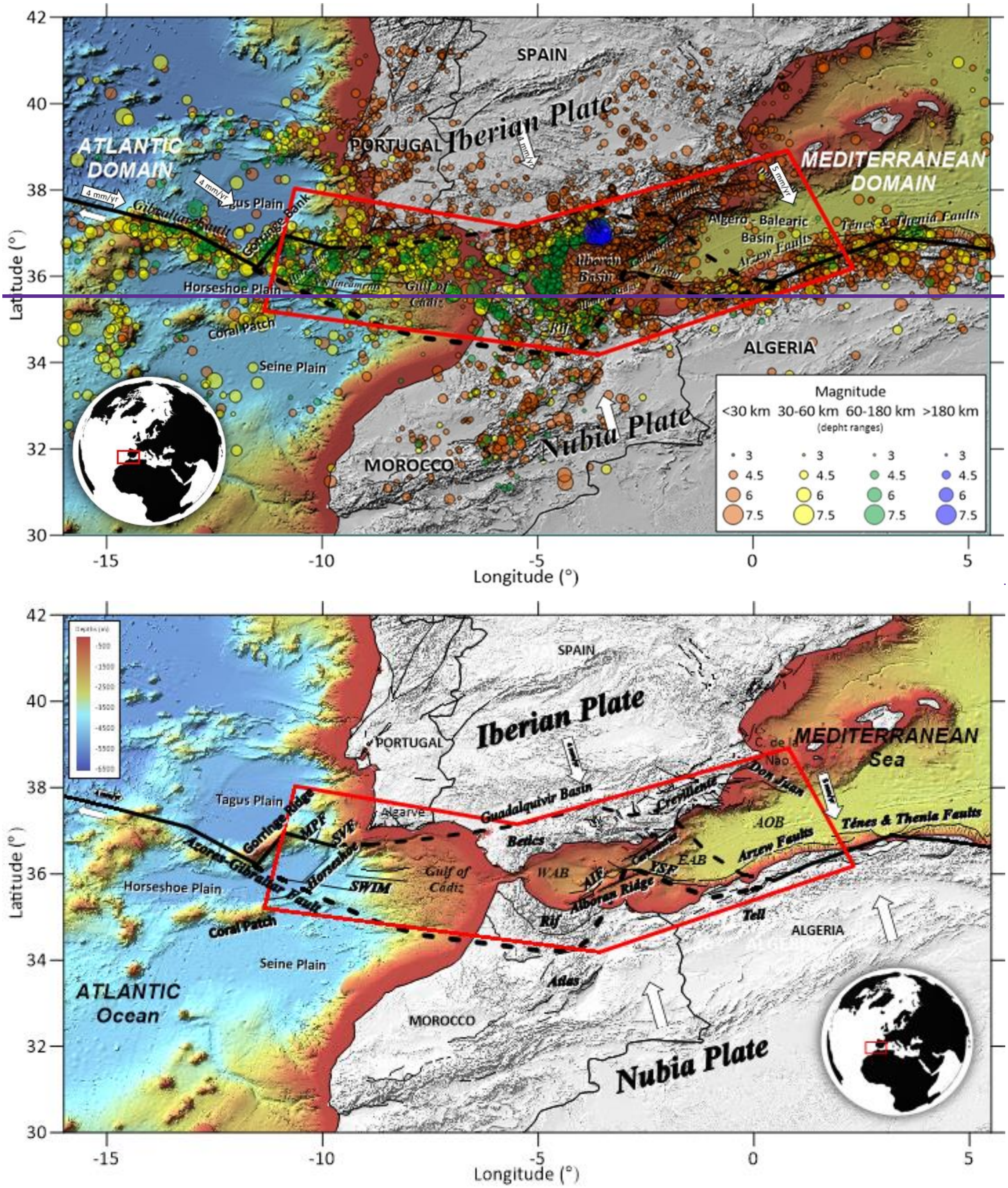
SPAIN
PORTUGAL
Iberian Plate
ATLANTIC DOMAIN
MEDITERRANEAN DOMAIN
4 mm/yr
5 mm/yr
Tagus Plain
Gorringe Bank
Gibraltar Fault
Horseshoe Plain
Gulf of Cadiz
Algero - Balearic Basin
Ténès & Thenia Faults
Arzew Faults
Alboran Basin
Rif
Coral Patch
Seine Plain
ALGERIA
MOROCCO
Nubia Plate
Magnitude
<30 km
30-60 km
60-180 km
>180 km
(depht ranges)
3
4.5
6
7.5
Latitude (°)
Longitude (°)
42
40
38
36
34
32
30
-15
-10
-5
0
5
SPAIN
PORTUGAL
Iberian Plate
MEDITERRANEAN Sea
C. de la Nao
Don Juan
Crevillente
Guadalquivir Basin
Algarve
Betics
Tagus Plain
Gorringe Ridge
MPF
SVF
Horseshoe
SWIM
Azores-Gibraltar Fault
Horseshoe Plain
Gulf of Cadiz
WAB
AIF
YSF
EAB
AOB
Alboran Ridge
Arzew Faults
Ténès & Thenia Faults
Rif
Tell
ALGERIA
Atlas
Coral Patch
Seine Plain
ATLANTIC Ocean
MOROCCO
Nubia Plate

Figure 1. -Location of the area of interest of Red polygon shows the study Ibero-Magrebi-Algerian area in -this work in relation to the tectonic setting. Abbreviations are as follows: WAB: Western Alboran Basin, EAB: Eastern Alboran Basin, AOB: Algerian Oceanic Basin, SVF: Sao Vicente Fault, MPF: Marques de Pombal fault, SWIM: Southwest Iberian Margin lineaments (1, 2 and 3). AIF: Al Idrisi fault, YSF: Yusuf fault. comprising west Gulf of Cadiz to east Alboran Basin. Simplified seismotectonic map of study area between Nubia and Iberian Plates (infered modern boundary: thick black line, white arrows: relative movement direction between plates). Earthquake epicenters located according to their magnitudes and depth (circle size and colour in legend) distribution from IGN catallogue (available from https://www.ign.es/web/ign/portal/sis-catalogo-terremotos). Background: shadowed Digital Terrain Model (altimetry and coloured bathymetry) in the study area (extracted from GEBCO; https://www.gebco.net, 2020).

The Gulf of Cadiz is located on the contact boundary between the Eurasian and African plates, . which runs, in its westernmost partIt extends, from the Azores Islands to the Strait of Gibraltar, through the Iberian massif and the Algarve basin region to the north, and, in the eastern part, through the orogenic arc of the Betic-Rifeñaenean mountain range, the westernmost of the Mediterranean alpine chains. It is characterised by a NW-SE oblique convergence regime, mainly controlled by the formation of the Betic-Rifeño Orogenne orogen range and by the accommodation of post-orogenic compressional tectonic activity (IGN, 2023). This tectonic configuration makesmeans that seismic activity in the Gulf of Cáadiz is importantsignificant, with moderately deepmainly shallow earthquakeso (h < 40 - 6030 km), but not subduction zone has bben without clearly marked (Custódio et al., 2016)ing a subduction zone., and of Some moderate magnitude earthquakes have also been recorded (Martín-Dávila and Pazos, 2003). Most of the focal mechanisms in this area are reverse and rifting type with a maximum horizontal compression in a NW-SE direction. However, tThere is also historical and instrumental evidence of several high-magnitude earthquakes in the region. These include the earthquakes of 1755, with an approximate magnitude of (Mw ~7.5; Mendes-Victor et al., 2009)8.5), and of 1969, with a magnitude of (Mw 7.8;, López Arroyo and Udías, 1972)), both which causinged a small tsunamis that affected on the coasts of Morocco, Portugal, and Spain. Geological structures such as tThe Gorringe Bank, the Saoan Vicente submarine canyon (Sao -Vicente fault), Horseshoe, Marqués de Pombal, and the Nazaré and Cadiz-AlicanteSWIM faults coincide with the areas of show the greatest seismicity in the region surrounded by the Gorringe Ridge, the Coral Patch, and the Horseshoe an Seine abysisal plains.

The Alboran Sea is the westernmost part of the Mediterranean Sea, . It is bordered both to the north and to the south by the Alpine Mmountain ranges of the Betic,, to the south of in the Iberian Peninsula, and the Rif in the north of the African continentAfrica. It is a complex contact zone between the Eurasian and Nubian tectonic plates, whoseits genesis and evolution are related to the process of convergence between these plates, due to the northward motionpush of the African plate. This process gave rise to a westward displacement of the Alboran block (a small microplate detached from the large African plate), to the formation of the Alpine mountain ranges mentioned above, and to a lithospheric thinning of the continental crust with associated volcanism present on the island of Alboran. Among the tectonic structures, the submarine mountain ranges stand out, with a length of more than 50 km, orientedwith a NE-SW orientation, and delimited to the north and south by reverse faults with opposite dip. On the other hand, there are two sets of conjugate directional faults: NNE-SSW sinistral faults such as the Al-Idrisi fault, or NE-SW faults such as the Carboneras fault,~~,~~ and NW-ESE dextral faults such as the Yusuf fault. The maximum magnitudes recorded in the Alboran Sea have lower values. ~~The most important events are the Adra earthquakes in 1910 with Mw 6.1 (Stich et al., 2003), 1994 with Mw 6.4 (e.g., El Alami et al., 1998), 2004 with Mw 6.3 (Galindo-Zaldívar et al., 2009) and 2016 with Mw 6.3 (Galindo-Zaldivar et al., 2018).~~ Also, the~~Its~~ seismic activity in the Alboran Sea is interconnected with the activity in the southern Iberian Peninsula through the complex tectonic system running E-W from the Rif and Alboran Ridge, Eastern Alboran Basin, to the Arzew faults and~~ alpine~~ Tell Atlas~~chain~~ (e.g., Mourabit el al., 2014; Lepêtre et al., 2018).

~~The Maghreb-Algerian region as far as Tunisia is a key area in the western Mediterranean to understand the active tectonics and stress pattern across the slowly converging oblique Africa-Eurasia plate boundary. Its seismic activity is interconnected with seismic activity in the Iberian Peninsula (Mantovani et al., 1989), given its location in the complex tectonic system resulting from the interaction between both plate boundaries and alternating systems of rift and reverse faults (e.g., Mourabit et al., 2014; Leprêtre et al., 2018) running E-W from the Rif in the Western Alboran Basin, eastern margin of the Strait of Gibraltar, to Tunisia along the Sardania Channel, on the Alpine Tell/African Maghrebides chain (Buforn et al., 2004; Meghraoui and Pondrelli, 2012). Its seismotectonic configuration, which forms an extensive belt of northwest African folds and thrusts and fault systems, where a complex compressional regime prevails, is what gives this region its seismicity. In particular, the current active contraction of the West Africa-Eurasia boundary is accommodated by a strike-slip fault regime with a normal component in the Alboran/Rif block, a predominantly NE-SW thrust fault with a strike-slip component in the western part of the Tell, and an E-W strike-slip fault with a reverse component along the eastern Tell and the Saharan-Tunisian Atlas (Soumaya et al., 2018), Subordinate NE-SW left-lateral strike-slip faults are also present. The seismic events and corresponding stress distribution generated by these fault systems are distributed with a general E-W trend and a NW-SE shortening component along the Africa-Eurasia plate boundary (Ousadou et al., 2014).~~

~~Large earthquakes occur in the areas of the Gulf of Cadiz-SW of Cape St. Vincent and NW of Algeria. Smaller earthquakes occur in the S and SE Iberia and N Morocco.~~ Many recorded~~The vast majority of~~ earthquakes ~~(Fig. 1)~~ have shallow foci (h < 50 km; IGN catalogue), although a significant number of earthquakes are also generated at intermediate depth (50 - 200 km) and some occur at great~~very~~ depth~~ep~~ ~~earthquakes~~ (600 - 670 km). Deep earthquakes are ~~located~~ in the province of Granada (south of Dúrcal-Alborán Sea) (Molina Palacios, 1998; Buforn and Udías, 2007). Intermediate seismicity is mainly located in the areas of the Gulf of Cadiz, mainly located within the crust up to a depth of 100 km; about 90% of the observed seismicity occurs at approximate depths up to 55-60 km in the Gorringe Bank, High Atlas and ~~in~~ the Granada-Malaga-O of~~de~~ Alboran area. In the Alboran Sea there is also significant shallow seismicity at depths of less than 30 km, especially in the active Betica-Alboran-Rif shear zone; from here onwards to the W it becomes much deeper.

3. Materials

3.1 Ocean and land digital terrain models

The mid-resolution digital terrain model (DTM) employed~~used~~ in this study was constructed ~~from a~~ after the gridded data set developed by the four Regional Centres of the Nippon Foundation-GEBCO Seabed 2030 Project (Mayer et al., 2018; GEBCO Compilation Group 2022, 2022) ~~compiled with~~ using satellite altimetry~~,~~ from the European Marine Observation and Data Network (EMODnet; http://www.emodnet.eu/).~~.~~ This global terrain model for ocean and land ~~with~~ has a spatial resolution of 15 arc seconds. ~~-~~The vertical component that the DTM incorporates, for each point over which the hazard is assessed, is used in the estimation of the relative distances, from the site to the seismogenic source, used by some of the GMPEs.

The open source DTM downloaded from GEBCO web site (Fig. 1) has been resampled by averaging to 0.1º grid resolution, corresponding to cells with approximately 10 km in latitude, to simplify the comparison of our work with previous studies. Computationally, our estimated PGA using the improved DSHA was performed on a grid of 3,854 sites, generated from the above resampled. This grid size was chosen on the basis of experience and approximately equal to the standard error in earthquake epicentre determination (Panza et al., 1990; Suhadolc, 1990). ~~is produced from version 2.4 of the SRTM15+ base grid (Tozer et al., 2019) augmented with measured and estimated seafloor topography from shipboard beam echosounders and depths predicted using satellite altimetry, from the European Marine Observation and Data Network (EMODnet; http://www.emodnet.eu/). This global continuous terrain gridded model provides elevation data (altimetry > 0 and bathymetry < 0) in metres. The GEBCO_2022 Grid compilation was carried out at the Seabed 2030 Global Centre, hosted at the National Oceanography Centre, UK.~~

~~The original DTM GEBCO grid for this paper has been downloaded over a rectangle area 12ºW 34ºN to 3ºE 39ºN (background in Fig. 1), from the Internet in netCDF (CF Compliant), Esri ASCII raster, or GeoTiff data formats. To adjust the comparison of the results obtained in this work with those obtained in the seismic hazard analysis in areas comprising the study area, the original spatial resolution of 15 arc-seconds (about 450 m x 450 m) raster file, which data values are pixel-centre registered,~~ The model ~~has been resampled by averaging to 0.1º x 0.1º grid resolution, corresponding to cells with approximately 10 km in latitude~~ ~~(Figure 1) to simplify the comparison of our work with previous studies.~~

3.2 Seismogenic Source Catalogues and Seismicity Parameters

~~Currently, the Ibero-Maghreb-Algerian region does not have its own seismogenic source zonation model that covers it in its entirety or, at least, the regions of the Gulf of Cadiz, the Alboran Sea, and North Africa as a whole, which are included in the study area of this work. However, several models already proposed and accepted by the scientific community, which, if correctly integrated, could be used to compose such a zonation. These three regions, although governed by the same regional~~

tectonic framework resulting from the oblique interaction of the Eurasiatic and Nubian-African plates, have very heterogeneous seismic and seismotectonic characteristics, resulting in a diversity of seismogenic zones when forming models to characterise the distribution of seismicity in these regions.

There are several seismogenic zonation models thatSeveral seismogenic zonation models partially cover the study area (TableFig. 2). However, there is no single seismogenic zonation that fully covers the area of interest and surrounding areas to affectively account for their effects (Fig. 2). The ZESIS or COMMISSION zonation model (García Mayordomo, 2015), used to update the seismic hazard map in Spain (IGN-UPM, 2017), whose southern boundary runs along the NW-SE Gibraltar-Azores fault to the Moroccan Rif where it takes a WSW-ENE direction, running parallel to the Algerian Mediterranean coast. Models considered for the development of the Portuguese seismic hazard map include the ERSTA (Carvalho and Malfeito, 2018) and the EC8 (CEN, 2004) whose southern edge runs similarly to the Spanish model. The zonation of the Harmonisation of Seismic Hazards in Europe Project, or SHARE project (Giardini et al., 2014; Woessner et al., 2015), designed for the 2013 Euro-Mediterranean Seismic Hazard Model (ESHM13) at the European scale for the Euro-Mediterranean region. All of these partially cover the regions of the Gulf of Cadiz and the Alboran Sea, and very slightly cover the seismogenic activity of North Africa. Therefore, the zonation for the North African region proposed by Poggi et al. (2020) has also been considered. All these models use seismogenic sources of an areal type, with the incorporation of certain active faults as independent and complementary seismogenic sources to the characterisation of the areal zones.Thus, iIn this study we opted to integrate different models into an areal seismogenic zonation model covering our studied region, analysing their compatibility. Among the previous seismic zonation models, the selected models, together with their corresponding characteristic seismic parameters, were the ZESIS (Fig. 2a) and the NAF model proposed by Poggi et al. (2020) (Fig. 2b). , These models were chosen because the ZESIS model has been used in the SHA for Spain and the NAF is the most recent model for the North African area. Additionally, both models cover geographically and almost entirely overlapping the study area of this workas they are the most recent models and are in the best geographical conditions as they overlap widely in the study area of this work., considering Iinitially, of interest the areal seismogenic sources that are within the limit (perimeter marked in red in Fig. 2) in both models were considered of interest., Byin this way, in addition to making an integrationg of both models, the NAF in the north can be complemented with the ZESIS, and the ZESIS east in the south with the NAF.

Table 2: Seismogenic zonation models partially covering the study area.

Zonation model	**Covered extension**	**Reference**	**Implementation**
ZESIS or COMMISSION	Iberian Peninsula	García Mayordomo (2015)	Seismic hazard map of Spain
SA and SB	Portugal	Vilanova and Fonseca (2007)	Seismic hazard map of Portugal
EC8 and ERSTA	Portugal	Carvalho and Malfeito (2018)	Seismic hazard map of Portugal
ESHM13 and ESHM20	Euro-Mediterranean region	Woessner et al. (2015); Danciu et al. (2021)	Seismic hazard map for Europe
NAF	North Africa	Poggi et al. (2020)	Seismic hazard map of North Africa

4. Seismic hazard assessment

Seismic hazard is -a concept commonly used to express the probability that the intensity threshold is exceeded, by one or more an earthquakes, during theoccurs in a given geographic area, within a given time period, within a region of interest and with a ground motion intensity exceeding a given threshold (McGuire, 2004; Kijko, 2019). It is generally conveyed as a year or multi-year percentage to reach or surpass certain values of peak ground distance, velocity or acceleration, distributed in an area It is generally quantified as the frequency with which the amplitude of ground motion caused by seismic events at a given point on the ground surface is exceeded during a specified period of time Seismic Hazard Analysis (SHA) performs the assessment of the expected ground motion caused by a seismic event for a given location (Kijko, 2019) by describing the potential for an earthquake related natural hazard phenomenon to occur, such as strong vibrations, soil liquefaction processes, etc. Seismic hazard can be expressed in different ways, but most often in terms of values or probability distributions of accelerations, velocities, or displacements of bedrock or ground surface. Several methods are used to assess seismic hazard. The most commonly used are DSHA, PSHA, and current variants of DSHA such as the NDSHA (Panza et al., 1996, 2001, 2012; Magrin et al., 2017; Panza and Bela, 2020). SIn DSHA, seismic hazard is defined in DSHA as the 2nd quartile or other selected percentile (e.g., 84% or 98% as used in this work) of ground motion intensity (PGA measured in g for this work) from a single earthquake or set of earthquakes, and is calculated from simple earthquake information and ground motion attenuation relationships statistics -(Krinitzsky, 1995, 2002) that assumes a particular earthquake scenario. Seismic hazard in PSHA is determined by calculating ground motion frequencies or exceedance rates using a mathematical model based on statistical earthquake (size, time and location distributions) and ground motion functionsrelationships (McGuire, 2004, 2008). This model takes into account uncertainties related to earthquake size and moment (Kramer, 1996). PSHA methods can be categorized into parametric, using the total probability theorem (Cornell, 1968; Kramer, 1996), and nonparametric methods that utilize extreme value distribution functions (Epstein and Lomnitz, 1966) in SHA. Although both SHA methods use seismological and geological information, they define and calculate seismic hazard differently, which improves the understanding of seismic hazard forecasting at the studied site or region (US NRC, 1997; Benito and Jiménez, 1999; Orozova and Suhadolc, 1999; Wang and Cobb, 2012). Theeis complementarity and practicality of the DSHA in submerged areas with uncertain and difficult to obtain information are two is one of the main reasons why in this work , in the absence of a probabilistic seismic hazard map of the entire proposed area, it has been chosen as ato start the preliminary SHA alternative to other more complex and data-intensive hazard assessment methodsstudy with the DSHA. A key component of SHAs is the ground motion attenuation equationratio, which. It account for the energy loss of the motion due to the distance travelled by the shock. Models of such Aattenuation models are referred to as ground motion prediction equations (GMPEs).

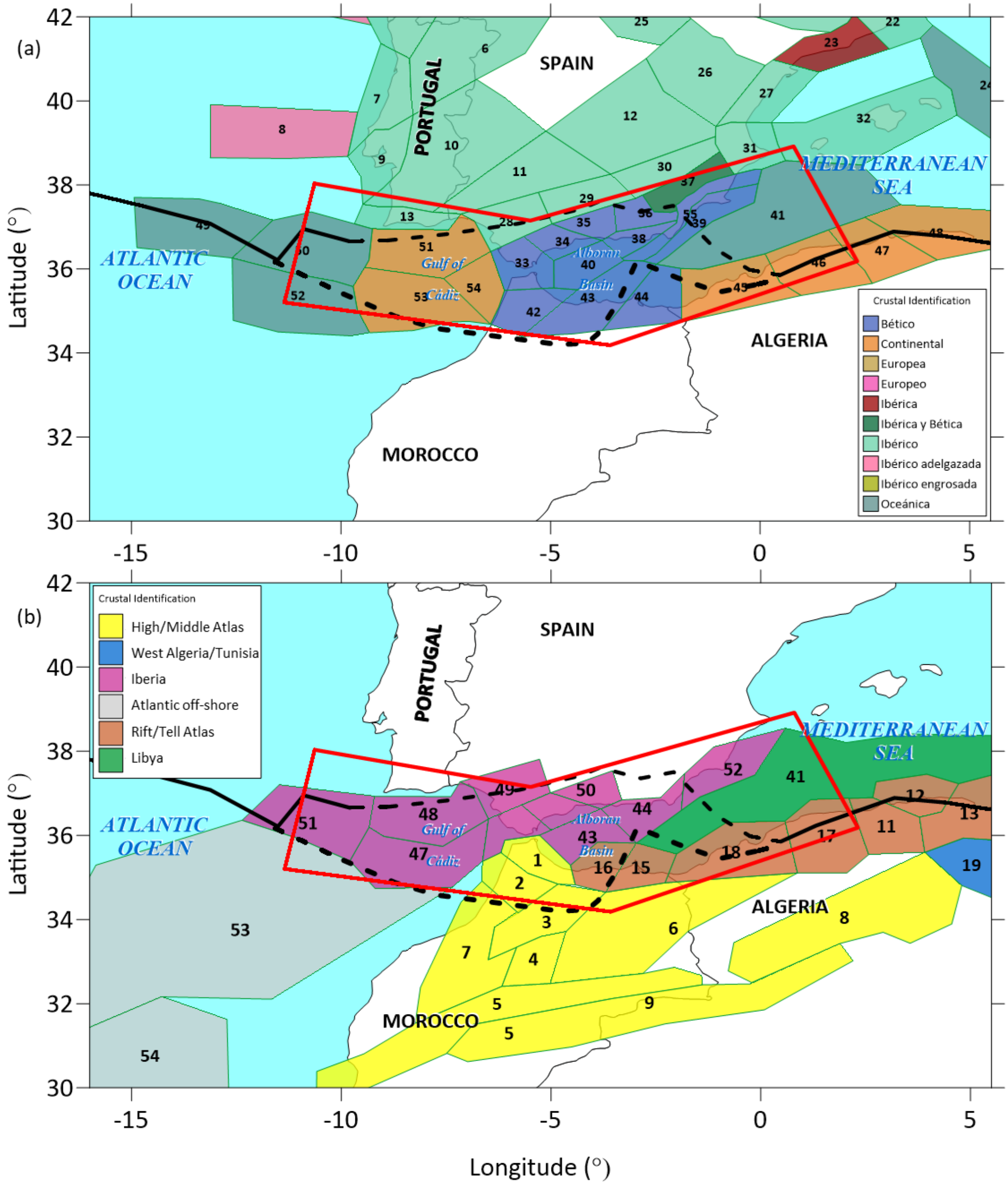

Figure 2. Seismogenic ~~zones~~ zoning in the active shallow~~stable continental~~ crustal~~ in the~~ region (~~S~~ASCR). Colours are used to represent the tectonic groups of the ~~S~~ASCR: (a) model for South Iberia (modified from ZESIS: IGN-UPM, 2017) and (b) model for North Africa (modified from NAF: Poggi et al., 2020). The number marked in each zone corresponds to its reference in the original zoning ZESIS or NAF model.

4.1 Ground motion prediction equations (GMPEs)

~~One of the most important parts of evaluating seismic hazards is determining the ground motion model, which is a mathematical formula that predicts how an earthquake will affect the ground. This formula is known as the ground motion prediction equation (GMPE). These attenuation~~ Attenuation functions are commonly derived from strong ground-motion records for an earthquake (i.e., Campbell and Bozorgnia, 2003). Functions relate the ~~of~~ magnitude M ~~occurring at~~ and the ~~a~~ distance R ~~or~~ of the seismic scenario (M,R)~~, where M is the moment magnitude, and R is the distance metric related to the energy path between the source and the site, over a range of magnitudes and distances that are meaningful for the analysis~~. With an appropriate set of quality records, it is possible to fit a parametric ~~{pi}~~ model f(M,R,ϕ_k~~{pi}~~) to estimate the intensity of strong motion (Y) for a given seismic scenario. The fitted parameters reflect the characteristics of magnitude, and distance scaling, but also near and far -source, faulting mechanism, and hanging wall effects. The ~~heterogenous~~heterogeneous geological media causes a dispersion in the ~~Due to the dispersion of the recorded data~~ ~~recorded pair~~s ~~dispersion~~ (M,R) sampled pairs. ~~, resulting from the randomness introduced by the natural environment,~~So, the correlation between variables can be strong, but never perfect, ~~so~~ that means there is an unavoidable ~~error~~ uncertainty or random deviation ε in these regression models. If the expected seismic intensity at the project site Y is interpreted as a conditional random variable on the pair (M,R), the fitted model:

$$\sim s\; Y \sim f(M,R,\phi_k \{p_i\}) + \varepsilon \qquad (1)$$

provide an estimate of the median ground motion and the ~~error~~ term ε, ~~οφ τηε ιντενσιτψ~~ the intensity ~~of the ground motion~~ in terms of magnitude of the earthquake, distance ~~and~~ to site, ~~and~~ rupture mechanism~~ode~~ and geological conditions (Douglas, ~~2001,~~ 2020). The deviation term ε is identified by a Gaussian distributed random variable, with null mean E[ε] =0 and variance Var[ε] = σ^2 or random dispersion around the behaviour of the model.

~~. Due to the frequent lognormal behaviour of the recorded Y values at different locations and conditions, it depends on the energy released by the earthquake and how this is dissipated in the path from its hypocentre to a site located at a certain distance, which is usually formulated as:~~

~~$L(Y) = f(M,R,\{p_i\}) + \square = f_1(M^{\square}) + f_2(R^{\square\square}) + f_3(e^M) + f_4(R) + f_5(\{p_i\}) + \square$~~

~~□□□□□□□□□□□□□□□□□□□□□□□□□□□□~~

~~This formula, in which L(Y) is the natural or in base 10 logarithm of the seismic intensity Y, provides an estimate of the maximum ground motion at a point, after attenuation with the distance that the original shaking level in a forthcoming earthquake, based on its magnitude M, the distance from the source to the evaluation point R, the lithological characteristics of the geological medium traversed, and the rupture mechanism involved in the earthquake, mainly.~~

This expression (1) of the GMPE is composed of the sum of different terms $\{f_i(\cdot)\}$ that quantify the attenuation of the energy transported by the seismic wave train through the geological medium. In general, these terms are: f_1, is a term proportional to M□, since the magnitude is defined as the logarithm of some maximum motion parameter.; f_2 is a term proportional to $R^{-□}$ since the propagation away from the earthquake source through the geological medium of the energy waves causes the amplitudes of the body waves to decrease as a function of R^{-1}, and the amplitudes of the surface waves to decrease as a function of $1/R^{-0.5}$; . f_3 is a term that incorporates that the area in which fault rupture occurs increases with increasing earthquake magnitude, so that some of the waves that produce strong motion at a location arrive from a distance, R, and others arrive from greater distances, so the effective distance is therefore greater than R by an amount that increases as the magnitude increases; . f_4 includes the damping of the energy carried by the deformation waves by the geological material traversed which causes the ground motion amplitudes to decrease exponentially with R; . and, lastly, f_5 introduces through a series of parameters $\{p_i\}$ the possible effect of source characteristics or geological ground conditions on the ground motion. Finally, tThe error term □ is identified by a Gaussian distributed random variable, with null mean E[□] =0 and variance Var[□] = $□^2$ or random dispersion around the behaviour of the model expressed in (1), resulting from the recorded seismic data used in its empirical regression. Catalogues of GMPEs for different regions of the world and various Y-motion parameters contain some relationships that use all these terms, their combinations in varying degrees of complexity, and others that do not (Douglas, 2001, 2020).

Most GMPEs (1) are defined in terms of finite metrics of relative fault distance to the SHA site assuming a planar rupture geometry. These metrics are usually incorporated in GMPEs, such as a distance to the surface projection of the rupture so called Joyner-Boore (R_{JB})., or the closest distance to the rupture plane (R_{RUP}). (Fig. 3). The rupture trace is defined as the projection of the upper edge of the rupture onto the ground surface. The rupture plane, trace, and surface projection allow the definition of four finite fault distance metrics used in GMPEs: R_{RUP}, R_{JB}, R_X, R_Y, Z_{TOR} (Fig. 3). The rupture distance R_{RUP} is the distance from the site to the nearest point of the rupture plane. The Joyner-Boore distance R_{JB}, is the closest distance between the site and the surface projection of the rupture plane, and the auxiliary parameters R_X, R_Y, and Z_{TOR} are the coordinates from the site to the closest point of the top of the rupture (Kaklamanos et al., 2011). Depending on which distance metric the GMPE is formulated, there may be cases where the estimation of the intensity of the movement is affected by the relief of the terrain where the site is located. HoweverTherefore, there are other distances considered in the GMPEs catalogue formulations where if the terms of expression (1) involving R distance in Eq. (1) are givening as a function of dephtdepth (i.e., R_{RUP},) R_Y, or Z_{TOR}.. In these cases, the estimation of the intensity of the motion is affected by the terrain relief (altimetry or bathimetry) where the site is located. Thus, the estimated shake motionvement Y in mountain areas will be loweress than in marine abyssal plains because effect will be more noticeable if Y is evaluated in mountainous areas, providing lower values as the distance increases, or at marine depths, obtaining higher Y because they are closer to seismogenic sources, and. S, so it is expected that the results of the estimation of Y in regions with significant unevenness will be sensitive to the use or notlack of a DTM of the area.

Unfortunately, tThe scarce availability of strong motion records for the whole Ibero-Maghrebian region-Algerian marine area, due to the lack of sufficient records in the southern Iberian Peninsula and North Africa, -merits a selection of a set of more drive us to select a representative set of GMPEs, without the possibility of direct comparison -(Atkinson et al., 2014) with local earthquake records, in a meaningful range for the (M,R) scenarios. Therefore, instead, nondirectnon-direct selection criteria have to be used, relying on SHA works that has been carried out in the emerged surrounding zones to the study area, and paying special attention to the adequacy of the tectonic context and the suitability of the GMPE functional form (Cotton et al., 2006; Poggi et al., 2020)., relying on SHA work that has been carried out in the emerged zones, southern Iberian Peninsula and North Africa, bordering the study area.. The fact that the Ibero-Maghrebian-Algerian study area is a mainly off-shore submarine region geographically located at the confluence of oceanic crust, active continental crust, and stable continental crust complicates the selection of suitable ground motion models. The GMPEs for active tectonic regions strongly underestimate the response spectrum ordinates for western Iberia. However, the analysis does not support that the ground motion attenuation for offshore earthquakes is anomalously low, because GMPEs developed for stable continental regions can in general reproduce them by applying a higher weighting (Vilanova and Fonseca, 2012). Recent tectonic classifications (Chen et al., 2018; Poggi et al., 2020; Hasterok et al., 2022) describeistinguish much of the study region as a zone of active Variscan-Hercynian zone in an active shallowsurface crustal region (ASCR). This region is, surrounded by stable continental cratons in the central African area to the south and the central Iberian Peninsula to the north, and by a stable Atlantic oceanic region to the west. Hence, it is assumed that in the ASCR there is a homogeneous behaviour of the crust in the ground motion response to seismic shaking, and the set of GMPEs chosen for the area can be applied uniformly over the whole area without distinction.

Recent tectonic classifications (Chen et al., 2018; Poggi et al., 2020; Hasterok et al., 2022) distinguish much of the study region as a zone of active Variscan-Hercynian surface crust (ASCR), surrounded by stable continental cratons in the central African area to the south and the central Iberian Peninsula to the north, and by a stable Atlantic oceanic region to the west. The fact that the Ibero-Maghreb-Algerian off-shore area is geographically located at the confluence of oceanic crust, active continental crust, and stable continental crust complicates the selection of suitable ground motion models. The GMPEs for active tectonic regions strongly underestimate the response spectrum ordinates for western Iberia. However, the analysis does not support that the ground motion attenuation for offshore earthquakes is anomalously low, because GMPEs developed for stable continental regions can in general reproduce them by applying a higher weighting (Vilanova and Fonseca, 2012). Therefore, the set of GMPEs chosen for the area can be applied uniformly over the whole area without distinction, as it is assumed that in the ASCR there is a homogeneous behaviour of the crust in the ground motion response to seismic shaking. According to this classification, two equally weighted models (Chiou and Youngs, 2008 and Akkar and Bommer, 2010) are applied (Poggi et al., 2020) for the stable continental crust and the ASCR of the North African zone. In addition, from the latest update of seismic hazard maps in the Iberian Peninsula developed in Portugal (Vilanova and Fonseca, 2007; Silva et al., 2015) and Spain (IGN-UPM, 2017), the discrimination of GMPEs applied for the continental coastal zone has been made according to their range of validity on the seismic scenarios that may occur in the study area for magnitudes greater than 5 by selecting three GMPEs (Boore and Atkinson, 2008; Cauzzi and Faccioli, 2008; Bindi et al., 2011) that complement the two provided by the North African model. For deep seismogenic zones, two attenuation functions (Youngs et al., 1997 and Zhao et al., 2006) incorporated in the Spanish hazard update model (IGN-UPM, 2017) have been taken.

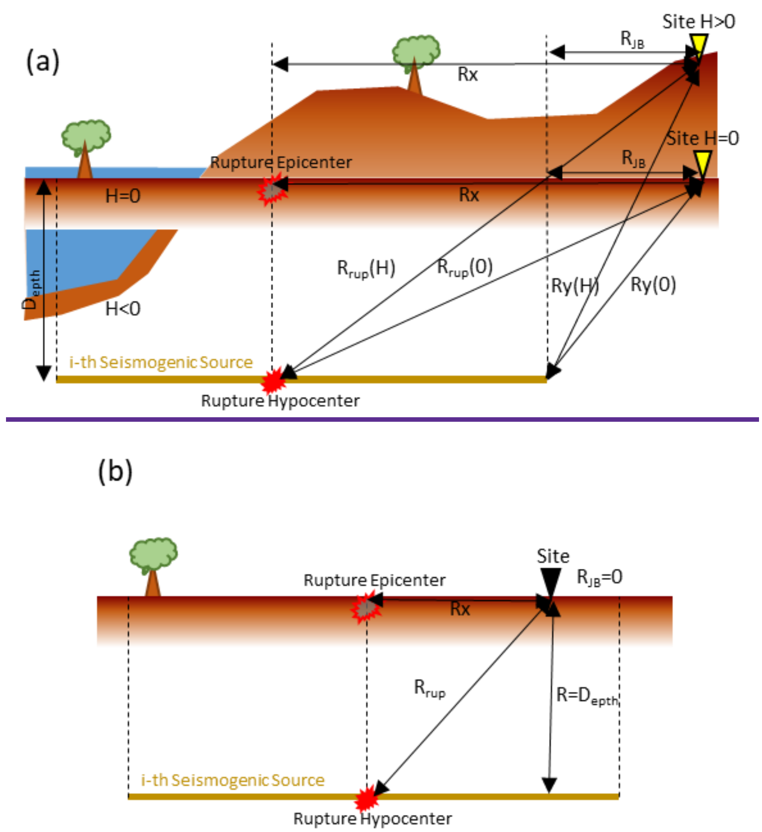

Figure 3. Earthquake source and distance measures from a evaluation site in a vertical cross-section trought a seismogenic source area: RJB: Joyner-Boore distance, Rrup: rupture distance Rx: horizontal ground surface projection of rupture distance. (a) Site outside the ground projection of the seismogenic source, with (H≠0) and without surface altimetry or bathimetry (H=0). (b) Site inside the ground projection of the seismogenic source, without surface altimetry or bathimetry (H=0).

At the European scale, in the ESHM13 of the SHARE project, GMPEs and their weights have been established so that the logic tree captures the epistemic uncertainty in ground motion prediction for six different tectonic regimes in Europe (Delavaud et al., 2012). For active shallow crustal regions with compression-dominated zones (a), including thrust or reverse faults, associated transcurrent faults (e.g., rift faults), Delavaud et al. (2012) recommend three GMPEs (Cotton et al., 2006; Cauzzi and Faccioli, 2008; Bindi et al., 2011) if a European database is used, or three alternative (Boore and Atkinson, 2008; Chiou and Youngs, 2008; Akkar and Bommer, 2010) if a European database is not used, which are first in their ranking based on log-likelihood and have an appreciably higher data support index (DSI) than the rest. From the preselection of these six models, the authors extract the models selected by experts for the ASCR, which are the majority of those considered in this paper. Lastly, the European-scale probabilistic SHA model has also been implemented in the Global Earthquake Map OpenQuake Engine (GEM-OQ; Pagani et al., 2014, 2020) engine, with the selection of the four SHARE strong motion models (Zhao et al., 2006; Cauzzi and Faccioli, 2008; Chiou and Youngs, 2008; Akkar and Bommer, 2010) for the ASCR (Woessner et al., 2015).

SHence, the seven GMPEs have been selected for their compatibility (Fig. 34a for the GMPEs in the ASCR) considering the updating works of the seismic hazard maps in Portugal, Spain, and North Africa and the European revisions of the SHARE and GEM-OQ homogenisation projects with the set of seismotectonic characteristics of the study region, considering the updating works of the seismic hazard maps in Portugal, Spain, and North Africa and the European revisions of the SHARE and GEM-OQ projects.. Although tThe degree of relative importance or weighting of each GMPE has been adjusted, considering that they apply equally over the entire extent of the ASCR, according to the values observed at points (control cities) in emerged territory. The PGA is the seismic intensity Y used in all the GMPE models selected in this work. Two equally weighted models for the stable continental crust region (SCCR) and the ASCR of the North African zone: Chiou and Youngs (2008) and Akkar and Bommer (2010) were applied (Poggi et al., 2020). Specifically, the coefficients inFor AKBO10 fromin particular, the coefficients of Bommer et al. (2012) have been incorporated, and the distance applied in CAFA08 is limited to 15 km below, in accordance with the recommendations made as recommended by GEM-OQ in its inventory of GMPEs (Douglas et al., 2010) GEM-OQ in its inventory of GMPEs. The magnitude of the seismic intensity Y used in all selected GMPE models is the PGA.

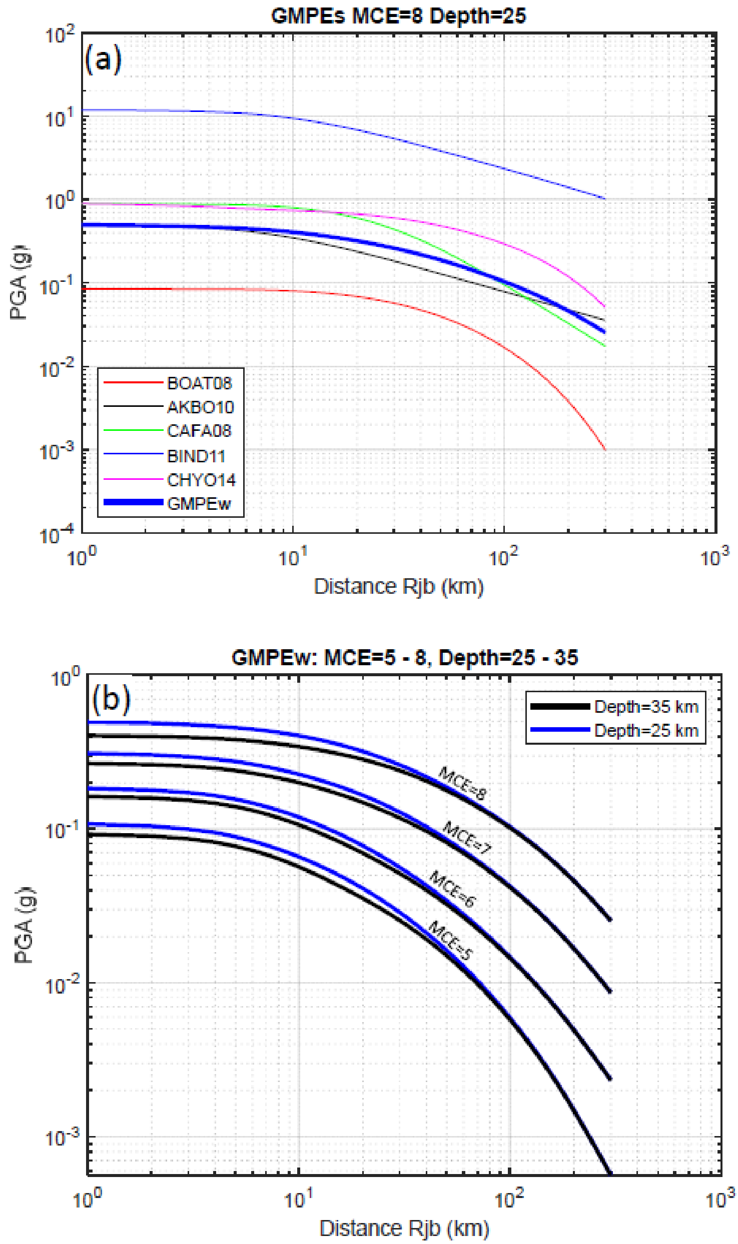

Figure 34. Ground motion prediction equations used, and the resulting weighted composition (GMPEw) applied in the DSHAthis work. (a) plot of the different ones: GMPEs BOAT08, AKBO10, CAFA08, BIND11, and CHYO14 in the case of (for reverse rupture mode, magnitude 8 Mw~8 and seismogenic 25 km of source depth 25 km). (b) plots of weighted composition of GMPEs for a magnitude range (MCE 5 to 8), 25 km and 35 km seismogenic source depths, and reverse rupture mode. reverse rupture,, 25 to 35 km of source depths and magnitude Mw range from 5 to 8.

~~The types of strong motion considered include the full range of MCE for the zonings used in this work, since the minimum MCE is 5.7, higher than the maximum level (M = 5) of application of the model for low magnitudes, according to the range of magnitudes for Spain and North Africa.~~ The BOAT08 model (Boore and Atkinson, 2008) has an uncertainty in Ln(Y) of σ = 0.564, with Y in g, is valid for the entire magnitude range~~,~~. It uses ~~the Joyner-Boor~~the ~~e~~ R_{JB} distance ~~distance~~ o~~in~~ it~~s formulation,~~ is recommended when the fault geometry is unknown, for focal depths between 2 km and 31 km. Its~~, and a~~ formulation is parameterised according to the focal rupture mechanism (reverse, normal, or rupture-tear). The AKBO10 model (Akkar and Bommer, 2010) has been used in its updated rock version (Bommer et al., 2012), as recommended by GEM-OQ (Giardini et al., 2013; Woessner et al., 2015), to obtain log(Y)~~., with the PGA in cm/s^2, considering a~~ It is formulated~~ion~~ in three categories according to the failure mechanism, it uses~~ing~~ ~~the~~ R_{JB} ~~distance~~ and uncertainties σ_1 = 0.2610 (intra-event) and σ_2 = 0.0994 (inter-event). The CAFA08 model (Cauzzi and Faccioli, 2008) provides log(Y) has ~~where Y is in m/s^2, with~~ an uncertainty of σ = 0.344 for the horizontal PGA, taking a reference shear wave velocity in the upper 30 m (V_{s30}) of 800 m/s, corresponding to soil type A, according to Eurocode-8 and ~~the~~ RJB distance modified ~~with~~ by the depth to the source.

The ~~EC~~MCEs in this work are very close to the upper bound of the low magnitudes used in the Spanish hazard model~~, so~~. Hence the possible effect of the BIND11 model (Bindi et al., 2011) has been considered with an uncertainty of σ = 0.337, similar to the rest of the models, using R_{JB} to obtain log (Y), where Y is in cm/s^2, in rock (V_{s30} > 800 m/s) as a function of the different classes of failure mechanisms. The last of the strong shallow ground motion models used is CHYO14 (Chiou and Youngs, 2014)~~, which~~. It obtains Ln(Y)~~, with Y in g in the rock,~~ as a function of the R_{JB} and R_{rup} distances, for which a value of Z_{TOR} = 40 km has been taken as the upper limit of the mean rupture depth, an average dip of 60º, and the different types of rupture mechanisms that act predominantly in each seismogenic area. In this GMPE model~~,~~ the random variability includes the magnitude dependence with~~, as long as the threshold of~~ MCE >~~=~~ 5 as magnitude threshold~~is exceeded~~, and the nonlinear response of the ground was~~that has been~~ fitted as a function of V_{s30} (Chiou and Youngs, 2014). Finally, the two GMPE models applied in deep areas are ~~(~~Youngs et al., (1997) and~~;~~ Zhao et al.~~,~~ (2006). They correspond to~~with~~ those of the model developed for Spain, based on subduction data and~~or~~ global databases, applied for seismogenic sources at about 60 km depth, three located S and SW of the Gulf of Cadiz and one E of the Strait of Gibraltar, in the Iberian Peninsula (IGN-UPM, 2017). These models are adaptable for scenarios with high magnitudes (up to Mw ~8.5) and long distances with slow attenuations, such as those observed in these areas.

4.2 Deterministic Seismic Hazard Assessment (DSHA)

~~DSHA was the first methodology proposed in the late 1960s to assess seismic hazard in nuclear power plant design and engineering projects and was later applied to large industrial infrastructures (NRC, 1973; AEIS-IGN, 1979). This method assumes that seismicity behaves stationary by assuming that future earthquakes will occur in a similar way as they did in the past. The simplicity of its application is based on the fact that the seismic information required for its implementation uses~~

geology and seismic history (Krinitzsky, 2005) to identify earthquake sources and interpret the strongest earthquake that each source is capable of producing regardless of time or MCE(Krinitzsky, 2005). Therefore, the DSHA is a method that does not provide information on the return period of the MCE. The MCE earthquake is the largest possible occurrence along a recognised fault under currently known or assumed tectonic activity (USCOLD, 1995), which will cause the most severe consequences at the site..

Since it is based on the maximum effect that can reach the site of an earthquake produced in the area of influence, The mainerefore, the most important input parameters en the classic DSHA (Reiter, 1990) are the maximum magnitude associated with the characteristic earthquake as the maximum credible earthquake (MCE) for each seismic source area and an a set of attenuation relationship or GMPEslaw appropriate to the rupture mechanisms, tectonic regime, validity distance, and transmission characteristics of the wave (e.g., according to V_{s30}), which led to its widespread use for many years . For reasons of prudence, and despite the fact that the Althoug DSHA does not explicitly incorporate uncertainties through the probability and recurrence functions of seismic events in an area, the seismic hazard can be obtained as a certain percentile of ground motion. It should be noted that although the probability density of the 50th percentile, or average value, is the highest, it is very unlikely that an actual movement will be exactly equal to this estimate. Therefore, in general, tThe 50th percentile movement is mostly used in preliminary DSHA studies with DSHA, and the as well as the 84th percentile when it is used movement is sometimes used for critical structures. Thus, some deterministic seismic risk analysesDSHA use the mean second quartile PGAmotion plus a standarddesign deviation, which is equivalent to an exceedance probability of 16% (Ben-Zion et al., 2003), calculated from simple earthquake and ground motion statistics (Krinitzsky, 1995, 2002) in a particular seismic scenario for which the ground motion risk assessment is based.

Moreover, depending on how the distribution of seismicity is considered, the application of the DSHA is not zoned, if it is done on a homogeneous seismicity region, with a single seismic source of global influence. On the contrary, if the diversity of seismic behaviour in different seismic areas with local influences is remarkable, the DSHA is zoned and the geometry of each seismogenic source is required for its use. Considering the work on the characterisation of seismogenic structures that has been developed so far and that reveals the enormous variety and heterogeneous spatial distribution, the DSHA used in this work is zoned.

The calculation of the seismic hazard was based on assuming here the occurrence of a large earthquake of a certain magnitude at a specific location that affects the site where the motion assessment is made. To perform these calculations, in For its computation, tTThis work we follows a series of steps as the classic DSHA scheme (Reiter, 1990b; Krinitzsky, 1995; Kramer, 1996; Campbell, 2005) that allow the deterministic derivation of the seismic hazard with a zone-based method:

(i) Build a A catalogue construction of N_F seismogenic sources SS_j: $\{SS_j\}_{j=1...Nf}$, which may affect the study area, such an inventory compiles their geometry, depth, and geographic location.

(ii) ~~Characterisation~~ Assign~~Characterise~~ ~~of~~ the seismic potential to~~of~~ each source SSj with its MCEj and the prevailing focal mechanism (normal, reverse~~thrust~~ or strike-slip). ~~SS_j that is capable of a significant ground motion at the site for MCE_j and the prevailing focal mechanism (normal, thrust, or strike-slip) of its seismicity.~~

(iii) ~~For the seismic ground motion intensity parameter Y, by which the hazard is to be characterised, s~~Select the set $\{f^i\}$ of the empirical ~~Ground Motion Prediction Equations (~~GMPEs~~)~~ or attenuation relationships ~~laws~~ $Y^i=f^i(M,R,\phi^i_k,\sigma^i_Y)$, with their corresponding parameters ϕ^i_k ~~that include possible dependence on focal mechanism, shear type or S-wave velocity,~~ and the random uncertainties σ^i_Y for each i-th prediction equation.

(iv) Arbitrarily select the desired probability of exceedance $PR_{exed}=Pr[Y>=y_{max}/M,R]$, for a seismic scenario given by the (M,R) pair.

(v) Calculate the p-th percentile equivalent to the probability of exceedance:

$$PC_{Pr}= Pr[Y<y_p/M,R]=1- Pr[Y>=y_p/M,R] \qquad (2)$$

(vi) Calculate the standard normal random variable Z_{01}, of mean 0 and variance 1, that matches the percentile PC_{Pr}.

(vii) Loop f~~F~~or each~~a~~ site P located at the geographic coordinate position (x,y,h) with latitude, longitude and hypsometry (height or depth above mean sea level) do,~~.~~

(viii.a) Loop f~~F~~or each j-th seismic source SS_j (j=1,.... N_F), assuming that the worst-case scenario (M,R, focal mechanism) is set, defined as the occurrence of an earthquake of magnitude M=MCEj from a point of the j-th seismogenic source at the shortest possible distance $R = R_{min} =\min\{d(P,SSj)\}$, based on the distance ~~(Fig. 3)~~ to be handled (R_{JB}, R_{ep}, R_{hip}, etc.) in the attenuation function (Fig. 3~~4~~).

(viii.a.1) Calculate the median ground motion (50th percentile or GMPE treated as deterministic) of the seismic parameter $Y^i_{50,j}$ at the site, with each i-th GMPE: $Y^i_{50,j} = f^i(M,R,\phi^i_k)$.

(viii.a.2) Calculate the p-th percentile of the seismic parameter at the site with the i-th equation of motion:

$$\log Y^i_{p,j} = \log Y^i_{50,j} + Z_{01}\, \sigma^i_Y \qquad (3)$$

(viii.a.3) Obtain the on-site seismic ground shaking parameter $Y_{p,j}$ on site P produced by each j-th earthquake source.

(viii.b~~ix~~) Deterministic evaluation of the th-percentile of the seismic hazard $Y_p(x,y,h)$ at the site located at (x,y,h) as the largest parameter of the intensity of ground shake obtained from each seismogenic source: $Y_p(x,y,h) = \max\{Y_{p,j}\}$

(ix) Write $Y_p(x,y,h)$ output to change to a new location of the P site to assess.

~~(xi) Repetition of this process at numerous locations spread over a geographical region allows mapping of the hazard assessment over the geographical study area.~~

~~Then, as a result we will obtain the estimate of the seismic action on the bedrock of the site studied, which, being a maximum impact value, will be characterised by the most unfavourable seismic scenarios for the seismic ground motion parameter Y. Specifically, according to the formulation of the GMPEs used, the results obtained for Y are PGA (g) in rock,~~

without quantifying the probability associated with the results obtained, although part of the random uncertainties involved in the estimation process have been incorporated in their calculation, as shown above.

The previous hazard estimation is based on the classical deterministic method; however, it is not statistically accurate considering that the intensity of the seismic motion Yp, obtained for a minimum p-percentile, turns out to be the maximum value of a set of independent random variables with a standard distribution function. However, Ssince in each GMPE the log Y value is distributed as a normal random variable of mean logY with standard deviation σ (Kramer, 1996), then, sinceand $Y_p(x,y,h) = \max\{Y_{p,j}\}$, both Y_p and $Y_{p,j}$ are random variables. Thus, if the p-th percentile Y_p is accurately calculated as follows:

$$\Pr\left[Y_p <= y_p/M,R\right] = F\left(\frac{\log Y_p - \log y_{max/M,R}}{\sigma}\right) = \frac{p}{100} \tag{4}$$

in accordance with the classical scheme, with a single dominant seismic source, and where F denotes the cumulative density function of the standard normal distribution (e.g., mean μ = 0, and variance = 1). Now, considering the distribution of $Y_{p,NS}$ as the extreme value of a set of values (Coles, 2001; Ang and Tang, 2007), the above approximation is computed as:

$$\Pr\left[Y_{p,NS} <= y_p/M,R\right] = \Pr\left[Y_1 <= y_p/M,R\right] x \Pr\left[Y_2 <= y_p/M,R\right] x \ldots x \Pr\left[Y_{NS} <= y_p/M,R\right] = \frac{p}{100} \tag{5}$$

This implies incorporation of the effect of the remaining NS seismic sources in the hazard percentile estimation in the hazard assessment. The estimation is more complicated than in the case of a single source, as it is now necessary to solve the nonlinear equation:

$$\prod_{j=1}^{NS} F\left(\frac{\log Y_{p,NS} - \log y_{j/M,R}}{\sigma}\right) = \frac{p}{100} \tag{6}$$

As this paper uses an approach based on a logic tree scheme that weights the GMPEs to capture the epistemic uncertainties in the hazard estimation, the above equation is rewritten to solve for each i-th GMPE $f^i(M,R,\phi^i_k)$ used and its corresponding i-th random uncertainty σ^i:

$$\varphi^i\left(\log Y^i_{p,NS}\right) = \prod_{j=1}^{NS} F\left(\frac{\log Y^i_{p,NS} - \log y_{j/M,R}}{\sigma^i}\right) - \frac{p}{100} = 0 \tag{7}$$

from which each $Y^i_{p,NS}$ is obtained.

4.3 Epistemic uncertainty treatment: logic tree scheme in DSHA

There are numerous uncertainties in the DSHA methodology that arise from a lack of knowledge or limited comprehensionunderstanding of the seismic process. This limited comprehension is due, on the one hand, to the extreme complexity of the process, which hinders its conceptual understanding for its correct modelling, to its irregular spatial and temporal distribution, interfering with the estimation of its frequency distributions, its representation and localisation, the estimation of its sizes, and the definition of the seismic sources. The extreme complexity of the process limits its discernment, which hinders its conceptual understanding for its correct modelling, to its irregular spatial, temporal, and magnitude distribution, to define the seismic sources. In addition, uncertainties arise on the GMPEs, which the statistical adjustment of their coefficients incorporates an estimation error, and arbitrary users choice is itself an unsure process. All these uncertainties can be classified as random and epistemic (McGuire and Shedlock, 1981; Kiureghian and Ditlevsen, 2009).

In this work, we have used a practical method to incorporate the uncertainties inherent in hazard studies that do not have a GMPE developed specifically for the study region, as in our case study, called the logic tree method. Its formulation uses weighting factors assigned to a particular GMPE based on its likelihood (Coppersmith and Youngs, 1986; EPRI, 1987; National Research Council, 1988). An approach to this method can be incorporated into DSHA (Kramer, 1996; Joshi and Sharma, 2008), which has an advantage over the classic scheme in that epistemic uncertainty is better addressed (Bommer et al., 2005; Bommer and Scherbaum, 2008). The logic tree is constructed from a series of branches connected through nodes from which the computational process twigs according to a possibility or appropriate weighting factors $\{w^i\}$, based on expert judgement (Budnitz et al., 1997), depending on the suitability, importance, of a particular GMPE model. Even after large earthquakes such as the 2011 Tohoku earthquake (Japan), significant ignorance has been revealed in the segmentation of seismic sources and the characterisation of their maximum characteristic earthquake (Stein et al., 2012; Beven et al., 2018). In addition to the lack of precise knowledge of the process that releases seismic energy and how it is transmitted through the geological medium, uncertainties are transferred to the seismicity models that are used, for example, to adjust the models of the GMPEs, whose arbitrary correct choice is itself an uncertain process, of which the statistical adjustment of their coefficients incorporates an estimation error. All these uncertainties, depending on their nature, can be classified as random and epistemic (McGuire and Shedlock, 1981; Kiureghian and Ditlevsen, 2009). Epistemic uncertainty is the scientific uncertainty in the process model, and although it can be reduced with improved knowledge, it is due to gaps in understanding, limited by the complexity of the processes underlying the different elements involved in the seismic hazard. Such gaps may include uncertainties about magnitude frequencies or recurrence rates, parameters of their distributions, maximum magnitudes, rupture mechanisms, consequences and impacts, and the significance of observations in the calibration and evaluation of simulation models. On the other hand, random uncertainty is due to the intrinsic variability due to natural chance, assumed to be irreducible and naturally inherent to the process under consideration. It is parameterised in the parameters involved by probability density functions. These uncertainties influence the hazard estimation and the results obtained, and their quantification has been analysed over time (Toro et al., 1997; Molina Palacios, 1998; McGuire, 2004).

To predict the representative level of PGA values, it is very necessary to properly select region-specific GMPEs (Bommer et al., 2010). Obtaining specific GMPEs for such tectonically complex regions as the one in this work and in a submerged area by means of strong motion records is very complex. The lack of strong motion records in the study area of this work does not allow for a specific ground motion model at the time of writing, and the usual practice is to select suitable ground motion models for similar or nearby tectonic regimes. Therefore, in this paper, we have used a practical method to incorporate the uncertainties inherent in hazard studies that do not have a GMPE developed specifically for the study region, called the logic tree. The formulation of this method, in which weighting factors are assigned to a particular model based on its likelihood, was done in the late 1980s by Coppersmith and Youngs (1986), EPRI (1987), and National Research Council (1988). The approach of this method, which makes use of many alternative prediction models (Kramer, 1996), can be incorporated into DSHA, which has an advantage over the basic scheme in that epistemic uncertainty is better addressed (Bommer et al., 2005; Bommer and Scherbaum, 2008). To this end, the logic tree is constructed from a series of branches connected through nodes from which the computational process branches according to a possibility or weight, whereby several models can be assigned to each node as different branches with different weights depending on the suitability, importance, or degree of a particular model. To effectively apply the logic tree method, it is essential to select the appropriate weighting factors $\{w^i\}$. The assignment of these weights to the different branches is subjective, based on expert judgement (Budnitz et al., 1997), which relies on the degree of uncertainty of the model, its accuracy, and the expected threshold in the seismic parameter calculated at control sites. Each of the weights $\{w^i\}$ reflect current scientific judgements on the relative merit of alternative models.

In the present study, the epistemic uncertainties have been simplified from a non-probabilistic perspective, considering the joint intervention by weighting the attenuation ratios that are applied to address the seismic ground motion estimation that best fits the known points on the emerged lands: the cities taken as control points and validation according to the PGA values obtained in other SHA studies. In other words, a linear combination model of ground motion prediction equations or attenuation relationships has been used to estimate the PGA in each scenario for each point where it is evaluated.

Specifically, fTFor this work, the composition of the logical tree used in this study incorporates a combinations of seven selected GMPEs tothe estimateion of the PGA at the site. The weights assigned to each GMPE in the tree are based on their suitability for different depths of seismic sources. The GMPEs used in this analysis are derived from studies conducted by IGN-UPM (2017) and Poggi et al. (2020) and take into account the specific rupture mechanisms associated with each source. Fig. 3b illustrates the use of our logical tree with various MCEs from sources at different depths of interest by DSHA, in which different GMPEs are combined, (Fig. 4b) is the product of the synthesis of the trees proposed by IGN-UPM (2017) and Poggi et al. (2020). The selection of GMPEs to be integrated into the synthesis of the logic tree was carried out by selecting analogues

~~in the source logic trees, as well as those with the highest assigned weight and equally applicable to all seismogenic regions, but considering their particular rupture style.~~ The treatment of uncertainties by the logic tree scheme is made mathematically explicit in the calculation process in the equations to obtain $Y_{p,j}$ at site P produced by each j-th earthquake source:

$$Y_{p,j} = \Sigma_i\, w^i\, Y^i_{p,j}$$

And also to obtain $Y_{p,NS}$ at each site P:

$$Y_{p,NS} = \Sigma_i\, w^i\, Y^i_{p,NS}$$

which includes the effects of the NS seismic sources. Th<u>e logic tree scheme shown here is used both for the estimation of the PGA</u> ~~ese equations are used when the PGA estimation at the site is~~ based on a single control source<u>,</u> with the most unfavourable seismic scenario<u>, and for</u>~~or where all sources are involved in~~ the PGA estimation<u> based on all seismogenic sources with</u>~~according to~~ their particular seismic scenario<u>.</u>~~, respectively.~~

4.4 ~~Geometric~~ <u>S</u>~~s~~ynthesis of seismogenic zonings

~~To integrate the ZESIS and NAF models of seismic zonation, which have been selected here to form the new model of seismogenic sources used as input parameter in the calculation of the seismic hazard in our study area, their compatibility was determined through the previous analysis of the seismic catalogue used and the type of seismogenic sources used to characterise the distribution of seismicity (areal, point or fault type) in each one of them.~~ <u>In a considerable extent of the study area, ZESIS and NAF zonings overlap (Fig.</u>~~ure~~ <u>2).</u> The selection of the areal seismogenic sources from ~~each~~ <u>both zonings</u> ~~zoning~~~~ZESIS and NAF~~ <u>used here for DSHA</u> was made by taking those that~~, intersecting with the study area,~~ contribute, either by proximity or by maximum magnitude, to the seismicity of the studied area. The seismic influence area was established within a buffer of 300 km (US NRC, 1997) from the study area (Fig. <u>4</u>~~5~~a). Additionally, some seismogenic sources adjacent to the area of seismic influence were selected, and their effect was quantitatively studied. Their seismic contribution was analysed by comparing the results ~~of ground-motion intensities~~ obtained from the DSHA ~~of models with and without the use of~~ <u>with or without</u> these sources.

<u>Geometrically, t</u>~~T~~he overlapping between seismogenic sources, ~~generated from the synthesis process of both zonings (ZESIS and NAF), which can cause the amplification of the seismic contribution in some areas due to the superposition of sources,~~ was treated by means of a topological ~~adjustment~~<u>tuning</u>. This operation allowed <u>a</u> geometric adjustment <u>to common perimeters</u> without overlap<u>s</u> ~~between the seismogenic sources, located mainly at the boundaries of the ZESIS and NAF models used~~ (Fig. <u>4</u>~~5~~b), considering <u>the seismotectonic features that control their boundaries</u>~~the seismotectonic considerations that control their boundaries and that are included in the models~~. ~~As each seismogenic source has associated~~ <u>The</u> seismic parameters <u>of each source</u>~~, the result of the origin zonings, these~~ have also been considered in the synthesis process~~to create the joint zonation, harmonising the seismicity contributed by the seismogenic sources to the study region~~, as <u>it has been carried out in</u>

similar studies (e.g., was carried out in the zonations resulting from the IBERFAULT, OPPEL, and SISMOGEN projects-; (García Mayordomo, 2015) to calculate the seismic hazard in the Iberian Peninsula. Furthermore, the procedure is supported by recent models for classification and segmentation of tectonic regions using fuzzy logic (Chen et al., 2018). This model is specifically designed for a seismic hazard analysis context based on the geophysical characteristics of the crust, including seismic moment release, seismic anelastic attenuation, and shear wave velocity variations. The tectonic similarity of the area addressed in this work is shown, as it presents similar characteristics in almost all its extensions in terms of the scale of the seismic source and the propagation of seismic waves. However, since this is a work on a global scale, more local studies can also be considered (Vilanova, 2018).

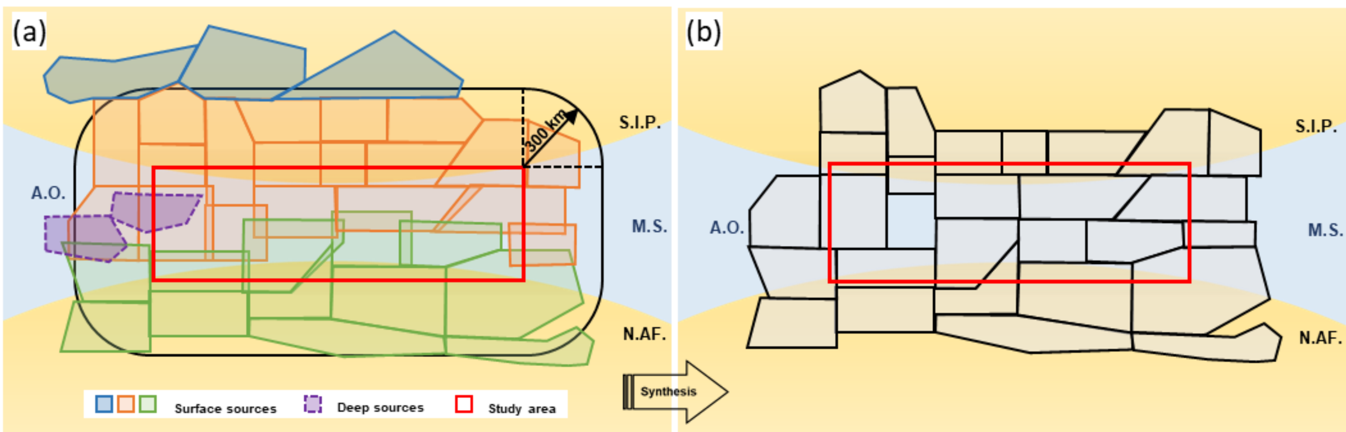

Figure 45. Graphical sketch of: (a) Initial schematic distribution of subsurface and deep seismogenic sources around the study area between the southern Iberian Peninsula (S.I.P.), north Africa (N.AF.), the Atlantic Ocean (A.O.) and the Mediterranean Sea (M.S.), and (b) mapping resulting from the synthesis and integration of seismogenic source zonation from the previous ones.

Once the synthesis of zones has been carried out and the catalogue of sources to be studied in the area has been prepared for its application in the evaluation by means of DSHA, it is necessary to assign a seismic characteristic to each of them, thus completing the inventory. The deterministic method that has been applied, being an extended version to 2.5D, since the value of the hazard on the earth's surface is evaluated taking into account the spatial position of the site (Long. X, Lat. Y, elevation Z) and the position of the source demands as geometric information of the source, in addition to its geometry, which is detailed by the geographical location of the vertices of the polygonal that delimits it, the average depth at which the seismicity is found. It also specifies its rupture mechanism and the characterisation of its seismic potential by means of the MCE.

The geometry of the sources has been obtained from the information provided in open access from the ZESIS website maintained by IGME-CSIC (https://info.igme.es/zesis/, last visited 15/02/2023) and from the GEM Foundation website in its version v2018.0.0 (2018-12-05, https://hazard.openquake.org/gem/models/NAF/, and https://platform.openquake.org/documents/261, last visited 15/02/2023) by downloading the shp files from both databases. The assigned depths for each source will be extracted from the information provided by both bibliographic references (downloaded files for ZESIS from https://info.igme.es/zesis/, and Fig. 7 for NAF, Poggi et al., 2020), as well as their corresponding predominant rupture mechanisms (as normal, reverse, or strike-slip).

The MCE values, ais the seismic characteristic of each seismogenic source as, are used for DSHAin the GMPEs to estimate the PGA values, setting the seismic scenario (M,R) at the selected grid point or site. Therefore, Tthe estimation of the MCE in a SHA becomes indispensable as it reflects the maximum energy capacity for a particular seismic source area that can be released in an earthquake. In practice, the value of the MCE for a given source in the synthesis zoning is determined by the level of information available. Usually the MCE isdoes not necessarilycorrespond to the largest magnitude earthquake on the nearest major fault. When there is insufficient geological information is lacking, the MCE is estimated by slightly increasing the historical maximum, usuallye.g., by one degree in intensity or half a degree in magnitude., However,although this adjustmentincrease depends on the seismic potential of the specific area (as Poggi et al. 2020 have done in NAF). The expected upper limit of the seismic magnitude that can be generated by a source is considered to be Tthe maximum credibleexpected MCE or magnitude of a seismicthat source is considered to be the upper limit, assuming that no source will cause an earthquake generated by that source will exceed this of magnitude greater than this (Joshi and Sharma, 2008). Therefore, the values of the MCEs used in this work for each source resulting from the synthesis have been extracted from the ZESIS (MM_{max} in Table 10; IGN-UPM, 2017) and NAF (M_{max} in Table 7; Poggi et al., 2020) zonings. Although MM_{max} and M_{max} are very similar values or for many sources the same, in others they present slight differences, so MCE = max $\{MM_{max}, M^{max}\}$ has been taken.

4.5 DSHA calculation specifications

The computer-programmed DSHA method can be found in the literature in various forms to perform the calculations efficiently over a geographical area, with its particular ground motion and seismotectonic characteristics. Published versions range from those that adapt their programming with Excel to the particular case studied (Loi et al., 2018), or in Igor Pro (Huang and Wang, 2012). Others, with a more general scope of application, are programmed on a computational system such as MATLAB (Vipin, 2013; Candia et al., 2019; Ramkrishnan et al., 2021), or with a high-level programming language such as FORTRAN. There are also specific programmes for SHA, such as Shakemap (Worden et al., 2020) in which BMKG (Badan Meteorologi, Klimatologi, dan Geofisika) modified in 2015 to incorporate DSHA (Zulkifli et al., 2017). Of these, in this paper an open source Visual Basic (VBA) script in Excel (Wang et al., 2012), which has been used in other studies from a deterministic perspective (Wang and Huang, 2014), has been selected for DSHA evaluation. Originally, the algorithm of this script is designed to perform standard deterministic hazard calculations on a given geographic coordinate location, and its input interface allows the incorporation of multiple linear or polygonal seismogenic sources, their seismic characterisation according to the MCE, and the calculation of the seismic hazard map by the deterministic method, by reproducing the same calculation that is done on a point on a grid of geographic coordinate data points.

As it is a programme built on a commonly used software tool for data analysis such as Excel and written in VBA, it uses an intuitive and easily arranged spreadsheet as the data input interface for the computation and output of results, which makes it a more user-friendly tool than other programmes written in high-level languages. The results obtained are given as PGA, PGV, or PGD values, according to the seismic parameter collected in the ground motion functions. The calculation performed at one point can be repeated on a geographical grid of points, which can then be spatially represented as hazard maps for the parameter in the study area. For the estimation of the DSHA, the study region in this work was incorporated as a grid of calculation points composed of 4,143 sites (Fig. 6a), separated by 0.1 degrees of latitude and longitude, equivalent to approximately 10 km. This grid size was chosen on the basis of experience and approximately equal to the standard error in earthquake epicentre determination (Panza et al., 1990; Suhadolc, 1990). Each point on the grid is considered an individual site. The PGA values in rock have been obtained at all grid points, following the standard DSHA procedure provided by Kramer (1996) and Villaverde (2009) with the improved calculation specifications given in the following. Once the PGA values for each grid point have been estimated, they are compiled into a single catalogue showing each grid point in latitude and longitude and the PGA value associated with that particular point. This file is then used to generate seismic hazard contour maps of the study area using 2D representation software.

The internal programming of the Excel script has been modified by editing the macro programmed in VBA, which allows the programme to be configured with the parameters of a new study, or to make modifications to extend the capabilities of the SHA calculation code. In this sense, the original script has been modified in the first phase to programme a series of user-defined functions and VBA subroutines that incorporate each of the GMPE that have been taken as attenuation functions for the study area and the logical tree scheme to weights them. When transferring the 2D flat calculation to a 3D space in which the sites where their hazard is assessed are located on a DTM adapted to the mesh size on which the DSHA is performed (Fig. 6a), each source has been assumed to be horizontally distributed at its corresponding depth (Table 1) and the distances (disregarding the curvature of the earth for the dimension of the study area) involved in the formulation of each GMPE (Rx, RJB, Rrup) must be reformulated appropriately for their correct calculation. To adapt the calculation with the correct 3D distances, it has been adapted using Haversine approximations to the distance on the great circle (on the basis of a spherical earth, i.e., ignoring ellipsoidal effects which is accurate enough for this paper purpose), the depth of the seismogenic source, and the elevation (altimetric or bathymetric) of the point where the evaluation is being carried out, with the minimum distance calculated with the original Scritp. Furthermore, some of the ground motion functions are specific to a type of rupture in the source that causes the shaking, so it has been necessary to include this information in the seismic characteristics of each source that are detailed in the spreadsheet for data entry.

Algorithms to compute a DSHA method have been implemented in varied ways and computer languages (i.e., Ramkrishnan et al., 2021, in MATLAB; Huang and Wang (2012), in IgorPro; Wang et al. (2012), in VBA-Excel). Given some of these codes are open-source available it eases the process of including further improvements. In this paper we have used the open-source code by Wang et al. (2012) modifying it to incorporate our selection of GMPEs and the account for the logical tree scheme to weights them. This is aiming at considering the relative 3D distances, from a site placed on the DTM (disregarding the curvature of the earth for the dimension of the study area), involved in the formulation of each GMPE. Hence R_x, R_{JB}, and R_{rup} must be reformulated for their correct calculation (using classic Haversine approximations; Gunawan and Prakoso, 2017).To account for uncertainty in ground motion models, the calculus for each site has evaluated, additionally to the 50%, ~~this article has evaluated~~ the effect on DSHA by choosing two values of 16% and 2% of the desired exceedance probability above the mean PR_{exed}=Pr[Y>y_{max}/M,R], for a seismic scenario. In DSHA, the 84th percentile movement to one standard deviation above the mean is usually adopted (Bommer, 2003), instead of the 50th percentile (mean movement). The 98th percentile has also been obtained corresponding to the probability of exceedance ~~probability~~ Pr[Y<=y_{max}/M,R]~~, in addition to the usual 50% or mean movement of the ground~~. Last, we consider the DSHA for a specific exceedance probability as the scenario in which all seismic sources contribute (maximum Y distribution in Eq. (5)) and with a logic tree approach (unlike the one used by Wang and Huang (2014), which only work with one GMPE) solving the nonlinear Eq. (7):   by means of a numerical Bisection method (halving, binary search, dichotomy or Bolzano method, Atkinson, 1991; Süli and Mayers, 2003).

~~The calculations performed above make it possible to obtain the value of the estimated hazard at the site caused by the seismic effect of a single source whose seismic scenario is the most adverse for the conditions of distance and magnitude, discarding the possible coupled effect which, although minor, could be contributed by the rest of the sources whose scenarios are less hazardous. Therefore, to assess the hazard for a specific exceedance probability, considering the scenario in which all seismic sources contribute (maximum Y distribution) and with a logic tree approach (unlike the one used by Wang and Huang (2014), which only work with one GMPE) a subroutine has been included in the program that solves the nonlinear equation lineal $\varphi^{i}\left(\log Y^{i}_{p,NS}\right) = 0$ by means of a numerical Bisection method, also known as halving, binary search, dichotomy or Bolzano (Atkinson, 1991; Süli and Mayers, 2003). This numerical approximation method, as the binary search algorithms popularly used in computer science (Knuth, 1998), is very robust, since it takes advantage of a corollary of the intermediate value theorem. The classical Bolzano theorem or the intermediate value theorem ensures that a continuous function that changes sign in an interval has a root. In our case, the continuous function $\varphi^{i}(x)$, if the values of $\varphi^{i}(a)$ and $\varphi^{i}(b)$ have opposite signs, at least exist one value $x^* \in (a,b)$ or root of φ^{i}, such that $\varphi^{i}(x^*) = 0$. Using as initial search interval (a,b) = (min{ $\log y_{j/M,R}$}, max{ $\log y_{j/M,R}$}+3σ^{i}), within it is verified that the Bolzano condition is fulfilled: $\varphi^{i}(a)\,\varphi^{i}(b) < 0$, the process of the bisection method process has been carried out to approximate numerically this root (Xo → X*):~~

~~Calculate Xo=(a+b)/2~~

If $\varphi^i(a)\,\varphi^i(Xo) < 0$, the root $X^* \in (a,Xo)$, then

assign b=Xo

Else If $\varphi^i(Xo)\,\varphi^i(b) < 0$, the root $X^* \in (Xo,b)$, then

assign a = Xo

End if

Back to calculate Xo

Since this process must be repeated at each site where the hazard is estimated and, in this case, for each GMPE, the convergence characteristics of this algorithm allow it to be repeated for a total of 100 iterations, which are sufficient to achieve an admissible error |Xo - X*| in the root X* solution of the Eq. (7)equation (Burden et al., 2015).:

$$|Xo - X^*| \leq |b - a|\, 2^{-100} \qquad (8)$$

The robustness of this method guarantees convergence without complex operations, although it is slower than other iterative numerical methods for solving non-linear equations . In addition, this technique has a guaranteed error bound, which is reduced by 12% with each iteration. To represent the new calculations made from the script with the above modifications, it has been necessary to adapt not only the input of new data (DTM, depth, rupture mode of the seismic sources, random error of the GMPEs, etc.), but also the output of results in the VBA script and its graphical representation has been tailored to represent the effects with the distance of each source and for various exceedance probabilities. In addition to providing the DSHA map, the output has been customized to represent the site effect of each source with distance from a particular site with its 3D location (longitude, latitude, and elevation) and to assess the joint or similar effect of sources, detect the most influential ones, and for a particular site study could determine the effect of its seismogenic zones in the worst-case scenario separately or together with DSHA .

4.6 Sensitivity and comparative analyses

The results obtained with the DSHA method implemented in this work may be significantly affected by the incorporation of the DTM, as some of the GMPEs, incorporated in the logic tree scheme, use a 3D distance metric in their set of independent variables (e.g., Rrup or Ry). Typically, the DSHA is plannimetric, and 2D relative soure-site distances are evaluated on a horizontal plane. The results obtained with the DSHA method with different exceedance probabilities, as implemented in this work, may be significantly affected by the incorporation of the DTM, as some of the GMPEs use a 3D distance metric in their set of independent variables (e.g., R_{rup} or R_y)and does not use 3D distances to deep sources from the DTM sites, as has been done here. These distances act on the hazard result by defining the seismic scenario affecting each point, and this is used on the set of GMPEs to evaluate the seismic acceleration of the PGA terrain. Likewise, the GMPEs used here incorporate certain rupture type particularities that are applied according to the type of rupture, so that the result of considering the same style in all the sources may give rise to unequal ~~disparate~~ results than if the specific predominant style of each source is used. ~~In order t~~To assess the sensitivity of the results to the effect of using the DTM and incorporating the information of the rupture style in each source, a descriptive statistical study has been carried out with parametric and nonparametric probabilistic methods on the resulting PGA maps and their absolute differences, with one or all seismic scenarios are used to evaluate PGA. ~~With the difference maps, it is possible to identify and contrast the areas with similar behaviour in all cases, or with little sensitivity to the TDM effect and type of rupture, or to detect areas with abnormally high PGA outliers.~~

~~The quality of~~ T~~t~~he PGA maps, obtained by DSHA with~~incorporating the~~ DTM and ~~the typology of the breakdown of each~~ source rupture style, have~~s~~ been benchmarked in ~~assessed through~~ two ways.~~comparison criteria.~~ First,~~1)~~ t~~T~~he geographical distribution of PGA values (g) with that obtained and published in four PGA maps (EHSM13-SHARE: Woessner et al. (2015); zoned PSHA: IGN-UPM (2017); unzoned PSHA: Crespo et al. (2014); and NAF zoned PSHA: Poggi et al. (2020)) that partially cover the study area. And second,~~2)~~ c~~C~~omparing the 50% percentile~~average~~ PGA values ~~(50% percentile)~~ obtained from the calculation with the model presented here in nine cities (Fig. 5~~6~~a) ~~uniformly distributed throughout the study area and for~~ which ~~six~~ previous studies ~~have published their calculated values~~ (Table 3~~1~~). ~~of the PGA hazard (Crespo et al., 2014; Rivas Medina, 2014; Salgado Gálvez et al., 2015; Woessner et al., 2015; IGN-UPM, 2017; Poggi et al., 2020).~~

Table 3~~1~~: Estimated PGA values (in g) presented from various authors (Annex VI in IGN-UPM (2017), NAF (Poggi et al. 2020), EHSM13-SHARE (Woessner et al., 2015), Crespo et al. (2014), Rivas Medina (2014) and CIMNE (Salgado Gálvez et al., 2015)) in each city used to control the results obtained from the DSHA calculation in the study area.

Main Region	City	Lat.	Long.	IGN-UPM	NAF	EHSM13 SHARE	Crespo	Rivas Medina	CIMNE
Southern Iberian Peninsula	Cádiz	36.533	-6.295	0.11	-	0.10	-	-	-
	Málaga	36.717	-4.424	0.16	-	0.11	-	0.20	-
	Almería	36.836	-2.464	0.19	-	0.13	-	0.30	-
	Huelva	37.267	-6.950	0.12	-	0.13	0.11	-	-
	Granada	37.183	-3.583	0.23	-	0.17	0.30	0.30	0.19
	Alicante	38.200	-0.483	0.18	-	0.11	0.22	0.25	-
North Africa	Tánger	35.791	-5.829	-	0.18	-	-	-	-
	Melilla	35.294	-2.936	-	0.24	-	-	-	-
	Orán	35.708	-0.637	-	0.32	-	-	-	-

~~Incorporating uncertainty in the ground motion models, this work has evaluated the effect on the DSHA of choosing two values of 16% and 2% of the desired exceedance probability above the mean, which translates into an effect on the spatial and statistical distribution of the PGA map values, which have also been analysed from a descriptive statistical perspective. The~~

consideration of different levels of uncertainty also affects the results obtained for the set of cities used as control ground motion values and how the control scenario varies in each of them and the rest of the scenarios with distance.

It is possible that in some of the 4,143 sites (Fig. 6a), over which the seismic movement is evaluated to construct the PGA map, the control scenario could be composed of several sources, not easily distinguishable if their uncertainty is considered. For this reason, the results obtained with the DSHA method, in which all seismic scenarios are used to evaluate, according to their random uncertainty, the different percentiles of the PGA, have also been contrasted by means of descriptive statistics, facilitating their comparison with the rest of the results in the previous cases.

5. Results

5.1 Seismic zonation

As a previous result to carry out the seismic hazard analysis in this work, a new seismic zonation of areal seismogenic sources was generated, The synthesis andof the integration of the described ZESIS and NAF catalogues over the geographical area in which they overlap within the study area has resulted in a 36 zones models. For this new zonation, 39 seismogenic sources were initially considered, of which 35 were those that formed the final zonation used in this work (Fig. 56b to d, and Table 4). This new zoning incorporates the sources from the NAF to the south and the ZESIS sources within and surrounding the study area. The ZESIS sources to the north (9 to 12, Fig. 2aTable 1), on the Iberian crust, have been discarded because of their deep (about 30 km) and low influence at the distances marked by the 300 km buffer around it. The constructed catalogue contains, in addition to the geometry of each source, its seismic parameters necessary for the DSHA calculation (Table 4)four deep sources located in the south and southwest of the Iberian Peninsula (between 40 and 65 km depth) were discarded, as their effect is negligible compared to the scenario of the rest of the ASCR sources at shallower depths and with a higher sympathetic intensity. The depths at which these sources are located vary between 20 and 36 km (Fig. 56b). The seismic characteristics derived from the ASCR seismogenic sources have maximum magnitudes (MCE magnitudes) ranging from 6.2 to 8.9 (Fig. 56c), where a clear relationship is observed between the zones of higher magnitude and the zones of higher instrumental seismicity. The predominant rupture mechanism is inverse in the band from the Gulf of Cádiz towards the Algerian Mediterranean coast, passing through the southern Rif and running parallel to the Atlas chain (Fig. 56d), which is the characteristic rupture mode in areas of plate collision where large compressive stresses act, as in the case of our study region. This mechanism reorganises in the form of shearing towards the Alboran Sea basin and the coastal area of the Iberian Peninsula and towards the interior of the Iberian Peninsula it becomes more extensive with a normal structure. The four deep sources located in the south and southwest of the Iberian Peninsula (between 40 and 65 km depth) were initially discarded, as they are rejected in the DSHA method when compared, in the search for the maximum PGA, with the seismic scenario of the rest of the ASCR sources at shallower depths.

The catalogue thus constructed contains, in addition to the geometry of the zonation, the seismic parameters of each source necessary for the DSHA calculation (Table 2). The MCE and the style of the predominant rupture mechanism in each zone according to the focal mechanisms analysed in the original ZESIS and NAF catalogues. The depth in kilometres has been calculated as the average of the depth range given in the seismic record for each source. The shallowest depth values are found in the 17 km of zones 40 and 41, (Table 2) in the western Alboran Sea (40), in the Betic crust that borders the Gibraltar Arc, and in the Algerian-Balearic basin, in the oceanic crust at the eastern edge of the study area (41). Both are predominantly driven by a transpressional shearing mechanism with NNW-SSE shortening direction resulting in moderate (40) to low (41) activity, with magnitudes slightly below 7. The deepest sources within the SACR are distributed over the emerged margin of the Baetic and its connection with the Rif through the Gibraltar Arc, at depths ranging from 33 km to 36 km, subjected to a strike-slip regime that becomes extensive toward the interior of the Iberian Peninsula (Fig. 7d) and with ECM magnitudes between 7 and 7.5. Most of the shallower sources, with depths of less than 23 km, are distributed on the southern border of the study area (sources 52 and 3 to 9), beneath the Atlas Mountains. These sources have been included in the catalogue because, although they have relatively low MCEs, they are close enough to the sites to contribute to their hazard. The remaining sources are located at intermediate depths around 26 km, between 23 and 30 km, in mainly rifting and reverse regimes. Notable among these sources are source 50, on the Gorringe submarine relief and the northern half of the Horseshoe Abyssal Plain, on the western edge of the study area, with an MCE of 8.9, and the sequence of 45 to 47 on the Arzew and Yousuf faults, off the Algerian coast, with an MCE of 7.9 to 8.1, all subject to a compressive stress regime with NNW-SSE directions of maximum shortening.

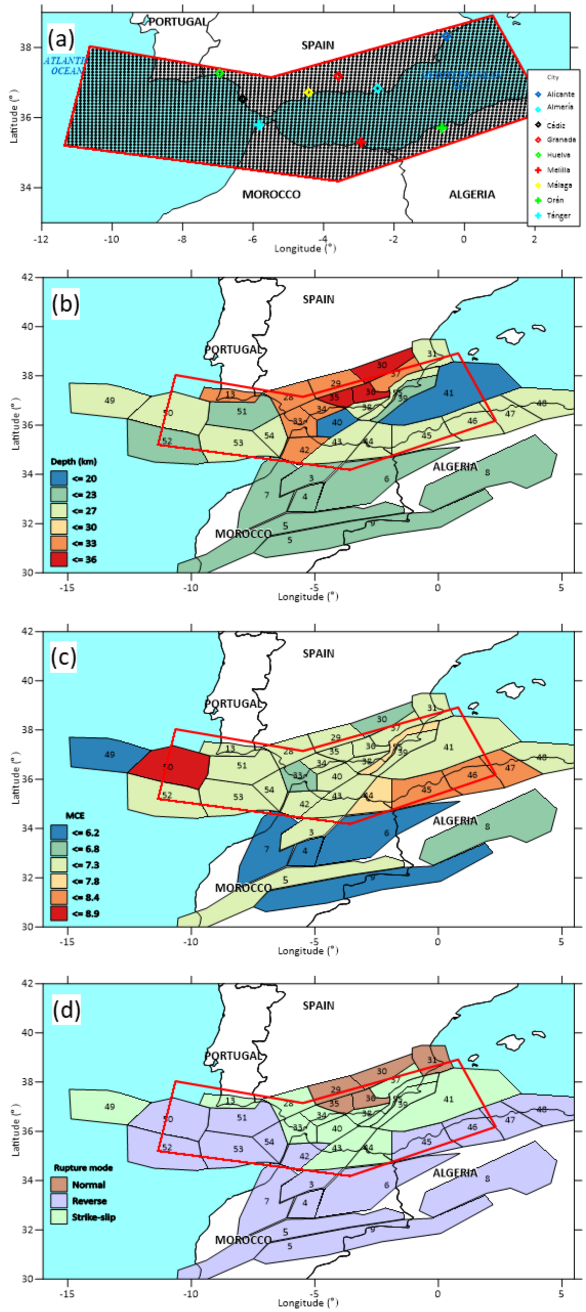

Figure 5~~6~~. (a) ~~Mesh of 4143 points with 0.1º spacing on which the DSHA calculation has been performed~~Calculation sites~~points~~ (black) and control cities (coloured crosses)~~. The nine cities used for the validation of results have been marked~~. Synthesis of the seismogenic source zonation considered in this work for DSHA evaluation on each (a) point, in both South Iberia and North Africa regions and the seismic and~~parameters~~ geographical distribution parameters ~~(~~(Table 4~~1~~) used in GMNAFI model for DSHA estimation: (b) depth (km), (c) magnitude of ~~máximum~~maximum credible~~onsidered~~ earthquake (MCE), and (d) main rupture mechanism~~ode~~ for each seismogenic source.

Table 4~~2~~: S~~Denomination of the s~~eismogenic sources and their seismic~~icity~~ parameters extracted from ZESIS (IGN-UPM, 2017) and NAF (Poggi et al., 2020) zoning models, used for the construction of the synthesis seismogenic model with which the DSHA has been calculated in the study area. The average~~mean~~ value MM_{avg}~~mean~~, standard deviation σ~~s~~MM, ~~and~~ minimum MM_{min}, and maximum MM_{max} truncation limits ~~MMmax,~~ are parameters of the maximum magnitude (MCE) distribution. MM — Maximum magnitude.

Main Region	Source No. Id.	Rupture Mechanism	Depth (km)	MCE Distribution			
				<MM_{avg}~~max~~>	σMM	M~~Max~~ MM_{min}	MM_{max}
Southern Iberian Peninsula **ZESIS**	**13**	Strike-slip	31	6.5	0.2	6.0	6.9
	28	Strike-slip	31	6.7	0.2	6.3	6.9
	29	Normal	31	6.6	0.4	6.2	6.9
	30	Normal	33	5.0	0.4	4.6	6.3
	31	Normal	25	6.6	0.4	6.5	7.1
	33	Strike-slip	30	5.8	0.4	5.4	6.4
	34	Strike-slip	30	6.6	0.3	6.3	7.0
	35	Normal	33	6.8	0.3	6.5	7.1
	36	Normal	36	6.6	0.4	6.2	7.0
	37	Strike-slip	32	6.8	0.2	5.4	7.0
	38	Strike-slip	24	6.7	0.2	6.5	6.9
	39	Strike-slip	22	6.7	0.1	4.9	6.9
	40	Strike-slip	17	6.5	0.3	6.0	6.8
	41	Strike-slip	17	6.5	0.4	4.7	6.9
	42	Reverse	30	6.8	0.3	6.5	7.1
	43	Strike-slip	25	7.0	0.2	6.2	7.3
	44	Strike-slip	24	6.4	0.4	6.0	7.4
	45	Reverse	26	7.3	0.5	6.8	7.9
	46	Reverse	26	7.5	0.3	7.2	7.9
	47	Reverse	26	7.6	0.4	7.3	8.1
	48	Reverse	26	6.8	0.1	6.6	7.1
	49	Strike-slip	24	6.0	0.1	5.9	6.2
	50	Reverse	26	8.7	0.2	8.5	8.9
	51	Reverse	23	6.8	0.3	6.6	7.1
	52	Reverse	23	6.4	0.2	6.2	7.1
	53	Reverse	24	5.7	0.2	5.5	7.0
	54	Reverse	24	6.9	0.4	6.5	7.3
	55	Strike-slip	25	6.7	0.3	6.6	7.4
	9	Reverse	26	6.8	0.3	6.5	7.2
	10	Reverse	31	6.3	0.3	5.7	6.8
	11	Reverse	30	6.1	0.2	5.9	6.3
	12	Strike-slip	31	5.1	0.3	4.9	6.4
North Africa **NAF**	**3**	Reverse	22	6.7	0.5	-	7.2
	4	Reverse	22	5.2	0.5	-	5.7
	5	Reverse	22	6.4	0.5	-	6.9
	6	Reverse	22	5.3	0.5	-	5.8
	7	Reverse	22	5.5	0.5	-	6.0
	8	Reverse	22	5.8	0.5	-	6.3
	9	Reverse	22	5.61	0.5	-	6.11

5.2 Seismic hazard maps, sensitivity and quality

The PGA (g) seismic hazard maps of PGA obtained (Fig. 6) for the MCE, considering the maximum control scenario in each of the 3,8544,143 sites onpoints used to obtain the map (Fig. 5a), have been obtained from several cases of input data: (i) Wwithout using the DTM, assigning 0 m coordinate attaking each point of the map, at 0 m elevation and the ASCR seismogenic sources with a the samea single rupture mechanism for all (inverse, as the most frequent, Table 4, to tear for all of them (Fig. 67a). (ii) Without using the DTM (Fig. 6b), but and assigning to each source its particular rupture mechanism (Table 41) (Fig. 7b).. (iii) With DTM (Fig. 1) and with the inverse rupture mechanism for all sources (Fig. 6d). And (iv) with DTM and the specific rupture mechanism for each source (Fig. 6e).The maximum calculated PGA values obtained are close to 0.83 g in both cases (PGA(0,reverse) and PGA(0,RM) in Fig. 67c), whilealthough the 75th, 50th and 25th percentiles are somewhat lower, in the case of the latter case assigning each source its particular rupture style, with a mean PGA (PGA_{50}) of about 0.317 g for both, as compared with 0.297 g. However, if each point on the map is assigned its corresponding elevation according to using the GEBCO DTM to the three-dimensional location for each calculation site(Fig. 1), the PGAmaps obtained (Fig. 7d and 7e) show very modest relief influence (Fig. 6d and 6e). PGAand have values slightly higher than the two previous ones without DTM of 1.1 g in both cases (PGA(H,reverse) and PGA(H,RM) in Fig. 67c), are slightly higher than the two previous one without DTM (Fig. 6a and b), although they do show higher percentile values than the two previous cases (Fig. 6c)., with an average PGA of 0.331 g and 0.30 g, respectively.

In the four cases presented, tThe highest PGA values are located oin the Gorringe submarine relief up to the Horseshoe plain in all four tested cases. These abussal, areas are affected by sources 50 and 52, withof moderate to strong seismicity, which produces and values in the range of the PGA distribution outliers in the area, approximately 0.6 g to 0.85 g without DTM and within the values of 0.65 g to 1.1 g with DTM. To the west, the sequence of sources 44 to 47 of moderate seismicity in the Algerian coastal zone in the area of the Arzew faults show values of 0.46 to 0.51 g without DTM, and 0.47 g to 0.54 with DTM. In the case of using a single rupture style, the PGA values show a smooth transition from N to S in the Alboran Sea basin area (Fig. 67a and 7d), however, when the style specific to each source is applied, this transition is more abrupt (Fig. 67b and e).

The behaviour at three points in the region (A, B, and C in Fig. 67a)) have been selected within the study area to analyse locally in detail the effect of DTM and PGA produced by the surrounding sources according to their relative distance .,They are located in areas with different seismic conditions: one in the Gorringe plainarea (10ºW, 36ºN), one in the Gibraltar Arc area (5ºW, 36ºN), and one in the Algerian coastal area. (0ºE, 36ºN), versus the effects of incorporating the DTM in the calculation (Fig. 8a), produce appreciably different increases in ground motion depending on the intensity of the seismicity in which they are located, for the same range of variability in Ttheir elevation has varied, evaluated from 1,000 m above sea level to 4,000 m depth to calculate the PGA on each (Fig. 7a). AtThe point A, the PGAover the Gorringe area suffers an increase of up to 17.5% between the resultPGA obtained if A were at 0 m (0.8328 g) and that which would be obtained if Athe point were at -4,000 m depth (0.970 g). This increase is reduced to 12.1% for the point Cin the Algerian area, and in Bthe Gibraltar Arc area it is reduced to 10.1%. The effect on the three points can be recognised for all sources within 100 km (Fig. 7b) of relative distance R. There are four relevant sources affecting point A (circles), four for point B (squares) and three for point C (diamonds), whose PGA are higher than 0.1 g. However, for distances greater than 100 km, there is no difference between using or not using the DTM in the calculation. By observing that the red symbols of A, B and C are superimposed on the blue symbols in Fig. 7b, the PGA values obtained with and without DTM at distances greater than 100 km are very similar and less than 0.1 g. The rate of change and increase of the PGA, as the distance to the control source varies, in the three cases shown, has a practicallyis negligible change, almost constant, for the range of elevations analysed. The individualised effect of each source on this behaviour for the extreme cases of elevation 0 m and -4000 m has been represented (Fig. 8b) according to its control earthquake and the distance R at which the source is located considering its depth. In this graph it is possible to recognise how up to 100 km distance there is an appreciable effect on the PGA value, higher than 0.1 g and up to 100 km distance. After 100 km, the difference in the PGA obtained using the DTM and without it is less than 1%. The effect on the three points, which have been taken over areas of different simian intensity, is more noticeable at 0.1 g and above, with the five seismic sources closer to the site, and attenuates to almost zero at 100 km and above.

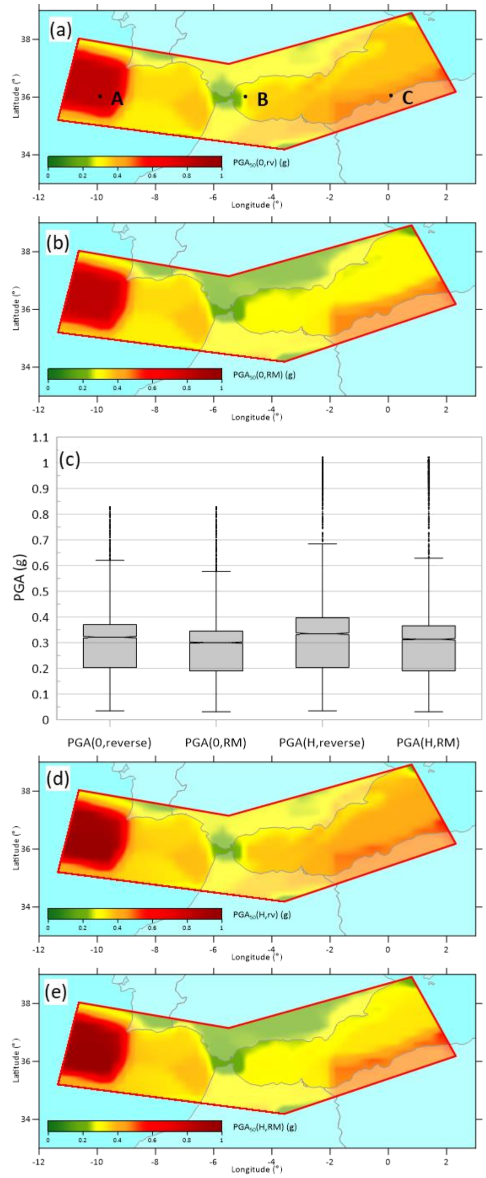

Figure 67. PGA maps from DSHA: (in g) obtained with the DSHA method in this work: (a) without DTM and considering only a reverse focal mechanism in all seismogenic sources. Probe points A (10ºW, 36ºN), B (5ºW, 36ºN), and C (0ºE, 36ºN) used for sampling PGA map results;.; (b) without DTM and considering a source-specific average focal mechanism (Table 42);. Probe points A (10ºW, 36ºN), B (5ºW, 36ºN) and C (0ºE, 36ºN) used for sampling PGA map results. (c) Box-Whisker plots for PGA -values used for Fig.ures 7a, b, d, and e. Center line represents the mean value. Box edges are limited by the quartiles (25% lower and 75% upper percentile). Whiskers are limited by the 1.5 times the inter-quartile range. The notch size factor is 1.7. The sample outliers are represented by dot symbols; . PGA maps (in g) form DSHA: (d) with DTM (Fig.ure 1) and considering a reverse rupture focal mechanism in all seismogenic sources; (e) with DTM (Fig.ure 1) and considering a source-specific average rupturefocal mechanism (Table 42).

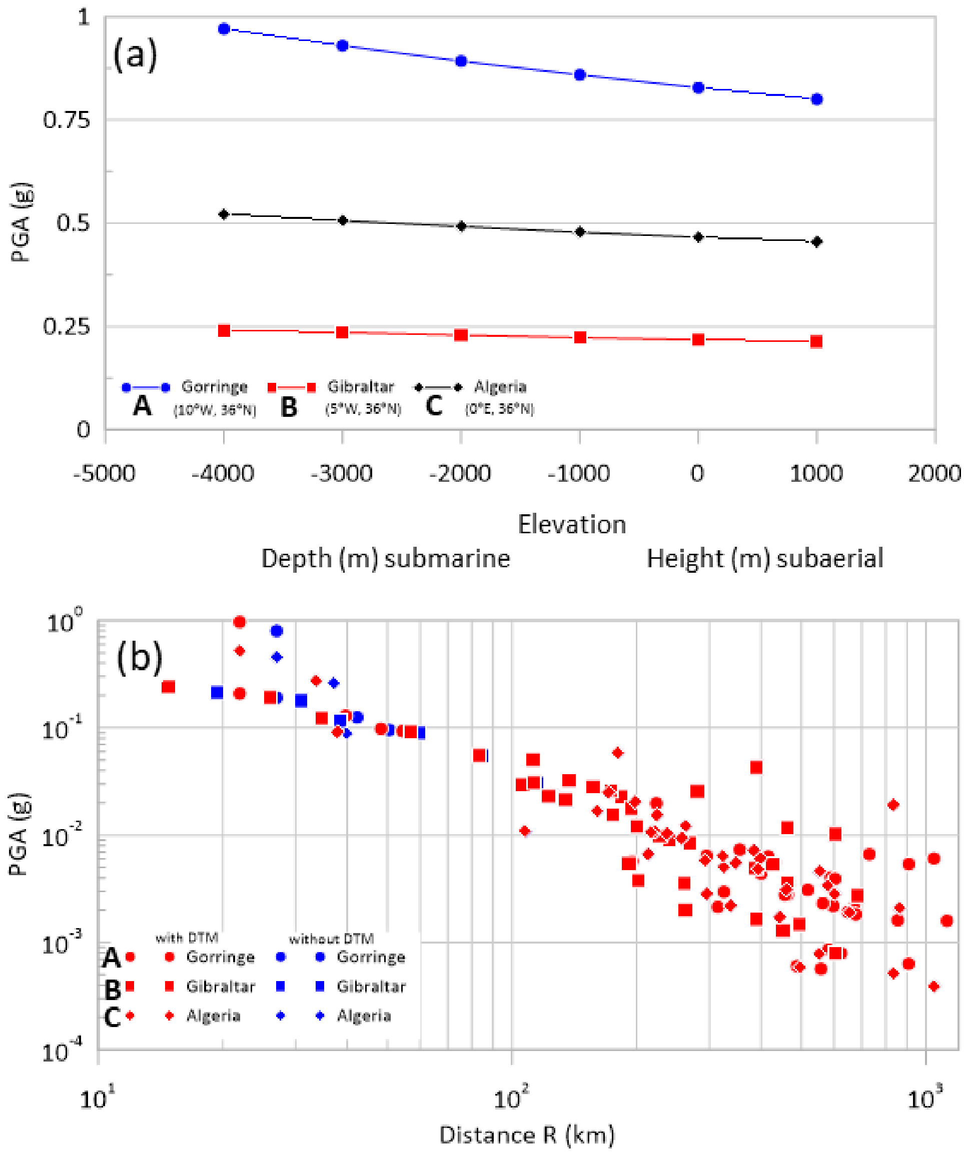

Figure 78. Effect of the DTM on the values obtained at three points distributed in the study area (Fig.ure 67a): A Gorringe (10ºW, 36ºN), B Gibraltar Arc (5ºW, 36ºN), and C Algeria coast (0ºE, 36ºN), (ae) considering that the points (A, B, and C) are at different elevations, : between 1000 m and -4000 m, and (bf) according to the MCEcontrol earthquake of each every source on each point (A, B, and C), considering that the points are at 0 m (red symbols, with DTM) and at -4,000 m depth (blue symbols, without DTM).

~~The spatial distribution of this behaviour is shown by the differences between the previous maps (Fig. 9a, 9b, 9d, and 9e) and their distribution statistics (Fig. 9c). The~~ D~~d~~ifference~~s in the~~ PGA maps (in Fig.8) ~~obtained with and without DTM, and in the same conditions applied for the calculation according to the case of the rupture mechanism (reverse only, Fig. 9a: PGA(H,reverse)-PGA(0,reverse) and source-specific rupture mode, Fig. 9c: PGA(H,RM)-PGA(0,RM)),~~ show that, regardless of whether DTM is used or not (Fig. 8a), the highest~~most important~~ difference~~s~~ between assigning or not a predominant rupture mechanism is~~in the whole area or the specific one in each seismogenic source are~~ less than 0. 2 g (Fig. 8~~9~~c). Geograpgically, t~~T~~he positive increases observed over the reference values calculated without using the DTM (red tones) are areas of the map whose depth is closer to the source, being more intense in the abyssal plains~~deeper oceanic zones~~. So, generally~~In other words~~, in ~~the areas of the~~ submarine areas~~domain~~, the PGA values obtained are higher if the DTM is used~~, being the highest in the areas with the highest PGA values~~ (e.g., Gorringe, Horseshoe and Coral Patch areas). The differences are negative (blue shades) in the subaerial~~rfaced~~ areas, although lower than the positive ones (they are below 0.01 g) i.e.,~~show that~~ the PGA value obtained using the DTM is lower than that obtained without using it. The differences between using a common rupture mechanism according to the predominant one and the specific one of each source do not exceed 0.08 g (Fig. 8~~9~~b: PGA(0,reverse)-PGA(0,RM) and Fig. 8~~9~~d: PGA(H,reverse)-PGA(H,RM), ~~being null the difference in the areas where the specific mechanism coincides with the reverse one used and~~ highlighting the difference of 0.7 to 0.8 g in the extensional rupture zones (NE of the Betic) and with a moderate difference of 0.05 to 0.07 g in the rifting zones distributed in the Alboran basin and East of the Rif.

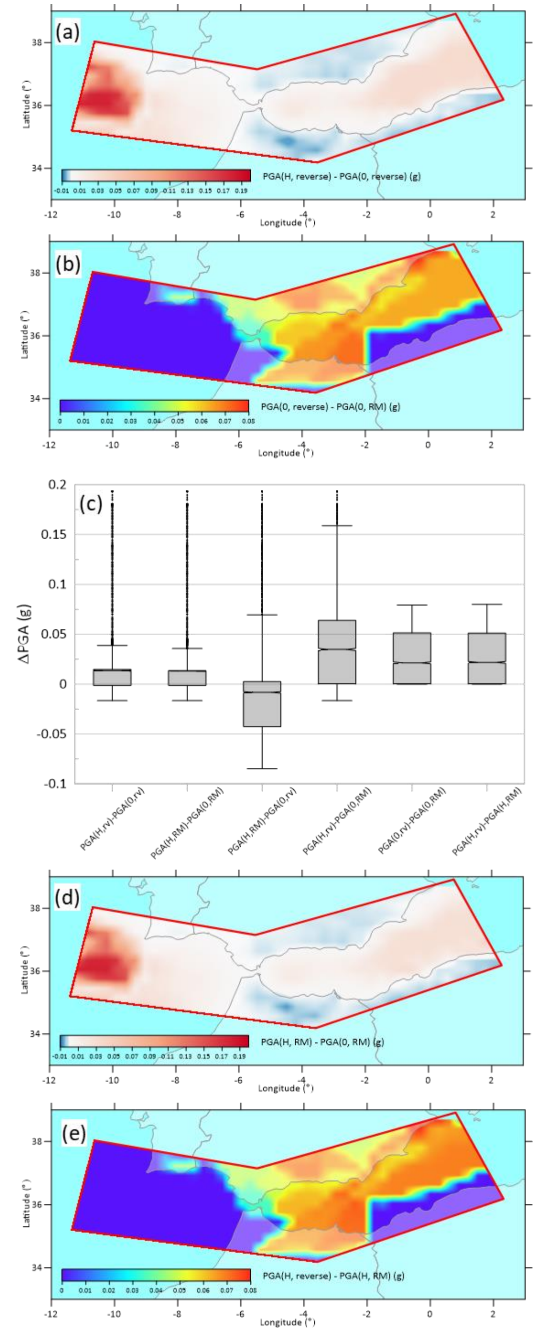

Figure 89. Difference maps between DSHA results in PGA from Fig.ure 68. Substraction: (a) between Fig.ure 67d and a; (b) between Fig.ure 67a and b; (c) Box-Whisker plots for PGA differences used for Fig.ures 9a, b, d, and e. Center line represents the mean value. ~~Box edges are limited by the quartiles (25% lower and 75% upper percentile). Whiskers are limited by the 1.5 times the inter-quartile range. The notch size factor is 1.7.~~ The sample outliers are represented by dot symbols; (d) difference between Fig.ure 67e and b; (e) difference between Fig.ure 67d and e.

The results obtained for PGA (g) in the nine selected point-cities (Table 3~~1~~) show variations according to the ~~parameters~~ specified information ~~for their calculation on the assignment of the rupture mode and the use of the~~ (DTM and rupture mechanism) for their PGA ~~in the~~ calculation (columns DSHA^{1} to DSHA^{4} in Table 5~~3~~). Some cities show relevant ~~important variations between the different calculation options~~ of up to 31% in Granada, while others show no variation in the calculated PGA, such as Huelva or Orá~~a~~n, although most of them are between 20.8% in Malaga and 23% in Almerí~~i~~a. ~~The values obtained with the DSHA methodology used in this work show values higher than those obtained with the probabilistic methodology. Some of them are twice as high as those obtained with PSHA in some previous studies, and the differences are reduced in more recent studies (Table 1).~~ Despite these differences, the spatial ~~correspondence and complete~~ distribution of the PGA

Table 5~~3~~: Estimation of PGA (g) at bedrock level by DSHA at each control city and according to the test cases ~~considered in this work:~~. DSHA^{1} ~~result~~ without ~~bathymetric DTM~~bathymetry and considering a single reverse rupture mechanism equal for all seismogenic sources~~;~~. DSHA^{2} ~~result~~ without ~~bathymetric DTM~~bathymetry and considering a source-specific rupture mechanism (Table 4~~);~~). DSHA^{3} ~~result~~ with ~~bathymetric DTM~~bathymetry and considering a reverse rupture mechanism in all seismogenic sources~~;~~. DSHA^{4} ~~result~~ with ~~bathymetric DTM~~bathymetry and considering a source-specific rupture mechanism (Table 4~~);~~). DSHA$_{84}^{5}$ 84th percentile with ~~bathymetric DTM~~bathymetry and considering a source-specific rupture mechanism (Table 4~~);~~). DSHA$_{98}^{6}$ 98th percentile with ~~bathymetric DTM~~bathymetry and considering a source-specific rupture mechanism (Table 4~~); columns~~). Columns 7 to 9 are the same as 4 to 6, but using the control and all non-control sources (NS).

Main Region	City	DSHA^{1}	DSHA^{2}	DSHA^{3}	DSHA^{4}	DSHA$_{84}^{5}$	DSHA$_{98}^{6}$	DSHA^{7} all NS	DSHA$_{84}^{8}$ all NS	DSHA$_{98}^{9}$ all NS
Southern Iberian Peninsula	Cádiz	0.27	0.22	0.27	0.23	0.43	0.82	0.59	0.79	1.26
	Málaga	0.29	0.24	0.29	0.24	0.46	0.87	0.50	0.48	1.08
	Almería	0.32	0.26	0.32	0.27	0.52	1.01	0.61	0.83	1.33
	Huelva	0.3	0.3	0.3	0.3	0.57	1.10	0.58	0.81	1.31
	Granada	0.29	0.22	0.29	0.22	0.41	0.78	0.49	0.64	0.99
	Alicante	0.38	0.31	0.38	0.31	0.59	1.15	0.59	0.81	1.31
North Africa	Tánger	0.22	0.18	0.22	0.18	0.34	0.65	0.47	0.63	0.99
	Melilla	0.39	0.32	0.39	0.32	0.61	1.18	0.56	0.79	1.31
	Orán	0.47	0.47	0.47	0.47	0.90	1.74	0.59	0.92	1.75

values in the region, compared to the distributions partially ~~distributions~~ covered by previous work (Fig. 9~~10~~) are very similar to those ~~that~~ obtained in this work. Although it is not the purpose of this paper to discuss the compatibility, lateral, and comparative continuity of the presented maps, it is possible to appreciate some differences between them. However, there is a good fit, both regionally as a whole and locally in specific zones, of the results obtained ~~the isovalue curves extracted~~ from ~~the case where~~ the DSHA ~~is calculated~~ with ~~the~~ DTM and ~~the~~ source-specific rupture mechanism~~ode~~ with ~~(Fig. 7d) plotted on each of~~ the PGA maps obtained by zoned (Fig. 9~~10~~a, b and d) and non-zoned (Fig. 9~~10~~c) PSHA probabilistic methods ~~fit both regionally as a whole, and locally in specific areas, to the geometry of the regions~~. The~~is~~ best fit are~~is~~ found in areas with high PGA values: Gorringe, Horseshoe and Coral Patch to the west, Atlas Mountains and Algerian coast to the southeast, and the Betic mountain range from Má~~a~~laga to Alicante to the north; as well as in the areas with lower values in the Alboran Sea basin to the east and south of the Gulf of Cá~~a~~diz.

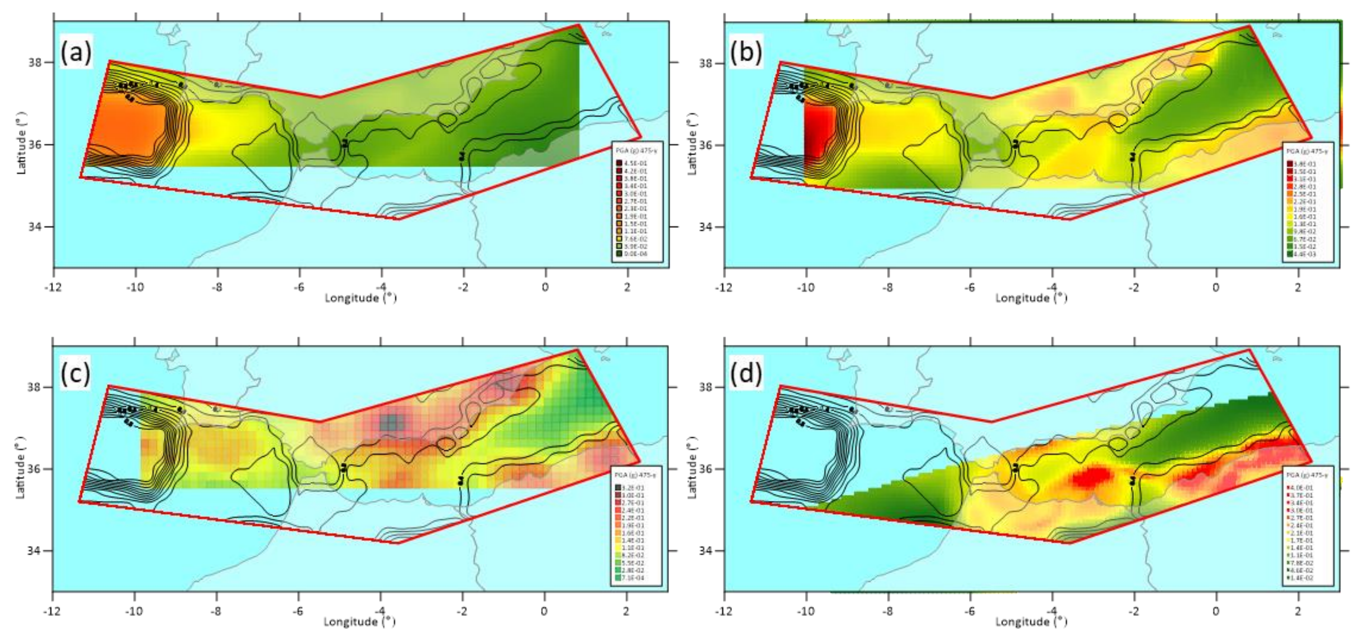

Figure 9~~10~~. Available PGA (g) maps used in this work for calibrate the results on SHA. South Iberia regio~~ó~~n PGA map in g from zoned PSHA (a) modified from EHSM13-SHARE (Woessner et al. ~~(~~2015), (b) modified from UPM-IGN (2017), (c) from un-zoned PSHA modified from Crespo et al. (2014), and (d) North Africa region PGA map in g from zoned PSHA modified from Poggi et al. (2020).

5.3 Hazard assessment with exceedance rates and cumulative effect of sources

~~The results obtained incorporating the uncertainty due to the GMPEs have been carried out considering the DTM in the DSHA calculation, the particular rupture mode of each source, and the random uncertainties σ^i_Y for each i-th prediction equation, as constants for AKBO10, CAFA08, BOAT08 and BIND11, or evaluated particularly in CHYO14 for the seismic scenario being assessed.~~ The PGA ~~(g)~~ maps ~~obtained~~ using DTM and the rupture mechanism on each source, for the 16% and 2% exceedance probability ~~values~~ ~~associated with each of them, corresponding to the 84% and 98% percentiles, respectively, of PGA~~ (PGA_{84} and PGA_{98} percentiles, Fig. 10~~1~~a and b, respectively) associated with the GMPEs uncertainties, show a geographical distribution of the maximum values over the Atlantic areas of Gorringe, Horseshoe and Coral Patch, and off the Algerian coast in the area of the Mediterranean Alboran basin. As in the 50% PGA percentile (or PGA_{50}), they are similar ~~in both cases of exceedance rates, corresponding~~ to the areas of highest seismogenic potential. The PGA maximum values (Fig. 10~~1~~c), reach 2 g (maximum at 2.07 g) for PGA_{84} ~~exceedable by 16% of the cases~~, with an interquartile range between 0.34 and 0.69 g, with a mean of 0.60 g ~~(PGA(H,RM,84) or PGA_{84})~~, and up to 4 g (maximum at 4.26 g) for PGA_{98} with a mean of 1.17 g in a range between 0.66 and 1.33 g. ~~, only exceedable by 2% of the cases (PGA(H,RM,98) or PGA_{98}). Therefore, considering random uncertainties in the estimation of hazard by DSHA results in an increase of 103% and 318% for the probability of exceedance of 16% and 2%, respectively, in the maximum PGAs, with smaller increases for the remaining quartiles: 89% and 267% increases for the first quartile of PGA_{84} and PGA_{98}, respectively, and 92% and 269% for the third quartile of the PGA_{84} and PGA_{98} distributions.~~ The multimodal frequency distribution ~~of all these values~~ (Fig. 10~~1~~d) of PGA_{50}, PGA_{84}, and PGA_{98} percentiles mapped values preserves the shape in~~as~~ the cumulative distribution functions. There are~~show, maintaining a number of~~ three major frequency maxima and smaller but higher PGA values mainly located over the outlier set of the Box-Whisker diagram ~~(PGA(H,RM) on another scale in Fig. 7c)~~. ~~The modal maxima shift from 0.25, 0.40, 0.55 and 1 g, for a PGA percentile of 50%, towards higher PGA values as a lower exceedance rate is considered, from 0.5, 0.65, 0.85 and 2.1 to 84%, until they are located at 0.8. 1.25, 1.75 and 4.3 at 98%, showing an increase in dispersion around each mode.~~ The modal maxima in the distribution functions, for each PGA percentiles, shift to higher PGA values as a lower exceedance rate is considered, with an increase in dispersion around each mode. The entire distribution of PGA values on the maps computed with Eq. (7) has been stretched to higher PGAs. Most of the distribution, comprised of the second and third quartiles, rises in the diagram (Fig. 10d) with the interquartile range of the values remaining almost the same without considering all sources. Although the shape of these distribution functions is preserved, they are slightly shifted towards higher values of the PGA. Even the minima of the PGA for the three PGA percentiles have increased, as seen in the small shift to the right of the cumulative frequency distribution curves (Fig. 10d).

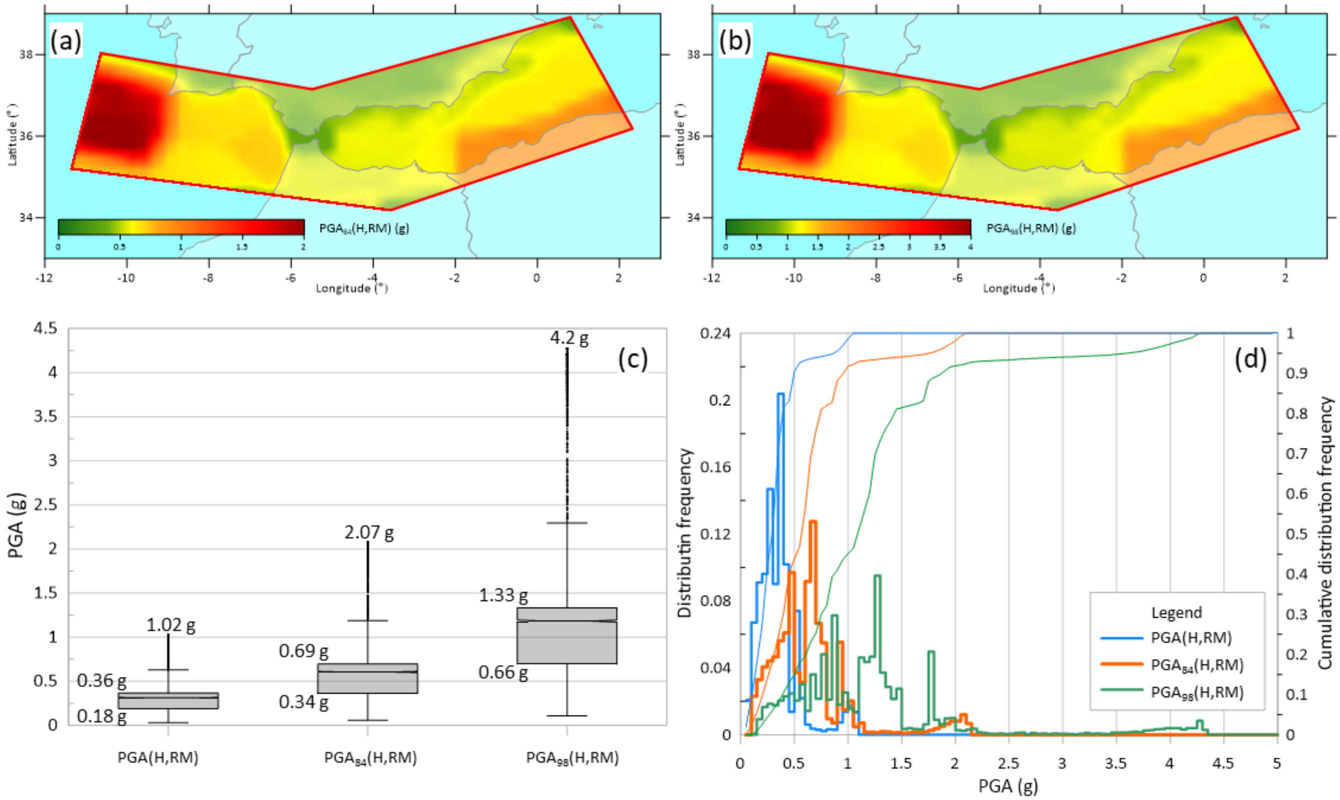

Figure 10~~1~~. PGA~~percentile~~ 84 (a) and PGA_{98} (b) hazards maps obtained including the ~~with the DSHA method with~~ DTM ~~(Figure 7a)~~, considering a source-specific average rupture ~~focal~~ mechanism (Table 4~~1~~) and random uncertainty for each GMPE. (c) Box-Whisker plots for PGA values in f~~F~~igures (a), (b) and Fig.~~ure~~ 6~~8~~c~~d~~ (for comparison). Centre~~r~~ line represents the mean value. ~~Box edges are limited by the quartiles (numbers indicated 25% lower and 75% upper percentile). Whiskers are limited by the 1.5 times the inter-quartile range. The notch size factor is 1.7.~~ The sample outliers are represented by dot symbols. (d) Histograms, as distribution of relative frequencies, and experimental cumulative distribution functions for PGA values in f~~F~~igures (a), (b) and Fig.~~gure~~ 6~~8~~c~~d~~ (for comparison).

~~The regional behaviour shown in the previous results over the studied area is particularly reproduced over the control cities (Fig. 12) in the strong motion they receive, for the control earthquake of each seismogenic source, as a function of distance. In fact, compared to the average values of the PGA marked with blue symbols, the values of the PGA_{84} (yellow dots) increase in the order of 100% and those of the PGA_{98} (red dots) up to 300% approximately and in the same way for all the sources individually, both if the seismic scenario received by the city site is important and if the strong motion is low. Specifically, the values of PGA_{84} (Table 3, column $DSHA_{84}$[5]) in the cities of Almeria and Orán do not exceed an increase of 92%, while in Cádiz and Granada they only increase by 86%. As for the PGA_{98} values (Table 3, column $DSHA_{98}$[6]), the maximum increases reach 270% in Almeráa and Orán, with the lowest increases being 255% in Cádiz and Granada. However, the way in which this movement is received is not the same for all cities. The distribution of the PGA in the distance is homogeneously~~

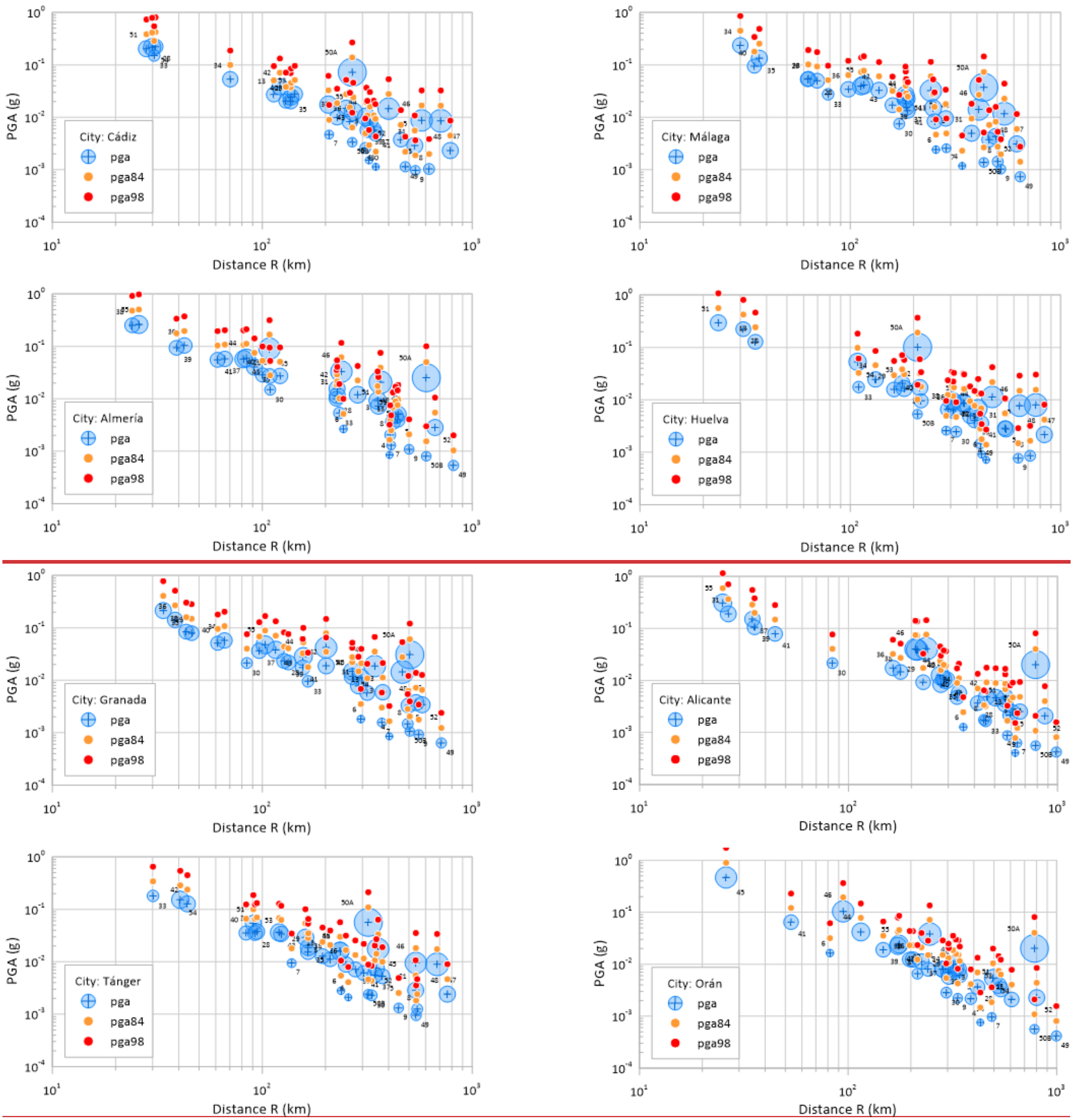

Figure 12. Effect of strong seismic motion in each of the control cities triggered from each seismic source, according to its MCE and distance from it, for each of the percentiles (50th median, 84th and 98th) of random uncertainty in the composition of GMPEs. The PGA (in g) has been evaluated considering the type of rupture at each source, and the distance taking into account the DTM, and the depth of each source.

~~distributed in cities such as Málaga, Granada, and Orán, and there are less homogeneous distributions forming weakly differentiated aggregates such as in Cádiz or Alicante, and two clearly distinguishable source aggregates such as in Almeria, Huelva, or Tánger.~~

Using the same input data as for the previous~~0.5, 0.16 and 0.02~~ exceedance probabilities maps, three new maps have been obtained solving~~shown in Fig. 7 and 11 and calculated with the DSHA method above, using the seismogenic source that produces the maximum ground motion or control earthquake at the site, the hazard calculation for the different percentiles, the DSHA has been calculated using all sources, including those that do not control (Fig. 13). In other words, for this new map,~~ Eq.~~equation~~ (7) ~~has been solved~~ for each point. As a general result in these three maps (Fig. 11a to 11c)~~, considering the effect of the distribution of the rest of the seismic scenarios that each source originates, as a non-homogeneous distribution of the seismic scenarios, as found in the control cities (Fig. 12), and the random uncertainty produced by the GMPEs. After considering the joint effect of the 35 sources to create the maps for the mean PGA (PGA(H,RM,NS) in Fig. 13a) and the 84th and 98th percentiles (PGA_{84}(H,RM,NS) and PGA_{98}(H,RM,NS) in Fig. 13b and 13c)~~, the joint effect of the 36 seismic sources a substantial increase in seismic hazard is observed at all points in the study region due to the overall seismic contribution from sources. ~~This increase is especially higher in areas close to confluences, contact zones, or common sides between seismic zones, being less relevant as the excess probability decreases, becoming barely perceptible in the case of probability 0.02 (Fig. 13c).~~ This geographical distribution reflects the joint nature of the effect of the sources when evaluating the DSHA, increasing by more than 155% in cities such as Cádiz (by 156%) or Tánger (by 161%) for their average GMPEs of 0.59 g and 0.47 g, respectively, when considering all sources in addition to the control source (Table 5~~3~~, column DSHA[7] all NS), compared to their average PGA values considering only the control source in the calculation of the DSHA with DTM and a particular rupture mechanism (Table 5~~3~~, column DSHA[4]). ~~The hazard values in these cities can be as high as 1.26 and 0.99 g, 447% and 450%, respectively, when considering probability of exceedance rates of 0.16 and 0.02 over the random uncertainty (Table 3, columns $DSHA_{84}$[8], and $DSHA_{98}$[9] all NS). The cities with the smallest increase are Melilla and Orán, with an increase of 75% and 25% compared to their average comparison PGA values (Table 3, column DSHA[4]).~~ For the rest of the cities, the effect of the increase in their hazard values when including all random sources (Table 5~~3~~, columns DSHA[7], $DSHA_{84}$[8], and $DSHA_{98}$[9] all NS) against the comparison PGA averages is between the extreme values indicated, according to the evaluated AMP percentile.

An overview of the statistical quartile of the increase in the distribution of the PGA-mapped values distributed over the study area can be seen in the Box-Whisker graph (Fig. 11~~3~~d) and the cumulative frequency distributions for the mean and the 84th and 98th percentiles (Fig. 11e), compared to the corresponding ones obtained in the DSHA study evaluated with the control source alone (Fig. 10~~1~~c and ~~11~~d). The entire distribution of PGA values has increased. Although the maximum values are almost similar, most of the distribution, comprised of the second and third quartiles, rises in the diagram (Fig. 11~~3~~d) with the interquartile range of the values remaining almost the same without considering all sources. Even the minima of the PGA for the three evaluated percentiles of the PGA have increased, as seen in the small shift to the right of the cumulative frequency distribution curves (Fig. 11~~3~~e) which is as much as 470%, for example, between PGA(H,RM) with a minimum of 0.03 g and PGA(H,RM,NS) with 0.17 g, although these distribution functions preserve their shape in terms of the small jumps they present, they are slightly shifted towards higher values of the PGA.

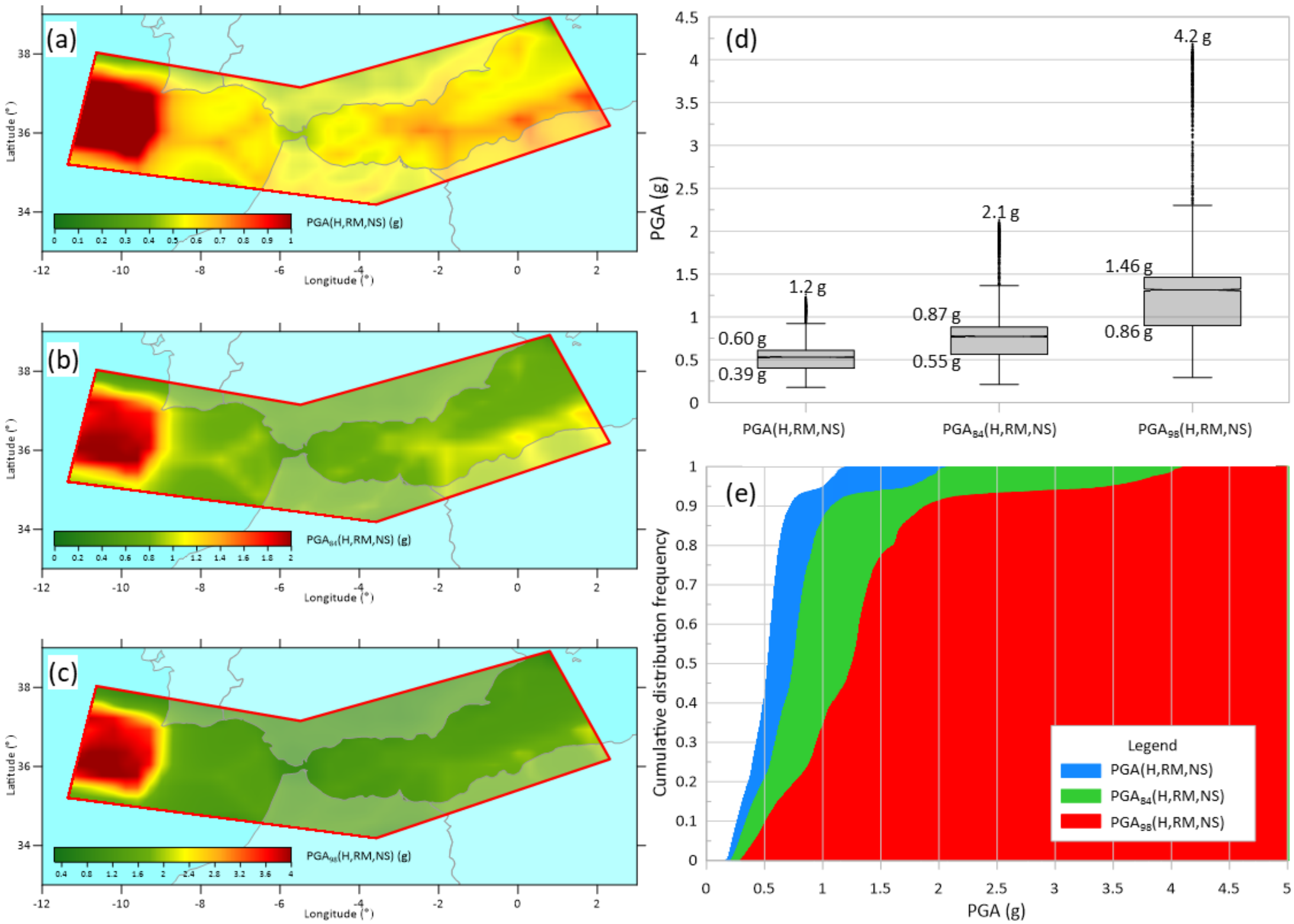

Figure 11~~3~~. PGA~~ percentile~~ $_{50}$ (a), PGA$_{84}$ (b), and PGA $_{98}$ (c) maps obtained including the ~~with the DSHA method with~~ DTM~~ (Figure 7a)~~, considering a source-specific average rupture~~focal~~ mechanism (Table 4~~1~~), random uncertainty for each GMPE, and cumulative effect on each site of all non-controlling seismogenic sources. (d) Box-Whisker plots for PGA values in (a), (b) and (c). Center line represents the mean value. ~~Box edges are limited by the quartiles (numbers indicated 25% lower and 75% upper percentile). Whiskers are limited by the 1.5 times the inter-quartile range. The notch size factor is 1.7.~~ The sample outliers are represented by dot symbols. (d) Experimental cumulative distribution functions for PGA values in (a), (b) and (c).

6. Discussion

With the integration of the relevant zonation models used in this work, a catalogue of 35 seismogenic sources has been created, compiling their essential seismic parameters: depth, MCE and rupture mode, to analyse the three-dimensional SHA, using the DTM of the area, according to the deterministic method and with the aim of studying the sensitivity of the results to the variation of these parametersAlthough . mMost seismic hazard analysis studies worldwide are presentedcarried out on emerged lands (e.g., ., ESHM20 from Danciu et al., 2021) in emerged terrain, the zonings incorporated in the computational models can be used, after an appropriate synthesis and integration process in the areas where they overlap, for seismically active underwater areas Giardini et al., 2014; IGN-UPM, 2017; Mourabit et al., 2014; Pailoplee et al., 2009; Poggi et al., 2020; Vilanova and Fonseca, 2007; Woessner et al., 2015), so not considering the DTM in the calculation is on the side of the most conservative safety. In additionHowever, as in the relativecase of underwater areas, the distance fromto the source to the calculation sites is one of the most relevanta factors that, analyses are more conservative if a DTM is includedif treated in the same way as for land above sea level, leads to incorrect results, underestimating the intensity of the seismic movement, which is this defect being more noticeable in abyssal activethe deeper zonesareas. On the other hand, the use of the characterisation of the predominant rupture mechanismode in each seismogenic zone is preferable to using a homogeneous global style for the whole study area to avoid uniformising the deformation-tectonic stress regime over the entire area. It is preferable to characterize the rupture mechanism specific to each seismogenic zone instead of applying a uniform style to the entire study area, as this avoids homogenizing the deformation-tectonic stress regimeAs the rupture regime of each source enters the calculation process through each GMPE in the structure of the logic tree, therefore only those GMPEs that consider a different formulation for each regime (Douglas, 2001, 2020) will be affected. As in the logic tree used in this work only the CAFA08 GMPE is independent of the rupture mode, the results obtained are affected, to a greater or lesser extent, especially in the areas of low-moderate seismic activity in the Alboran basin, since its predominant mode is rupture, and in the emerged territories of the south of the Iberian Peninsula where the mode is mostly normal. The influence of the differences between using or not using a DTM oin the analysis iscalculation of the DSHA are more significantimportant inthe highlyer the seismic areasactivity, whereas the impact although the contribution to these differences is practically negligible for sources overthat are more than 100 km away. TIt is precisely in these areas that the differences between incorponratsidering the local seismogenic characteristics frompeculiarities specified in the constructed catalogue and using athe DTM are most pronounced in these distant regionsgreatest.Regarding the PGA map obtained with the DTM and each source with its rupture mode, for an exceedance probability rate of 0.5 (50th percentile of the PGA) the qualitative differences, as they are not quantitatively comparable results with other maps that partially provide the offshore PGA distribution, are distinguishable local differences between one and the other. While the DSHA evaluates the worst-case scenario and presents the values of ground motion related to the worst-case scenario, the PSHA allows determining the exceedance rates of the specified ground motion at a desired time.

Seismic hazard analysis carried out in emerged terrain is useful to provide SHA for underwater areas. Including a DTM, although negligible for emerged land, is relevant for submerged zones and most noticeable in abyssal active zones. On the other hand, using rupture mechanism in seismic zones is preferable to using a homogeneous global style. The differences between incorporating local seismogenic characteristics from the constructed catalogue and using a DTM are most pronounced in these distant regions.

The geographical distribution ~~refore, a direct comparison between DSHA and PSHA results does not make sense, but the regional trend over the large zones~~ of maximum ~~values (Gorringe, Planicia Horseshoe, Coral Patch areas, in the Atlantic sector, and Arzew Faults Algerian zone, in the Mediterranean)~~, minimum and intermediate PGA values in SHA from previous published studies with probabilistic~~is similar to that obtained in this work with DSHA despite the maps obtained with PSHA~~ methods and partially covering our study area is very similar to the results obtained in this work with DSHA. This similarity holds true despite using different zonation methods (such as UPM-IGN 2017;~~, and~~ Poggi et al. 2020), ~~with a different zonation (Woessner et al. 2015),~~ or ~~with a~~ non-zoned approaches~~method~~ (like Crespo et al. 2014).

~~DSHA, unlike other SHA methods, is not affected by the uncertainty of the seismic parameters, as handled by the probabilistic method, which can be very relevant in areas where a complete comprehensive fault-specific catalogue of faults and their activity is not available for a robust estimation.~~ A~~lthough, a~~s Reiter (1990) points out, the DSHA does not contemplate the inherent uncertainty in the estimation of seismic hazard~~risk~~, since the frequency of occurrence and magnitudes are ~~is~~ not explicitly considered ~~taken into account, i.e., the recurrence interval or frequency and its associated uncertainty are not addressed~~. So, a~~A~~ less accurate version, ~~but one that at the same time~~ distributing~~es~~ the uncertainty due to randomness in the attenuation functions over a large region, is preferable, even though it provides larger values in this work.~~;~~ T~~t~~hese PGA values can be used as an upper bound of those that can be achieved, for different exceedance probabilities, such as those applied in this work of 0.16 and 0.02, rather than working with more precise, but less accurate, -PGAs~~values~~.

~~Finally, it should also be emphasised that this study introduces a modified DSHA method incorporating the attenuated effect of all sources in addition to the control source used in the classical DSHA, but does not conclude that the original framework is fundamentally flawed. Once the 36 noncontrol sources are considered, the PGA map indicates a substantial increase in seismic hazard, especially in areas close to the confluence of seismic zones. The joint contribution of the sources to the calculated exceedance probability differs according to the PGA vs. distance pattern at each site. Thus, in the cities used as control points, some cities such as Cadiz and Tánger show larger increases than others such as Melilla or Orán. Consequently, large noncontrollable risks lead to a high estimate (at the same percentile), with extreme probability estimates. The distribution of the PGA over the study area becomes more uniform, with less appreciable changes, as the percentile increases (or the probability of exceedance decreases) although its silhouette in the probability distribution is preserved by extending towards higher PGA values.~~

~~Taking this into account, the choice of a seismic hazard alternative should be closely related to the intended applications.~~ For industrial facilities of important socioeconomic position, where failure consequences are unsustainable, it is suggested to use the new DSHA to include the seismic hazard from non-controlling sources ~~in order~~ to ensure that the design is as safe as possible. ~~;~~ C~~c~~onversely, the conventional DSHA might be suitable for non-critical building or structure designs. In ~~Similarly, for~~ the study of landslide-triggering hazard that can cause a tsunamis, it is important to consider~~also relevant to include~~ all sources, preferably at the point event, noted by Collico et al. (2020). ~~(Colico et al., 2020~~Furthermore, it is crucial to utilize ~~)~~ ~~and to use~~ the entire PGA map when~~to~~ applying slope stability methods based on different models, as highlighted ~~(Wang et al., 2021~~ Wang et al. (2021),~~)~~ to avoid~~since~~ underestimating the amplitude of the tsunamigenic source, that can have catastrophic consequences for~~on~~ the affected coastline. Therefore, to ensure accurate assessments and appropriate ~~it reaches, so in order not to underestimate the effects and thus the~~ mitigation measures, it is recommended~~advisable~~ to account~~have~~ for~~an~~ upper bound ~~on the~~ uncertainties, as emphasized by ~~(~~Zengaffinen-Morris et al. (~~,~~2022).

T~~However, t~~he decision for the SHA method is based on its suitability for assessing earthquake hazards ~~not because the selected method is more scientific than another~~, as~~since~~ earthquakes are inherently random and unpredictable. It is important to acknowledge that~~and~~ hazard estimates cannot be fully~~are not~~ verified due to the nature os seismic events~~able~~ ~~-~~(Musson 2012a, b; Wang 2012). Therefore, the use of DSHA which include the seismic hazard from all sources could be recommended for industrial critical facilities of socioeconomic relevance. Likewise, since underestimating the amplitude of the tsunami wave can have catastrophic consequences on the reached coastline, in the study of earthquake-triggered landslide hazard, it is also relevant to include all sources to produce a conservative PGA map with which to apply slope stability methods (Wang et al., 2021) and evaluate maximum upper bound of displaced water volumes.~~The PSHA, for example, is questioned for its imperfect algorithm and unrealistic estimates (Castanos and Lomnitz 2002; Klugel 2007). Moreover, its use of a logic tree analysis to consolidate so-called epistemic uncertainty is considered unscientific (Krinitzsky 2003). Mualchin (2005) considered that no seismic hazard analysis is perfect given our limited understanding of the random process of earthquakes.~~

7. Conclusions

The assessment~~prediction~~ of tsunamigenic sources, both seismic and co-seismic submarine landslides, has become a ~~controversial~~ topic of current scientific and technical interest in the context of recent tsunamis. Under these circumstances, seismic hazard analysis in marine areas should become a best practice for assessing coastal tsunami hazard ~~in order~~ to develop effective coastal inundation prevention and mitigation programmes. However, ~~even~~ the analysis of seismic hazard in underwater areas is subject to debate. . One reason is that it is typically excluded from ~~due not only to the fact that it is usually not shown on~~ national seismic hazard maps as~~because~~ it is ~~of~~ not relevant unless there are~~interest in the absence of~~ structures affected~~resting on the ground shaken~~ by the earthquake. Additionally, ~~,~~there are concerns about the applicability of ~~but also because of its possible shortcomings using~~ standard methodologies for assessing seismic hazard in underwater regions. Among these, DSHA also faces this problem. The use of the 50th percentile motion (PGA_{50}) may be insufficient when field evidence indicates that actual seismic motions can sometimes be two (PGA_{84}) or even three standard deviations (PGA_{98}) above the central value, which could lead to seafloor dislocation or a landslide large enough to generate a tsunami.

The results have shown that if the influence of several relevant sources is not fully addressed in the DSHA analysis, it may result in an inadequate SHA, especially when there are numerous sources around the analysed site. In~~Therefore,~~ this study we have applied ~~introduces a~~ DSHA framework that could arbitrarily consider the ~~s non-~~controlling seismic source~~s~~ and non-controlling seismic source~~s~~ using extreme likelihood theory to SHA. With this method applied to a submarine region and considering the DTM of bathymetries, a hazard map is presented for the Ibero-Maghrebian region, comprised between the western edge of the Gulf of Cá~~a~~diz and the eastern Mediterranean boundary of the Alboran basin, considering 36~~5~~ seismogenic sources with their seismic parameters, rupture mode and depth. Compared to the original DHSA, a substantial increase in the intensity of seismic motion is observed, especially at locations close to the confluence of seismic source zones. This acceleration increases as a lower random uncertainty exceedance probability is used. Therefore, this method based on DSHA is suggested to be preliminarily applied in submarine areas, to evaluate the genesis of tsunamis by strong motions triggering possible large tsunamigenic landslides, making the hazard assessment as safe as possible with the seismic risks provided by each of the seismic sources.

Code availability

~~Excel-based Visual Basic script used in this research can be obtained~~ F~~f~~rom the corresponding author upon reasonable request.

Data availability

This work used only published or public domain datasets~~: IGN-UPM (2017, https://doi.org/10.7419/162.05.2017) for Southern Iberian Peninsula; Poggi et al. (2020, https://doi.org/10.1007/s10518-020-00820-4) for North Africa~~.

Author contributions

AJRB, CPB and MLLI: Investigation. AJRB: literature review. AJRB, CPB and MLLI: conceptualization. AJRB and CPB: methodology. AJRB and CPB: software. AJRB and CPB: formal analysis. AJRB: writing (original draft). AJRB, CPB and MLLI: writing (review and editing). CPB and MLLI: supervision. MLLI: validation.

Competing interests

The authors have no relevant competitive or financial interests to disclose.

Acknowledgements

The authors would like to express their gratitude to the ~~anonymous~~ reviewers João Fonseca and Alexandra Carvalho, whose suggestions helped improve and clarify this manuscript. We would also like to thank Giuliano Panza for his comments. The Open Access publishing for this study has been covered thanks to a CSIC agreement with Copernicus Publications. Thanks to the EMODnet Bathymetry Consortium (2020), EMODnet Digital Bathymetry (DTM). (https://doi.org/10.12770/bb6a87dd-e579-4036-abe1-e649cea9881a) to allow the download and use of the current EMODnet DTM version of December 2020, which has a resolution of 1/16 * 1/16 arc minutes.

References

AEIS-IGN: Seminario sobre criterios sísmicos para centrales nucleares y obras públicas: Madrid, 29-30 de marzo de 1978, Asociación Española de Ingeniería Sísmica (AEIS) and Instituto Geográfico Nacional (IGN), 1979.

Akkar, S. and Bommer, J. J.: Empirical Equations for the Prediction of PGA, PGV, and Spectral Accelerations in Europe, the Mediterranean Region, and the Middle East, Seismological Research Letters, 81, 195–206, https://doi.org/10.1785/gssrl.81.2.195, 2010.

Ang, A. H. and Tang, W. H.: Probability Concepts in Engineering Planning: Emphasis on Applications to Civil and Environmental Engineering, John Wiley and Sons, 2007.

~~Arenillas, M., C, S., and A, S.: CRITERIA TO DETERMINE SEISMIC RISK ON SITES: APPLICATION TO SPANISH DAMS, 1982.~~

Atkinson, K.: An Introduction to Numerical Analysis, John Wiley & Sons, 726 pp., 1991.

~~Atkinson, G. M., Bommer, J. J., and Abrahamson, N. A.: Alternative Approaches to Modeling Epistemic Uncertainty in Ground Motions in Probabilistic Seismic-Hazard Analysis, Seismological Research Letters, 85, 1141–1144, https://doi.org/10.1785/0220140120, 2014.~~

Ayadi, A. and Bezzeghoud, M.: Seismicity of Algeria from 1365 to 2013: Maximum Observed Intensity Map (MOI2014), Seismological Research Letters, 86, 236–244, https://doi.org/10.1785/0220140075, 2014.

~~Benito, B. and Jiménez, E.: Peligrosidad sísmica, Física de la Tierra, 11, 13–47, 1999.~~

Ben-Zion, Y., Lee, W. H. K., Kanamori, H., Jennings, P. C., and Kisslinger, C.: Key formulas in earthquake seismology, International handbook of earthquake and engineering seismology, 81, 1857–1875, 2003.

~~Beven, K. J., Almeida, S., Aspinall, W. P., Bates, P. D., Blazkova, S., Borgomeo, E., Freer, J., Goda, K., Hall, J. W., Phillips, J. C., Simpson, M., Smith, P. J., Stephenson, D. B., Wagener, T., Watson, M., and Wilkins, K. L.: Epistemic uncertainties and natural hazard risk assessment – Part 1: A review of different natural hazard areas, Natural Hazards and Earth System Sciences, 18, 2741–2768, https://doi.org/10.5194/nhess-18-2741-2018, 2018.~~

~~Bezzeghoud, M., Ayadi, A., Caldeira, B., Fontiela, J., and Borges, J. F.: Los mayores sismos en Argelia en la época moderna: las fallas de El Asnam y Zemmouri-Boumerdès, Fis. Tierra, 29, 183, 2017.~~

Bindi, D., Pacor, F., Luzi, L., Puglia, R., Massa, M., Ameri, G., and Paolucci, R.: Ground motion prediction equations derived from the Italian strong motion database, Bull Earthquake Eng, 9, 1899–1920, https://doi.org/10.1007/s10518-011-9313-z, 2011.

~~Bommer, J. J.: Deterministic vs. probabilistic seismic hazard assessment: an exaggerated and obstructive dichotomy, J. Earthq. Eng., 06, 43–73, https://doi.org/10.1142/S1363246902000644, 2002~~.

Bommer, J. J.: Uncertainty about the uncertainty in seismic hazard analysis, Eng. Geol., 70, 165–168, https://doi.org/10.1016/S0013-7952(02)00278-8, 2003.

Bommer, J. J. and Scherbaum, F.: The Use and Misuse of Logic Trees in Probabilistic Seismic Hazard Analysis, Earthq. Spectra, 24, 997–1009, https://doi.org/10.1193/1.2977755, 2008.

Bommer, J. J., Scherbaum, F., Bungum, H., Cotton, F., Sabetta, F., and Abrahamson, N. A.: On the Use of Logic Trees for Ground-Motion Prediction Equations in Seismic-Hazard Analysis, Bull. Seismol. Soc. Am., 95, 377–389, https://doi.org/10.1785/0120040073, 2005.

~~Bommer, J. J., Douglas, J., Scherbaum, F., Cotton, F., Bungum, H., and Fäh, D.: On the Selection of Ground-Motion Prediction Equations for Seismic Hazard Analysis, Seismological Research Letters, 81, 783–793, https://doi.org/10.1785/gssrl.81.5.783, 2010.~~

Bommer, J. J., Akkar, S., and Drouet, S.: Extending ground-motion prediction equations for spectral accelerations to higher response frequencies, Bull Earthquake Eng, 10, 379–399, https://doi.org/10.1007/s10518-011-9304-0, 2012.

Boore, D. M. and Atkinson, G. M.: Ground-Motion Prediction Equations for the Average Horizontal Component of PGA, PGV, and 5%-Damped PSA at Spectral Periods between 0.01 s and 10.0 s, Earthquake Spectra, 24, 99–138, https://doi.org/10.1193/1.2830434, 2008.

Budnitz, R. J., Apostolakis, G., and Boore, D. M.: Recommendations for probabilistic seismic hazard analysis: Guidance on uncertainty and use of experts, US Nuclear Regulatory Commission (NRC), Washington, DC (United States). Div. of Engineering Technology; Lawrence Livermore National Lab. (LLNL), Livermore, CA (United States); Electric Power Research Inst. (EPRI), Palo Alto, CA (United States); US Department of Energy (USDOE), Washington DC (United States), https://doi.org/10.2172/479072, 1997.

Buforn, E. and Udías, A.: Sismicidad y mecanismo focal de los terremotos de la región Cabo de San Vicente-Argelia, Revista de la Sociedad Geológica de España, 20, 301–310, 2007.

Buforn, E., Sanz de Galdeano, C., and Udías, A.: Seismotectonics of the Ibero-Maghrebian region, Tectonophysics, 248, 247–261, https://doi.org/10.1016/0040-1951(94)00276-F, 1995.

~~Buforn, E., Bezzeghoud, M., UdÍas, A., and Pro, C.: Seismic Sources on the Iberia-African Plate Boundary and their Tectonic Implications, Pure Appl. Geophys., 161, 623–646, https://doi.org/10.1007/s00024-003-2466-1, 2004.~~

Buforn, E., Udías, A., and Pro, C.: Large Earthquakes at the Ibero-Maghrebian Region: Basis for an EEWS, Pure Appl. Geophys., 172, 2387–2396, https://doi.org/10.1007/s00024-014-0954-0, 2015.

Buforn, E., Udías, A., and Pro, C.: Source mechanism studies of earthquakes in the Ibero-Maghrebian region and their tectonic implications, J Seismol, 20, 1075–1088, https://doi.org/10.1007/s10950-015-9551-7, 2016.

Burden, R. L., Faires, J. D., and Burden, A. M.: Numerical Analysis, Cengage Learning, 918 pp., 2015.

Campbell, K. W. and Bozorgnia, Y.: Updated Near-Source Ground-Motion (Attenuation) Relations for the Horizontal and Vertical Components of Peak Ground Acceleration and Acceleration Response Spectra, Bull. Seismol. Soc. Am., 93, 314–331, https://doi.org/10.1785/0120020029, 2003.

~~Campbell, K.: Overview of Seismic hazard Approaches with Emphasis on the Management of Uncertainties.", in: 2nd ICTP Workshop on Earthquake Engineering for Nuclear Facilities: Uncertainties in Seismic Hazard", Trieste, Italy, 14–25, 2005.~~

Carvalho, A. M. and Malfeito, N.: Mapas de perigosidade sísmica para Portugal Continental: Uma análise crítica - Parte I – Períodos de recorrência de sismos, 2018.

Castaños, H. and Lomnitz, C.: PSHA: is it science?, Engineering Geology, 66, 315–317, https://doi.org/10.1016/S0013-7952(02)00039-X, 2002.

Cauzzi, C. and Faccioli, E.: Broadband (0.05 to 20 s) prediction of displacement response spectra based on worldwide digital records, J Seismol, 12, 453–475, https://doi.org/10.1007/s10950-008-9098-y, 2008.

~~CEN: Design of structures for earthquake resistance – part 1: General rules, seismic actions and rules for buildings, European Committee for Standardization (CEN), Brussels, BS EN 1998–1:2004, 2004.~~

Chen, Y.-S., Weatherill, G., Pagani, M., and Cotton, F.: A transparent and data-driven global tectonic regionalization model for seismic hazard assessment, Geophysical Journal International, 213, 1263–1280, https://doi.org/10.1093/gji/ggy005, 2018.

~~Cheng, C.-T., Chiou, S. J., Lee, C.-T., and Tsai, Y.-B.: Study on probabilistic seismic hazard maps of Taiwan after Chi-Chi earthquake, J. Geoengin., 2, 19–28, https://doi.org/10.6310/jog.2007.2(1).3, 2007.~~

Chester, D. K.: The 1755 Lisbon earthquake, Progress in Physical Geography: Earth and Environment, 25, 363–383, https://doi.org/10.1177/030913330102500304, 2001.

Chiou, B. S.-J. and Youngs, R. R.: Update of the Chiou and Youngs NGA Model for the Average Horizontal Component of Peak Ground Motion and Response Spectra, Earthquake Spectra, 30, 1117–1153, https://doi.org/10.1193/072813EQS219M, 2014.

Chiou, B.-J. and Youngs, R. R.: An NGA Model for the Average Horizontal Component of Peak Ground Motion and Response Spectra, Earthquake Spectra, 24, 173–215, https://doi.org/10.1193/1.2894832, 2008.

Coles, S.: An Introduction to Statistical Modeling of Extreme Values, Springer, London, https://doi.org/10.1007/978-1-4471-3675-0, 2001.

Collico, S., Arroyo, M., Urgeles, R., Gràcia, E., Devincenzi, M., and Peréz, N.: Probabilistic mapping of earthquake-induced submarine landslide susceptibility in the South-West Iberian margin, Mar. Geol., 429, 106296, https://doi.org/10.1016/j.margeo.2020.106296, 2020.

Coppersmith, K. J. and Youngs, R. R.: Capturing uncertainty in probabilistic seismic hazard assessments within intraplate tectonic environments, in: Proceedings of the Third US national conference on earthquake engineering, 301–312, 1986.

Corbi, F., Sandri, L., Bedford, J., Funiciello, F., Brizzi, S., Rosenau, M., and Lallemand, S.: Machine Learning Can Predict the Timing and Size of Analog Earthquakes, Geophys. Res. Lett., 46, 1303–1311, https://doi.org/10.1029/2018GL081251, 2019.

Cornell, C. A.: Engineering seismic risk analysis, Bulletin of the Seismological Society of America, 58, 1583–1606, https://doi.org/10.1785/BSSA0580051583, 1968.

Cornell, C. A., Howells, D. A., Haigh, I. P., and Taylor, C.: Probabilistic analysis of damage to structures under seismic loads, Dyn. Waves Civ. Eng., 473–488, 1971.

Cotton, F., Scherbaum, F., Bommer, J. J., and Bungum, H.: Criteria for Selecting and Adjusting Ground-Motion Models for Specific Target Regions: Application to Central Europe and Rock Sites, J Seismol, 10, 137–156, https://doi.org/10.1007/s10950-005-9006-7, 2006.

Crespo, M. J., Martínez, F., and Martí, J.: Seismic hazard of the Iberian Peninsula: evaluation with kernel functions, Natural Hazards and Earth System Sciences, 14, 1309–1323, https://doi.org/10.5194/nhess-14-1309-2014, 2014.

Custódio, S., Lima, V., Vales, D., Cesca, S., and Carrilho, F.: Imaging active faulting in a region of distributed deformation from the joint clustering of focal mechanisms and hypocentres: Application to the Azores–western Mediterranean region, Tectonophysics, 676, 70–89, https://doi.org/10.1016/j.tecto.2016.03.013, 2016.

Danciu, L., Nandan, S., Reyes, C. G., Basili, R., Weatherill, G., Beauval, C., Rovida, A., Vilanova, S., Sesetyan, K., and Bard, P.-Y.: The 2020 update of the European Seismic Hazard Model-ESHM20: Model Overview, EFEHR Tech. Rep., 1, https://doi.org/10.3929/ethz-b-000590386, 2021.

Delavaud, E., Cotton, F., Akkar, S., Scherbaum, F., Danciu, L., Beauval, C., Drouet, S., Douglas, J., Basili, R., Sandikkaya, M. A., Segou, M., Faccioli, E., and Theodoulidis, N.: Toward a ground-motion logic tree for probabilistic seismic hazard assessment in Europe, J. Seismol., 16, 451–473, https://doi.org/10.1007/s10950-012-9281-z, 2012.

Douglas, J.: A comprehensive worldwide summary of strong-motion attenuation relationships for peak ground acceleration and spectral ordinates (1969 to 2000), Imperial College of Science, Technology and Medicine, Civil Engineering …, 2001.

Douglas, J.: Ground motion prediction equations 1964–2020, Dept. Civil Environ. Eng., Univ Strathclyde, Glaskow, UK, 670, 2020.

Douglas, J., Faccioli, E., Cotton, F., and Cauzzi, C.: Selection of ground-motion prediction equations for GEM1, GEM Technical Report 2010-E1, GEM Foundation, Pavia, Italy. www.globalquakemodel.org, 2010.

EPRI: Seismic hazard methodology for the central and eastern United States, Seysmicity Own. Group Electr. Power Res. Inst. EPRI, P101-38-45–46, 2256–14, Report NP-472, 1987.

El Alami, S. O., Tadili, B. A., Cherkaoui, T. E., Medina, F., Ramdani, M., Brahim, L. A., and Harnafi, M.: The Al Hoceima earthquake of May 26, 1994 and its aftershocks: a seismotectonic study, 1998.

EPRI: Seismic hazard methodology for the central and eastern United States, Seysmicity Own. Group Electr. Power Res. Inst. EPRI, P101-38-45–46, 2256–14, Report NP-472, 1987.

Epstein, B. and Lomnitz, C.: A Model for the Occurrence of Large Earthquakes, Nature, 211, 954–956, https://doi.org/10.1038/211954b0, 1966.

Estrada, F., Galindo-Zaldívar, J., Vázquez, J. T., Ercilla, G., D'Acremont, E., Alonso, B., and Gorini, C.: Tectonic indentation in the central Alboran Sea (westernmost Mediterranean), Terra Nova, 30, 24–33, https://doi.org/10.1111/ter.12304, 2018.

Fonseca, J. F. B. D.: A Reassessment of the Magnitude of the 1755 Lisbon Earthquake, Bulletin of the Seismological Society of America, 110, 1–17, https://doi.org/10.1785/0120190198, 2020.

Galindo-Zaldívar, J., Chalouan, A., Azzouz, O., Sanz de Galdeano, C., Anahnah, F., Ameza, L., Ruano, P., Pedrera, A., Ruiz-Constán, A., Marín-Lechado, C., Benmakhlouf, M., López-Garrido, A. C., Ahmamou, M., Saji, R., Roldán-García, F. J., Akil, M., and Chabli, A.: Are the seismological and geological observations of the Al Hoceima (Morocco, Rif) 2004 earthquake (M=6.3) contradictory?, Tectonophysics, 475, 59–67, https://doi.org/10.1016/j.tecto.2008.11.018, 2009.

Galindo-Zaldivar, J., Ercilla, G., Estrada, F., Catalán, M., d'Acremont, E., Azzouz, O., Casas, D., Chourak, M., Vazquez, J. T., Chalouan, A., Sanz de Galdeano, C., Benmakhlouf, M., Gorini, C., Alonso, B., Palomino, D., Rengel, J. A., and Gil, A. J.: Imaging the Growth of Recent Faults: The Case of 2016–2017 Seismic Sequence Sea Bottom Deformation in the Alboran Sea (Western Mediterranean), Tectonics, 37, 2513–2530, https://doi.org/10.1029/2017TC004941, 2018.

Galindo-Zaldivar, J., Gil, A. J., Tendero-Salmerón, V., Borque, M. J., Ercilla, G., González-Castillo, L., Sánchez-Alzola, A., Lacy, M. C., Estrada, F., Avilés, M., Alfaro, P., Madarieta-Txurruka, A., and Chacón, F.: The Campo de Dalias GNSS Network Unveils the Interaction between Roll-Back and Indentation Tectonics in the Gibraltar Arc, Sensors, 22, 2128, https://doi.org/10.3390/s22062128, 2022.

García Mayordomo, J.: Creación de un modelo de zonas sismogénicas para el cálculo del Mapa de Peligrosidad Sísmica de España, CSIC - Instituto Geológico y Minero de España (IGME), 2015.

García-Fernández, M., Vaccari, F., Jiménez, M.-J., Magrin, A., Romanelli, F., and Panza, G. F.: Chapter 24 - Regional application of the NDSHA approach for continental seismogenic sources in the Iberian Peninsula, in: Earthquakes and Sustainable Infrastructure, edited by: Panza, G. F., Kossobokov, V. G., Laor, E., and De Vivo, B., Elsevier, 491–514, https://doi.org/10.1016/B978-0-12-823503-4.00006-3, 2022.

GEBCO Compilation Group 2022: The GEBCO_2022 Grid - a continuous terrain model of the global oceans and land, NERC EDS British Oceanographic Data Centre NOC, https://doi.org/10.5285/e0f0bb80-ab44-2739-e053-6c86abc0289c, 2022.

Geller, R. J., Jackson, D. D., Kagan, Y. Y., and Mulargia, F.: Earthquakes Cannot Be Predicted, Science, 275, 1616–1616, https://doi.org/10.1126/science.275.5306.1616, 1997.

Giardini, D., Woessner, J., Danciu, L., Crowley, H., Cotton, F., Grünthal, G., Pinho, R., Valensise, G., Akkar, S., and Arvidsson, R.: Seismic hazard harmonization in Europe (SHARE): online data resource, Swiss Seism. Serv ETH Zurich Zurich Switz, 10, 2013.

Giardini, D., Wössner, J., and Danciu, L.: Mapping Europe's Seismic Hazard, Eos, Transactions American Geophysical Union, 95, 261–262, https://doi.org/10.1002/2014EO290001, 2014.

Goded, T., Buforn, E., and Muñoz, D.: The 1494 and 1680 Málaga (Southern Spain) Earthquakes, Seismological Research Letters, 79, 707–715, https://doi.org/10.1785/gssrl.79.5.707, 2008.

Gómez de la Peña, L., Gràcia, E., Maesano, F. E., Basili, R., Kopp, H., Sánchez-Serra, C., Scala, A., Romano, F., Volpe, M., Piatanesi, A., and R. Ranero, C.: A first appraisal of the seismogenic and tsunamigenic potential of the largest fault systems in the westernmost Mediterranean, Marine Geology, 445, 106749, https://doi.org/10.1016/j.margeo.2022.106749, 2022.

Gonzalez-Castillo, L., Galindo-Zaldivar, J., de Lacy, M. C., Borque, M. J., Martinez-Moreno, F. J., García-Armenteros, J. A., and Gil, A. J.: Active rollback in the Gibraltar Arc: Evidences from CGPS data in the western Betic Cordillera, Tectonophysics, 663, 310–321, https://doi.org/10.1016/j.tecto.2015.03.010, 2015.

Grasso, S. and Maugeri, M.: The Seismic Microzonation of the City of Catania (Italy) for the Etna Scenario Earthquake (M = 6.2) of 20 February 1818, Earthquake Spectra, 28, 573–594, https://doi.org/10.1193/1.4000013, 2012.

Gunawan, P. H. and Prakoso, N. B.: Solution path of Newton's method for determining epicenter earthquake hazard in Italy 24 august 2016, in: 2017 International Conference on Control, Electronics, Renewable Energy and Communications (ICCREC), 2017 International Conference on Control, Electronics, Renewable Energy and Communications (ICCREC), 202–206, https://doi.org/10.1109/ICCEREC.2017.8226707, 2017.

Gumbel, E. J.: Statistics of Extremes, Columbia University Press, https://doi.org/10.7312/gumb92958, 1958.

Hamming, R. W. and Hamming, R. W.: Numerical Methods for Scientists and Engineers, Courier Corporation, 756 pp., 1986.

Hasterok, D., Halpin, J. A., Collins, A. S., Hand, M., Kreemer, C., Gard, M. G., and Glorie, S.: New Maps of Global Geological Provinces and Tectonic Plates, Earth-Science Reviews, 231, 104069, https://doi.org/10.1016/j.earscirev.2022.104069, 2022.

Hays, W. W., Algermissen, S. T., Espindsa, A. F., Perkins, D. M., and Rinehart, W. A.: Guidelines for developing design earthquake response spectra, Final Report Army Construction Engineering Research Lab, 1975.

Herraiz, M., De Vicente, G., Lindo-Ñaupari, R., Giner, J., Simón, J. L., González-Casado, J. M., Vadillo, O., Rodríguez-Pascua, M. A., Cicuéndez, J. I., Casas, A., Cabañas, L., Rincón, P., Cortés, A. L., Ramírez, M., and Lucini, M.: The recent (upper Miocene to Quaternary) and present tectonic stress distributions in the Iberian Peninsula, Tectonics, 19, 762–786, https://doi.org/10.1029/2000TC900006, 2000.

Huang, D. and Wang, J.-P.: Seismic hazard map around Taiwan through a catalog-based deterministic approach, in: 15th World Conference on Earthquake Engineering, 2012.

IGN: Instituto Geográfico Nacional: Geology and tectonics of Gulf of Cadiz, https://www.ign.es/web/resources/sismologia/tproximos/sismotectonica/pag_sismotectonicas/golfocadiz.html, 2023.

IGN-UPM: Actualización de mapas de peligrosidad sísmica de España 2012, Instituto Geográfico Nacional (IGN), 267, https://doi.org/10.7419/162.05.2017, 2017.

Joshi, G. C. and Sharma, M. L.: Uncertainties in the estimation of Mmax, J. Earth Syst. Sci., 117, 671–682, https://doi.org/10.1007/s12040-008-0063-5, 2008.

Kaklamanos, J., Baise, L. G., and Boore, D. M.: Estimating Unknown Input Parameters when Implementing the NGA Ground-Motion Prediction Equations in Engineering Practice, Earthq. Spectra, 27, 1219–1235, https://doi.org/10.1193/1.3650372, 2011.

Kijko, A.: Seismic Hazard, in: Encyclopedia of Solid Earth Geophysics, edited by: Gupta, H. K., Springer International Publishing, Cham, 1–14, https://doi.org/10.1007/978-3-030-10475-7_10-1, 2019.

Kiureghian, A. D. and Ditlevsen, O.: Aleatory or epistemic? Does it matter?, Struct. Saf., 31, 105–112, https://doi.org/10.1016/j.strusafe.2008.06.020, 2009.

Klügel, J. U.: Error inflation in Probabilistic Seismic Hazard Analysis, Eng. Geol., 90, 186 192, https://doi.org/10.1016/j.enggeo.2007.01.003, 2007.

Knuth, D. E.: The Art of Computer Programming: Volume 3: Sorting and Searching, Addison-Wesley Professional, 804 pp., 1998.

Kossobokov, V. and Panza, G.: Seismic roulette: Hazards and risks, Terra Nova, 34, 475–494, https://doi.org/10.1111/ter.12617, 2022.

Koulali, A., Ouazar, D., Tahayt, A., King, R. W., Vernant, P., Reilinger, R. E., McClusky, S., Mourabit, T., Davila, J. M., and Amraoui, N.: New GPS constraints on active deformation along the Africa–Iberia plate boundary, Earth and Planetary Science Letters, 308, 211–217, https://doi.org/10.1016/j.epsl.2011.05.048, 2011.

Kramer, S. L.: Geotechnical Earthquake Engineering, Prentice-Hall Civil Engineering and Engineering Mechanics Series, Prentice Hall, Upper Saddle River, 653, 1996.

Krinitzsky, E. L.: Earthquake probability in engineering — Part 1: The use and misuse of expert opinion. The Third Richard H. Jahns Distinguished Lecture in Engineering Geology, Eng. Geol., 33, 257 288, https://doi.org/10.1016/0013-7952(93)90030-G, 1993a.

Krinitzsky, E. L.: Earthquake probability in engineering—Part 2: Earthquake recurrence and limitations of Gutenberg-Richter b-values for the engineering of critical structures: The third Richard H. Jahns distinguished lecture in engineering geology, Eng. Geol., 36, 1–52, https://doi.org/10.1016/0013-7952(93)90017-7, 1993b.

Krinitzsky, E. L.: Deterministic versus probabilistic seismic hazard analysis for critical structures, Engineering Geology, 40, 1–7, https://doi.org/10.1016/0013-7952(95)00031-3, 1995.

Krinitzsky, E. L.: How to obtain earthquake ground motions for engineering design, Engineering Geology, 65, 1–16, https://doi.org/10.1016/S0013-7952(01)00098-9, 2002.

Krinitzsky, E. L.: Comment on J.U. Klügel's "Problems in the application of the SSHAC probability method for assessing earthquake hazards at Swiss nuclear power plants", in Engineering Geology, vol. 78, pp. 285–307, Engineering Geology, 82, 66–68, https://doi.org/10.1016/j.enggeo.2005.09.004, 2005.

Leprêtre, R., Frizon de Lamotte, D., Combier, V., Gimeno-Vives, O., Mohn, G., and Eschard, R.: The Tell-Rif orogenic system (Morocco, Algeria, Tunisia) and the structural heritage of the southern Tethys margin, BSGF-Earth Sci. Bull., 189, 10, https://doi.org/10.1051/bsgf/2018009, 2018.

Lafosse, M., d'Acremont, E., Rabaute, A., Estrada, F., Jollivet-Castelot, M., Vazquez, J. T., Galindo-Zaldivar, J., Ercilla, G., Alonso, B., Smit, J., Ammar, A., and Gorini, C.: Plio-Quaternary tectonic evolution of the southern margin of the Alboran Basin (Western Mediterranean), Solid Earth, 11, 741–765, https://doi.org/10.5194/se-11-741-2020, 2020.

Loi, D. W., Raghunandan, M. E., and Swamy, V.: Revisiting seismic hazard assessment for Peninsular Malaysia using deterministic and probabilistic approaches, Natural Hazards and Earth System Sciences, 18, 2387–2408, https://doi.org/10.5194/nhess-18-2387-2018, 2018.

López Casado, C., Molina, S., Giner, J. J., and Delgado, J.: Magnitude-Intensity Relationships in the Ibero-Magrebhian Region, Nat. Hazards, 22, 269–294, https://doi.org/10.1023/A:1008142531071, 2000.

López Arroyo, A. and Udías, A.: Aftershock sequence and focal parameters of the February 28, 1969 earthquake of the Azores-Gibraltar fracture zone, Bulletin of the Seismological Society of America, 62, 699–719, https://doi.org/10.1785/BSSA0620030699, 1972.

Magrin, A., Peresan, A., Kronrod, T., Vaccari, F., and Panza, G. F.: Neo-deterministic seismic hazard assessment and earthquake occurrence rate, Engineering Geology, 229, 95–109, https://doi.org/10.1016/j.enggeo.2017.09.004, 2017.

Mantovani, E., Albarello, D., and Mucciarelli, M.: Evidence of interconnection between seismic activity in the Iberian Peninsula and North African belts, Phys. Earth Planet. Inter., 54, 116–119, https://doi.org/10.1016/0031-9201(89)90191-X, 1989.

Maramai, A., Brizuela, B., and Graziani, L.: The Euro-Mediterranean Tsunami Catalogue, https://doi.org/10.4401/ag-6437, 2014.

Martín-Dávila, J. and Pazos, A.: Sismicidad del Golfo de Cadiz y zonas adyacentes, Física de la tierra, ISSN 0214-4557, Nº 15, 2003, pags. 189-210, 2003.

Martínez-García, P., Soto, J. I., and Comas, M.: Recent structures in the Alboran Ridge and Yusuf fault zones based on swath bathymetry and sub-bottom profiling: evidence of active tectonics, Geo-Mar Lett, 31, 19–36, https://doi.org/10.1007/s00367-010-0212-0, 2011.

Mayer, L., Jakobsson, M., Allen, G., Dorschel, B., Falconer, R., Ferrini, V., Lamarche, G., Snaith, H., and Weatherall, P.: The Nippon Foundation—GEBCO Seabed 2030 Project: The Quest to See the World's Oceans Completely Mapped by 2030, Geosciences, 8, 63, https://doi.org/10.3390/geosciences8020063, 2018.

McGuire, R. K.: Seismic hazard and risk analysis, Earthquake Engineering Research Institute, Berkeley, 2004.

McGuire, R. K.: Probabilistic seismic hazard analysis: Early history, Earthquake Engineering & Structural Dynamics, 37, 329–338, https://doi.org/10.1002/eqe.765, 2008.

McGuire, R. K. and Shedlock, K. M.: Statistical uncertainties in seismic hazard evaluations in the United States, Bull. Seismol. Soc. Am., 71, 1287–1308, https://doi.org/10.1785/BSSA0710041287, 1981.

Mendes-Victor, L. A., Oliveira, C. S., Azevedo, J., and Ribeiro, A.: The 1755 Lisbon Earthquake: Revisited, Springer Netherlands, Dordrecht, https://doi.org/10.1007/978-1-4020-8609-0, 2009.

Medialdea, T., Vegas, R., Somoza, L., Vázquez, J. T., Maldonado, A., Díaz-del-Río, V., Maestro, A., Córdoba, D., and Fernández-Puga, M. C.: Structure and evolution of the "Olistostrome" complex of the Gibraltar Arc in the Gulf of Cádiz (eastern Central Atlantic): evidence from two long seismic cross-sections, Marine Geology, 209, 173–198, https://doi.org/10.1016/j.margeo.2004.05.029, 2004.

Meghraoui, M. and Pondrelli, S.: Active faulting and transpression tectonics along the plate boundary in North Africa, Ann. Geophys., 55, 955, https://doi.org/10.4401/ag-4970, 2012.

Molina Palacios, S.: Sismotectónica y peligrosidad sísmica del área de contacto entre Iberia y África, http://purl.org/dc/dcmitype/Text, Universidad de Granada, 1998.

Montessus de Ballore, F.: La península ibérica sismica y sus colonias, in: Anales de la Sociedad Española de Historia Natural, 175–184, 1894.

~~Morales, J., Benito, B., and Luján, M.: Expected ground motion in the south-east of Spain due to an earthquake in the epicentral area of the 1910 Adra earthquake, J. Seismol., 7, 175–192, https://doi.org/10.1023/A:1023506015307, 2003.~~

~~Moratto, L., Orlecka-Sikora, B., Costa, G., Suhadolc, P., Papaioannou, Ch., and Papazachos, C. B.: A deterministic seismic hazard analysis for shallow earthquakes in Greece, Tectonophysics, 442, 66–82, https://doi.org/10.1016/j.tecto.2007.05.004, 2007.~~

Mostafa, S. I., Abdelhafiez, H. E., and Abd el-aal, A. el-aziz K.: Deterministic scenarios for seismic hazard assessment in Egypt, Journal of African Earth Sciences, 160, 103655, https://doi.org/10.1016/j.jafrearsci.2019.103655, 2019.

Mourabit, T., Abou Elenean, K. M., Ayadi, A., Benouar, D., Ben Suleman, A., Bezzeghoud, M., Cheddadi, A., Chourak, M., ElGabry, M. N., Harbi, A., Hfaiedh, M., Hussein, H. M., Kacem, J., Ksentini, A., Jabour, N., Magrin, A., Maouche, S., Meghraoui, M., Ousadou, F., Panza, G. F., Peresan, A., Romdhane, N., Vaccari, F., and Zuccolo, E.: Neo-deterministic seismic hazard assessment in North Africa, J Seismol, 18, 301–318, https://doi.org/10.1007/s10950-013-9375-2, 2014.

~~Mualchin, L.: Seismic hazard analysis for critical infrastructures in California, Eng. Geol., 79, 177-184, https://doi.org/10.1016/j.enggeo.2005.01.009, 2005.~~

~~Munuera, J. M.: Datos básicos para un estudio de sismicidad en el área de la península Ibérica, Memorias del Instituto Geográfico y Catastral, 32, 1963.~~

Musson, R. M. W.: Probability in PSHA: Reply to “Comment on ‘PSHA Validated by Quasi-Observational Means’ by Z. Wang,” Seismol. Res. Lett., 83, 717–719, https://doi.org/10.1785/0220120036, 2012a.

Musson, R. M. W.: PSHA Validated by Quasi Observational Means, Seismol. Res. Lett., 83, 130–134, https://doi.org/10.1785/gssrl.83.1.130, 2012b.

National Research Council: Probabilistic seismic hazard analysis, Natl. Acad. Press Washintong DC, 97 pp., 1988.

~~Negredo, A. M., Bird, P., Sanz de Galdeano, C., and Buforn, E.: Neotectonic modeling of the Ibero-Maghrebian region, Journal of Geophysical Research: Solid Earth, 107, ETG 10-1-ETG 10-15, https://doi.org/10.1029/2001JB000743, 2002.~~

Neres, M., Carafa, M. M. C., Fernandes, R. M. S., Matias, L., Duarte, J. C., Barba, S., and Terrinha, P.: Lithospheric deformation in the Africa-Iberia plate boundary: Improved neotectonic modeling testing a basal-driven Alboran plate, Journal of Geophysical Research: Solid Earth, 121, 6566–6596, https://doi.org/10.1002/2016JB013012, 2016.

Nocquet, J.-M.: Present-day kinematics of the Mediterranean: A comprehensive overview of GPS results, Tectonophysics, 579, 220–242, https://doi.org/10.1016/j.tecto.2012.03.037, 2012.

NRC: Reactor site criteria. Appendix a: seismic and geology siting criteria for nuclear power plants, US Nuclear Regulatory Commission (NRC). Regulatory Guide 10CFR100, 1973.

Orozova, I. M. and Suhadolc, P.: A deterministic–probabilistic approach for seismic hazard assessment, Tectonophysics, 312, 191–202, https://doi.org/10.1016/S0040-1951(99)00162-6, 1999.

~~Ousadou, F., Dorbath, L., Ayadi, A., Dorbath, C., and Gharbi, S.: Stress field variations along the Maghreb region derived from inversion of major seismic crisis fault plane solutions, Tectonophysics, 632, 261–280, https://doi.org/10.1016/j.tecto.2014.06.017, 2014.~~

~~Pagani, M., Monelli, D., Weatherill, G., Danciu, L., Crowley, H., Silva, V., Henshaw, P., Butler, L., Nastasi, M., Panzeri, L., Simionato, M., and Vigano, D.: OpenQuake Engine: An Open Hazard (and Risk) Software for the Global Earthquake Model, Seismol. Res. Lett., 85, 692–702, https://doi.org/10.1785/0220130087, 2014.~~

~~Pagani, M., Garcia-Pelaez, J., Gee, R., Johnson, K., Poggi, V., Silva, V., Simionato, M., Styron, R., Viganò, D., Danciu, L., Monelli, D., and Weatherill, G.: The 2018 version of the Global Earthquake Model: Hazard component, Earthq. Spectra, 36, 226–251, https://doi.org/10.1177/8755293020931866, 2020.~~

~~Pailoplee, S., Sugiyama, Y., and Charusiri, P.: Deterministic and probabilistic seismic hazard analyses in Thailand and adjacent areas using active fault data, Earth Planets Space, 61, 1313–1325, https://doi.org/10.1186/BF03352984, 2009.~~

Palano, M., González, P. J., and Fernández, J.: Strain and stress fields along the Gibraltar Orogenic Arc: Constraints on active geodynamics, Gondwana Research, 23, 1071–1088, https://doi.org/10.1016/j.gr.2012.05.021, 2013.

Panza, G. F. and Bela, J.: NDSHA: A new paradigm for reliable seismic hazard assessment, Engineering Geology, 275, 105403, https://doi.org/10.1016/j.enggeo.2019.105403, 2020.

Panza, G. F., Prozorov, A. G., and Suhadolc, P.: Lithosphere structure and statistical properties of seismicity in Italy and surrounding regions, J. Geodyn., 12, 189–215, https://doi.org/10.1016/0264-3707(90)90007-H, 1990.

~~Panza, G. F., Vaccari, F., Costa, G., Suhadolc, P., and Fäh, D.: Seismic Input Modelling for Zoning and Microzoning, Earthquake Spectra, 12, 529–566, https://doi.org/10.1193/1.1585896, 1996.~~

~~Panza, G. F., Vaccari, F., and Cazzaro, R.: Deterministic Seismic Hazard Assessment, in: Vrancea Earthquakes: Tectonics, Hazard and Risk Mitigation: Contributions from the First International Workshop on Vrancea Earthquakes, Bucharest, Romania, November 1–4, 1997, edited by: Wenzel, F., Lungu, D., and Novak, O., Springer Netherlands, Dordrecht, 269–286, https://doi.org/10.1007/978-94-011-4748-4_25, 1999.~~

~~Panza, G. F., Romanelli, F., and Vaccari, F.: Seismic wave propagation in laterally heterogeneous anelastic media: Theory and applications to seismic zonation, in: Advances in Geophysics, vol. 43, edited by: Dmowska, R. and Saltzman, B., Elsevier, 1–95, https://doi.org/10.1016/S0065-2687(01)80002-9, 2001.~~

~~Panza, G. F., Mura, C. L., Peresan, A., Romanelli, F., and Vaccari, F.: Chapter Three - Seismic Hazard Scenarios as Preventive Tools for a Disaster Resilient Society, in: Advances in Geophysics, vol. 53, edited by: Dmowska, R., Elsevier, 93–165, https://doi.org/10.1016/B978-0-12-380938-4.00003-3, 2012.~~

~~Papadopoulos, G. A., Gràcia, E., Urgeles, R., Sallares, V., De Martini, P. M., Pantosti, D., González, M., Yalciner, A. C., Mascle, J., Sakellariou, D., Salamon, A., Tinti, S., Karastathis, V., Fokaefs, A., Camerlenghi, A., Novikova, T., and Papageorgiou, A.: Historical and pre-historical tsunamis in the Mediterranean and its connected seas: Geological signatures, generation mechanisms and coastal impacts, Marine Geology, 354, 81–109, https://doi.org/10.1016/j.margeo.2014.04.014, 2014.~~

~~Pastor, A. R.: Traits sismiques de la Peninsule Iberique, Ateliers de l'Institut géographique et cadastral, 1927.~~

Poggi, V., Garcia-Peláez, J., Styron, R., Pagani, M., and Gee, R.: A probabilistic seismic hazard model for North Africa, Bull Earthquake Eng, 18, 2917–2951, https://doi.org/10.1007/s10518-020-00820-4, 2020.

Ramkrishnan, R., Kolathayar, S., and Sitharam, T. G.: Probabilistic seismic hazard analysis of North and Central Himalayas using regional ground motion prediction equations, Bull. Eng. Geol. Environ., 80, 8137–8157, https://doi.org/10.1007/s10064-021-02434-9, 2021.

Reilly, W. I., Fredrich, G., Hein, G. W., Landau, H., Almazán, J. L., and Caturla, J. L.: Geodetic determination of crustal deformation across the Strait of Gibraltar, Geophysical Journal International, 111, 391–398, https://doi.org/10.1111/j.1365-246X.1992.tb00585.x, 1992.

Reiter, L.: Earthquake Hazard Analysis: Issues and Insights, Columbia University Press, 254 pp., 1990.

Rivas Medina, A.: Contribución metodológica para incorporar fallas activas en la modelización de la fuente dirigida a estimaciones de peligrosidad sísmica. Aplicación al sur de España, phd, E.T.S.I. en Topografía, Geodesia y Cartografía (UPM), 2014.

Rivas-Medina, A., Benito, B., and Gaspar-Escribano, J. M.: Approach for combining fault and area sources in seismic hazard assessment: application in south-eastern Spain, Natural Hazards and Earth System Sciences, 18, 2809–2823, https://doi.org/10.5194/nhess-18-2809-2018, 2018.

Rodriguez, M., Maleuvre, C., Jollivet-Castelot, M., d'Acremont, E., Rabaute, A., Lafosse, M., Ercilla, G., Vázquez, J.-T., Alonso, B., Ammar, A., and Gorini, C.: Tsunamigenic submarine landslides along the Xauen–Tofiño banks in the Alboran Sea (Western Mediterranean Sea), Geophysical Journal International, 209, 266–281, https://doi.org/10.1093/gji/ggx028, 2017.

Sá, L. F., Morales-Esteban, A., and Neyra, P. D.: A deterministic seismic risk macrozonation of Seville, Arab J Geosci, 14, 2392, https://doi.org/10.1007/s12517-021-08626-7, 2021.

Salgado Gálvez, M. A., Cardona Arboleda, O. D., Carreño Tibaduiza, M. L., and Barbat Barbat, H. A.: Probabilistic seismic hazard and risk assessment in Spain: national and local level case studies, Centre Internacional de Mètodes Numèrics en Enginyeria (CIMNE), 2015.

Silva, P. G., Elez, J., Giner-Robles, J., Perez-Lopez, R., Roquero, E., Rodriguez-Pascua, M., Azcárate, T., and Martínez-Graña, A.: ANÁLISIS GEOLÓGICO DEL TERREMOTO DE TORREVIEJA DE 1829 (ALICANTE, SE ESPAÑA), 2019.

~~Silva, V., Crowley, H., Varum, H., and Pinho, R.: Seismic risk assessment for mainland Portugal, Bull Earthquake Eng, 13, 429–457, https://doi.org/10.1007/s10518-014-9630-0, 2015.~~

Sinha, R. and Sarkar, R.: Seismic Hazard Assessment of Dhanbad City, India, by deterministic approach, Nat Hazards, 103, 1857–1880, https://doi.org/10.1007/s11069-020-04059-9, 2020.

~~Sokolov, V. Y., Wenzel, F., and Mohindra, R.: Probabilistic seismic hazard assessment for Romania and sensitivity analysis: A case of joint consideration of intermediate-depth (Vrancea) and shallow (crustal) seismicity, Soil Dyn. Earthq. Eng., 29, 364–381, https://doi.org/10.1016/j.soildyn.2008.04.004, 2009.~~

~~Somoza, L., Medialdea, T., Terrinha, P., Ramos, A., and Vázquez, J.-T.: Submarine Active Faults and Morpho-Tectonics Around the Iberian Margins: Seismic and Tsunamis Hazards, Front. Earth Sci., 9, 2021.~~

Soumaya, A., Ben Ayed, N., Rajabi, M., Meghraoui, M., Delvaux, D., Kadri, A., Ziegler, M., Maouche, S., and Braham, A.: Active Faulting Geometry and Stress Pattern Near Complex Strike-Slip Systems Along the Maghreb Region: Constraints on Active Convergence in the Western Mediterranean, Tectonics, 37, 3148–3173, https://doi.org/10.1029/2018TC004983, 2018.

Stein, S., Geller, R. J., and Liu, M.: Why earthquake hazard maps often fail and what to do about it, Tectonophysics, 562–563, 1–25, https://doi.org/10.1016/j.tecto.2012.06.047, 2012.

Stich, D., Batlló, J., Morales, J., Macià, R., and Dineva, S.: Source parameters of the MW= 6.1 1910 Adra earthquake (southern Spain), Geophysical Journal International, 155, 539–546, https://doi.org/10.1046/j.1365-246X.2003.02059.x, 2003.

Stich, D., Serpelloni, E., de Lis Mancilla, F., and Morales, J.: Kinematics of the Iberia–Maghreb plate contact from seismic moment tensors and GPS observations, Tectonophysics, 426, 295–317, https://doi.org/10.1016/j.tecto.2006.08.004, 2006.

Suhadolc, P.: Fault-plane solutions and seismicity around the EGT southern segment, R Freeman St Mueller Ed. Proc. Sixth Workshop Eur. Geotraverse Proj. Eur. Sci. Found. Strasbg., 371–382, 1990.

Süli, E. and Mayers, D. F.: An Introduction to Numerical Analysis, Cambridge University Press, 440 pp., 2003.

Tahayt, A., Feigl, K. L., Mourabit, T., Rigo, A., Reilinger, R., McClusky, S., Fadil, A., Berthier, E., Dorbath, L., Serroukh, M., Gomez, F., and Ben Sari, D.: The Al Hoceima (Morocco) earthquake of 24 February 2004, analysis and interpretation of data from ENVISAT ASAR and SPOT5 validated by ground-based observations, Remote Sensing of Environment, 113, 306–316, https://doi.org/10.1016/j.rse.2008.09.015, 2009.

Tehseen, R., Farooq, M. S., and Abid, A.: Earthquake Prediction Using Expert Systems: A Systematic Mapping Study, Sustainability, 12, 2420, https://doi.org/10.3390/su12062420, 2020.

Toro, G. R., Abrahamson, N. A., and Schneider, J. F.: Model of Strong Ground Motions from Earthquakes in Central and Eastern North America: Best Estimates and Uncertainties, Seismological Research Letters, 68, 41–57, https://doi.org/10.1785/gssrl.68.1.41, 1997.

Tozer, B., Sandwell, D. T., Smith, W. H. F., Olson, C., Beale, J. R., and Wessel, P.: Global Bathymetry and Topography at 15 Arc Sec: SRTM15+, Earth and Space Science, 6, 1847–1864, https://doi.org/10.1029/2019EA000658, 2019.

Udias, A. and Muñoz, D.: The Andalusian earthquake of 25 December 1884, Tectonophysics, 53, 291–299, https://doi.org/10.1016/0040-1951(79)90074-X, 1979.

US NRC: Identification and characterization of seismic sources and determination of safe shutdown earthquake ground motion, US Nuclear Regulatory Commission (NRC). Regulatory guide 1.165, 1997.

USCOLD: Committee on Earthquakes. Guidelines for earthquake design and evaluation of structures appurtenant to dams, U.S. Committee on Large Dams (USCOLD),Denver, CO., 75 pp., 1995.

Vázquez, J. T. and Vegas Martínez, R.: Acomodación de la convergencia entre África y la Península Ibérica, Golfo de Cádiz y Mar de Alborán, a partir del análisis de terremotos., Geogaceta, 172–174, 1999.

Vázquez, J. T. (Juan T., Galindo-Zaldívar, J., Palomino, D. (Desirée), González, L., Fernández-Puga, M. C., Naranjo, S., Pedrosa, M. T., Tendero-Salmerón, V., Bárcenas-Gascón, P. (Patricia), Estrada, F., and Ercilla, G.: SISTEMA DE PLIEGUES ACTIVOS EN EL MARGEN CONTINENTAL SEPTENTRIONAL DEL MAR DE ALBORÁN (MEDITERRANEO OCCIDENTAL), Servicio de Publicaciones de la Universidad de Zaragoza, 2022a.

Vázquez, J.-T., Ercilla, G., Alonso, B., Peláez, J. A., Palomino, D., León, R., Bárcenas, P., Casas, D., Estrada, F., Fernández-Puga, M. C., Galindo-Zaldívar, J., Henares, J., Llorente, M., Sánchez-Guillamón, O., d'Acremont, E., Ammar, A., Chourak, M., Fernández-Salas, L. M., López-González, N., and Lafuerza, S.: Triggering Mechanisms of Tsunamis in the Gulf of Cadiz and the Alboran Sea: An Overview, in: Historical Earthquakes, Tsunamis and Archaeology in the Iberian Peninsula, edited by: Álvarez-Martí-Aguilar, M. and Machuca Prieto, F., Springer Nature, Singapore, 65–104, https://doi.org/10.1007/978-981-19-1979-4_4, 2022b.

~~Vilanova, S. P.: The Seismicity of the Iberian Peninsula and interpretation of its genesis: implications for seismic hazard assessment, in: IX Simpósio sobre a Margem Ibérica Atlântica IX Simposio sobre el Margen Ibérico Atlántico IX Symposium on the Iberian Atlantic Margin, 25, 2018.~~

Vilanova, S. P. and Fonseca, J. F. B. D.: Probabilistic Seismic-Hazard Assessment for Portugal, Bulletin of the Seismological Society of America, 97, 1702–1717, https://doi.org/10.1785/0120050198, 2007.

Vilanova, S. P. and Fonseca, J. F. B. D.: Ground-Motion Models for Seismic-Hazard Assessment in Western Iberia: Constraints from Instrumental Data and Intensity Observations, Bulletin of the Seismological Society of America, 102, 169–184, https://doi.org/10.1785/0120110097, 2012.

~~Villaverde, R.: Fundamental Concepts of Earthquake Engineering, CRC Press, 976 pp., 2009.~~

~~Vipin, K. S.: Assessment Of Seismic Hazard With Local Site Effects : Deterministic And Probabilistic Approaches, Thesis, 2013.~~

Wang, J. P. and Huang, D.: Deterministic seismic hazard assessments for Taiwan considering non-controlling seismic sources, Bull. Eng. Geol. Environ., 73, 635–641, https://doi.org/10.1007/s10064-013-0491-6, 2014.

Wang, J.-P., Huang, D., and Yang, Z.: Deterministic seismic hazard map for Taiwan developed using an in-house Excel-based program, Computers & Geosciences, 48, 111–116, https://doi.org/10.1016/j.cageo.2012.05.014, 2012.

Wang, Y., Wang, R., and Zhang, J.-M.: Large-scale seismic seafloor stability analysis in the South China Sea, Ocean Eng., 235, 109334, https://doi.org/10.1016/j.oceaneng.2021.109334, 2021.

Wang, Z.: Comment on “PSHA Validated by Quasi Observational Means” by R. M. W. Musson, Seismol. Res. Lett., 83, 714–716, https://doi.org/10.1785/0220120016, 2012.

Wang, Z. and Cobb, J. C.: A critique of probabilistic versus deterministic seismic hazard analysis with special reference to the New Madrid seismic zone, Recent Advances in North American Paleoseismology and Neotectonics East of Rockies, 2012.

Woessner, J., Laurentiu, D., Giardini, D., Crowley, H., Cotton, F., Grünthal, G., Valensise, G., Arvidsson, R., Basili, R., Demircioglu, M. B., Hiemer, S., Meletti, C., Musson, R. W., Rovida, A. N., Sesetyan, K., Stucchi, M., and The SHARE Consortium: The 2013 European Seismic Hazard Model: key components and results, Bull Earthquake Eng, 13, 3553–3596, https://doi.org/10.1007/s10518-015-9795-1, 2015.

~~Worden, C. B., Thompson, E. M., Hearne, M., and Wald, D. J.: ShakeMap Manual Online: technical manual, user’s guide, and software guide, US Geological Survey, 2020.~~

Youngs, R. R., Chiou, S.-J., Silva, W. J., and Humphrey, J. R.: Strong Ground Motion Attenuation Relationships for Subduction Zone Earthquakes, Seismological Research Letters, 68, 58–73, https://doi.org/10.1785/gssrl.68.1.58, 1997.

Zengaffinen-Morris, T., Urgeles, R., and Løvholt, F.: On the Inference of Tsunami Uncertainties From Landslide Run-Out Observations, J. Geophys. Res. Oceans, 127, e2021JC018033, https://doi.org/10.1029/2021JC018033, 2022.

Zhao, J. X., Zhang, J., Asano, A., Ohno, Y., Oouchi, T., Takahashi, T., Ogawa, H., Irikura, K., Thio, H. K., Somerville, P. G., Fukushima, Y., and Fukushima, Y.: Attenuation Relations of Strong Ground Motion in Japan Using Site Classification Based on Predominant Period, Bulletin of the Seismological Society of America, 96, 898–913, https://doi.org/10.1785/0120050122, 2006.

~~Zulkifli, M., Rudyanto, A., and Sakti, A.: The view of seismic hazard in the Halmahera region, 050004 pp., https://doi.org/10.1063/1.4987082, 2017.~~